The Role of *vang-1/Van Gogh* in Neuronal Polarity in *Caenorhabditis elegans*

Jiravat Visanuvimol

Thesis submitted to the Faculty of Graduate and Postdoctoral Studies in partial fulfillment of the requirements for the degree of Doctor of Philosophy in Cellular and Molecular Medicine

Department of Cellular and Molecular Medicine (Neuroscience)
Faculty of Medicine, University of Ottawa

TABLE OF CONTENTS

STATEMENT OF CO-AUTHORSHIP

All experiments reported in this manuscript were performed by Jiravat Visanuvimol under the supervision of Dr. Antonio Colavita with the exception of the following: genetic screening and mapping of *vang-1(zy1)*, *vang-1(zy2)*, and *vang-1(zy10)* mutants were performed by Dr. Antonio Colavita; the identification of *prkl-1(zy11)* mutants and phenotypic characterization of *prkl-1(zy11)*, *vang-1(tm1422);prkl-1(zy11)* and *dsh-1(ok1445);prkl-1(zy11)* mutants were performed in our laboratory by Leticia Sanchez-Alvarez. Additionally, translational fusion proteins *Punc-4::gfp::prkl-1* and *Punc-4::gfp::dsh-1* were generated by Leticia Sanchez-Alvarez and *Pvang-1::gfp::vang-1* was made by Anna Su.

ABSTRACT

During neuronal development, the axonal and dendritic projections are polarized and oriented along specific body axis. To further explore the molecular basis of neuritogenesis *in vivo*, we used the nematode *Caenorhabditis elegans* as a developmental model and performed a forward genetic screen to identify genes that specify the polarity of neurite outgrowth. We examined the VC4 and VC5 neurons, members of the six VC motor neurons using the *Pcat-1::gfp* transgene *cyIs4*. The VC motor neurons are ventrally located neurons that extend two processes. VC1, VC2, VC3, and VC6 extend axons along the anterior-posterior (A/P) axis; VC4 and VC5 extend axons around the vulva along a mediolateral left-right (L/R) axis perpendicular to the A/P axis. We identified and showed that *vang-1/Van Gogh*, a core component of planar cell polarity (PCP) signalling pathway, acts cell-autonomously in VC4 and VC5 neurons and non-autonomously from the epithelial cells to restrict neurite formation along the A/P axis. *vang-1* mutant animals display ectopic neurites along the A/P axis. Using a candidate gene approach, we further identified and revealed two additional core members of PCP signalling, Prickle (PRKL-1) and Dishevelled (DSH-1), to play a role in A/P-directed neurite suppression. We also showed *prkl-1* and *dsh-1* genetically interact with *vang-1* and VANG-1 is required to suppress A/P-directed neurite outgrowth from larval stage 4 to adulthood. Overexpression of VANG-1 results in a *loss-of-function (lof)* phenotype, suggesting that an appropriate level of VANG-1 activity is important. Additionally, *vang-1/prkl-1*, and *dsh-1* may interact in parallel pathways. Our findings implicate PCP genes to play a previously unidentified role in maintaining polarized neuronal morphology by inhibiting neuronal outgrowth responses to environmental cues.

DEDICATION

I dedicate this thesis to:

- **My mother, Chanpen Karnjanavijaya**

  Who taught me the value of persistence, hard work, and discipline

- **My father, Vivat Visanuvimol**

  Who inspired me to challenge myself and be the best I can be

- **My wife, Atsuko Nakanishi**

  Who patiently supported me throughout my studies

- **My brothers and sisters, Robin, Lily, Patsy, Jenny, and Ron**

  Who constantly reminded me the importance of family

ACKNOWLEDGEMENTS

I would like to thank my thesis supervisor, Dr. Antonio Colavita, for the opportunity to work and learn in his laboratory. I would like to thank my thesis advisory committee members, Dr. Luc Sabourin, Dr. Marie-Andre Akimenko, and Dr. Johnny Ngsee, for their advice and for keeping me focused on my research.

I would like to also thank all the lab members, past and present, for their daily support and encouragements: Nasrin Habibi-babadi, Anna Su, Janice Imai, Vladimir Anikin, Claudia Arauz, Bobby Lanthier, Leticia Sanchez-Alvarez, Andrea McEwan, Cristina Slatculescu, and David Carr. I also would like to thank the past and present summer and honours students for assisting us in routine lab duty.

I would like to thank Dr. Charlie Thompson for taking care and being in charge of the confocal microscope. Thank you also to Zeiss microscope experts, Vincent Charboneau and Dr. Dan Stevens for their technical support.

I would like to thank you all my friends and staff at the Neuroscience Research Institute and Cellular and Molecular Medicine department for making everyday a filled with fun and laughter: the past members of the Sabourin lab, the past and present members of the Schlossmacher lab, the past and present members of the Hakim lab, Bea Robertson, Charlotte McCusker, Paul Andrea, Donna Hooper and Sylvie DeBlois.

Last but not least, I would like to thank my wife Atsuko Nakanishi and all members of my family for their unrelenting support. Mom, dad, Robin, Lily, Patsy, Jenny, Ron, Cheri, Yuki, and Nike, you all have contributed to my success in ways immeasurable. Thank you

TABLE OF CONTENTS

1: Chapter 1- General Introduction

LIST OF FIGURES

LIST OF TABLES

ABBREVIATIONS

AMP	**Ampicillin**
A/P	**Anterior-posterior**
aPKC	**a typical protein kinase C**
CNS	**Central Nervous System**
CE	**Convergence extension**
DS	**Dachsous**
DCC	**Deleted in Colorectal Carcinoma**
DSH	**Dishevelled**
D/V	**Dorsal-ventral**
EMS	**Ethyl methanesulfonate**
FT	**Fat**
FMI	**Flamingo**
FJ	**Four-jointed**
FZ	**Frizzled**
µg	**Microgram**
GDP	**Guanosine 5'-diphosphate**
GEF	**Guanine exchange factor**
GFP	**Green Fluorescence Protein**
GTP	**Guanosine triphosphate**
Hr	**Hour**
Invs	**inversin**
IPTG	**Isopropyl β-D-1-thiogalactopyranoside**
L	**Larval**
LB	**Luria-Bertani**

L/R	**Left-right**
LG	**Linkage group**
µl	**Microlitre**
µm	**Micrometer**
NGM	**Nematode growth medium**
NSC	**Neural stem cell**
PCP	**Planar Cell Polarity**
PIP3	**Phosphatidylinositol 3,4,5-triphosphate**
PKD	**Polycystic Kidney Disease**
P-Rvl	**Posterior-reversed vulval lineage**
PTEN	**Phosphatase lipid protein phosphatise and tensin homolog deleted on chromosome 10**
PRKL	**Prickle**
PD	**Proximal-distal**
SEC	**Second**
SPLE	**Spiny legs**
SOP	**Sensory Organ Precursor**
RGN	**Retinal Ganglion Cells**
ROBO	**Roundabout**
VANG	**Van Gogh**
VPC	**Vulva Precursor Cell**
WG	**Wingless**

CHAPTER 1

INTRODUCTION

1 Chapter 1- General Introduction

1.1 Neuronal development

Neurons are among the most highly morphologically and functionally diverse types of cells, typically extending a single long axon and multiple shorter dendrites. The development of neurons can be broadly categorized into three developmental processes: the initial acquisition of neuronal asymmetry, the polarization of axon and dendrite outgrowth, and the specification of axons and dendrites (Ou and Shen, 2010). The establishment of a single axon has been elegantly demonstrated *in vitro* via rodent hippocampal cell cultures, and can be divided into five stages. At stage 1, freshly plated immature post-mitotic neurons extend extensive networks of actin to form lamellipodia. At stage 2 the lamellipodia protrusions develop into short immature neurites. At stage 3, neurons undergo axon specification whereby one of the immature neurites rapidly grows to become an axon. At stage 4, the remaining neurites elongate and mature into dendrites. Finally at stage 5, the mature axon and dendrites form functional synapses (Dotti et al., 1988).

In vitro studies have uncovered important molecules and pathways that play a role in neuronal development. Some molecular complexes such as the PAR-3/PAR-6/aPKC (atypical protein kinase C) are well-characterized in regulating axon outgrowth and specification (Barnes and Polleux, 2009; Barnes et al., 2008; Insolera et al., 2011; Wiggin

et al., 2005). The PDZ-domain containing PAR-3 localizes in the soma and in all neurites during stage 2 of neuron development (Nishimura et al., 2004; Shi et al., 2003). At stage 3, both PAR-3 and PAR-6 are absent in dendrites and are only localized at the developing growth cone of the axon. Overexpression of PAR-3 and PAR-6 lead to multiple ectopic axons (Shi et al., 2003). PAR-3 and PAR-6 can directly bind and colocalize with the actin cytoskeleton regulators Rac1 and Cdc42 of the Rho family GTPases during neuronal development (Nishimura et al., 2005; Schwamborn and Puschel, 2004). It has been suggested that the PAR-3/PAR-6 complex acts downstream of Rho family GTPases and converts inactive GDP-bound Rac to active GTP-bound Rac by regulating Rac-specific guanine nucleotide exchange factors (GEFs) Tiam1 and STEF (Nishimura et al., 2005).

The role of the Par3/Par6/aPKC complex *in vivo* is challenging to interpret as the complex is also involved in regulating the apical-basal polarity of glial neuronal progenitors (Barnes and Polleux, 2009). Nonetheless, *in vivo* studies of neuronal development reveal that post-mitotic pyramidal neurons may acquire their axon-dendrite polarization from their progenitors' apical-basal polarity. In the mammalian neocortex, the neuronal progenitors extend a long basal process and project a short apical process toward the ventricle side. As the cells exit mitosis and migrate toward the top of the cortical plate, the post-mitotic neurons extend several short neurites and all but two of these neurites will be retracted, leaving the basally projected leading process and the apically projected trailing process. The leading process will eventually form dendrites and the trailing process will become an axon (Barnes and Polleux, 2009; Barnes et al., 2008; Morgan et al., 2006).

In vivo studies using time-lapse confocal microscopy, siRNA analysis and *ex vivo* cortical electroporation experiments in the mammalian cortex identified the bHLH transcription factor *Neurogenin2* (*ngn2*) and the mammalian ortholog of the polarity protein Par4 LKB1 kinase and its coactivator *Strad-α* as regulators of cortical neuron axon specification (Barnes et al., 2007; Hand et al., 2005; Shelly et al., 2007). NGN2 acts to specify the polarity of the dendrite-to-be leading process while LKB1 promotes axon formation in the trailing process (Hand et al., 2005; Ma et al., 2008b). Loss of LKB1 results in loss of axon formation and overexpression of LKB1 leads to formation of multiple axons (Barnes et al., 2007; Shelly et al., 2007). In addition, LKB1 can phosphorylate the SAD-A/B kinases and may function upstream of the SAD-A/B kinases. Activated SAD-A/B kinases in turn phosphorylate microtubule-associated proteins such as Tau, resulting in cytoskeleton modifications (Kishi et al., 2005). However, the *in vivo* extracellular cues that lead to the phosphorylation of NGN2 and LKB1 and the signalling pathway involved in the LKB1-mediated activation of SAD-A/B kinases and the accumulation of Par3/Par6/aPKC complex at the tip of nascent axon remain largely unknown.

In vivo studies of the development of retinal ganglion cells (RGC) in zebrafish revealed differences in neuronal development *in vivo* and *in vitro*. Unlike *in vitro* development, *in vivo* time-lapse analysis of RGC development revealed that post-mitotic RGCs do not project multiple processes and instead extend only two neurites along the apical-basal axis. The basally projected neurite will mature into an axon and the apically directed process will give rise to a dendrite (Zolessi et al., 2006). An extracellular cue Laminin1 (Lamα1) is required for correct polarization of a basally projected axon-to-be

neurite toward the basal lamina of the neural retina (Choi et al., 2010; Randlett et al., 2011). In contrast to the localization observed in *in vitro* hippocampal pyramidal neurons culture, PAR3 and aPKC are localized to the tip of the apical dendrite-to-be neurite (Zolessi et al., 2006). Observations obtained from *in vivo* studies underline the importance of interaction between extracellular cues and intracellular signalling during neuritogenesis. Furthermore, recent reports demonstrate that the extracellular guidance cues Netrins and Slits play a role in the induction of the nematode *Caenorhabditis elegans* neuronal asymmetry and initiation of neurite emergence (Adler et al., 2006; Quinn et al., 2006).

In our study, we showed that *vang-1*, the sole *C. elegans* homolog of the Planar Cell Polarity (PCP) gene *Van Gogh*, plays a role in regulating neuronal polarity. Therefore, the goals of this literature review are to provide an overview of the development of neurite outgrowth in *C. elegans* and to highlight the role of non-canonical Wnt PCP signalling pathway in both invertebrates and vertebrates' development.

1.2 *Caenorhabditis elegans* as a genetic model

1.2.1 *C. elegans* as an experimental model

The nematode *C. elegans* is an excellent experimental model for studying the development of neurons. It has a rapid life span of 3 days from the time the egg is laid to the time the animal reaches sexual maturity and develops through four easily identifiable larval stages prior to reaching adulthood (Jorgensen and Mango, 2002). In addition, *C. elegans* are hermaphrodites and thus produce progeny that are clones of themselves, eliminating extensive breeding work necessary to maintain desired genotypes. Adult

nematodes are about 1mm in length, and they can be easily grown on agar plates containing bacteria as the food source. In addition, the embryo's development follows an invariant cell lineage; therefore, the origin of most cells can be traced back to the blastomeres that they were derived from (Deppe et al., 1978; Maduro, 2010; Sulston et al., 1983). The hermaphrodite consists of 959 cells, of which 302 are neurons (Jorgensen and Mango, 2002). The complete wiring and synaptic connectivity maps have been thoroughly illustrated and described by electron microscopy (Hall and Altun, 2008). Additionally, neurons in *C. elegans* can be visualized *in vivo* by using GFP promoter or translational fusions. Moreover, its relatively small, fully sequenced genome of 100 million base pairs makes it a powerful genetic tool. Furthermore, the nematode can be stored frozen at -80 $^{\circ}$C (Jorgensen and Mango, 2002).

1.2.2 *C. elegans* as an experimental model for genetic investigations

C. elegans is an ideal organism for genetic analysis due to its small genome size of approximately 19,500 genes and its ease of manipulation (Coghlan, 2005). Mutations in *C. elegans* can be readily induced by soaking the animals in a mutagen such as ethyl methanesulfonate (EMS) to generate point mutations (Jorgensen and Mango, 2002). A number of genetic screens can be utilized to identify genetic mutants and to uncover additional genes that modulate the same process as an existing mutant. Most known mutants were identified via simple forward F2 screens where a population of larval stage (L) 4 wild-type hermaphrodites were exposed to a mutagen to induce mutations in the sperm and oocytes (Jorgensen and Mango, 2002). The mutagenized worms, termed P0, are plated and allowed to lay F1 eggs. The P0s are then removed and the hatched F1s are permitted to grow to adulthood and to lay F2 eggs. The F1s are removed and the F2

progeny are then examined for phenotypes of interest. The frequency of EMS-induced point mutations is one in every 2,000 copies of a gene; therefore, approximately 1000 F1s are required in a genetic screen to obtain a *loss-of-function (lof)* mutant (Jorgensen and Mango, 2002).

Other variations of genetic screens include enhancer, suppressor, drug selection, and laser ablation screens. An enhancer screen for an increase in the frequency or severity of the defective phenotypes in the obtained mutants to identify additional mutations that regulate the same biological process (Rocheleau et al., 2002). Similarly, a suppressor screen surveying for the suppression of frequency or severity of the starting phenotype can also be used (Colavita and Culotti, 1998). Drug-selection screens identify mutants that are resistant to drugs of interest (Artal-Sanz et al., 2006). Laser ablation screens use a laser microbeam to ablate cells of interest in mutagenized worms and screen for restoration of biological function (Ziel et al., 2009).

1.2.3 Neuronal outgrowth and polarization in *C. elegans*

1.2.3.1 Netrin/UNC-6 and DCC/UNC-40 regulate neurite polarization along the dorsal-ventral axis

One of the well-studied aspects of neuronal development is axon guidance in the central nervous system (CNS). In bilaterally symmetric organisms, the majority of the CNS axons cross the midline of the body and form synaptic contacts with their targets on the contralateral side (Hou et al., 2008). Recent studies have suggested that some of the molecules involved in guiding axons may also play roles in modulating axon outgrowth. These include the ligands Netrin, Slit, and Semaphorins and their respective cell-surface

receptors Deleted in Colorectal Carcinoma (DCC), Roundabout (ROBO), and Neuropilins. These axon guidance molecules are highly conserved across invertebrates and vertebrates. In *Drosophila*, the midline cells secrete both the attractive Netrin and repulsive Slit cues. Commissural axons are guided toward the midline by the presence of DCC receptors on the growth cones. Once across the midline, the receptors to the repulsive Slit cues, ROBO, are upregulated to prevent midline re-crossing (Killeen and Sybingco, 2008; Mitchell et al., 1996). Non-crossing axons, in contrast, always express ROBO receptors and therefore are repelled from crossing the midline (Killeen and Sybingco, 2008). Similarly in mice, the commissural axons expressing DCC receptors are attracted to Netrin secreted by the floor plate cells of the spinal cord. The commissural axons extend ventrally to the floor plate and switch their responsiveness to Slit upon crossing the floor plate (Evans and Bashaw, 2010; Serafini et al., 1996). Semaphorins and Eph4A are additional repulsive cues present in vertebrates (Evans and Bashaw, 2010).

In *C. elegans*, the mechanisms of axon guidance function in the same manner as in *Drosophila* and in vertebrates. The mechanosensory neurons AVM and PVM send out axons first in the ventral direction and then anteriorly along the ventral nerve cord. The ventrally extending axons express the DCC ortholog UNC-40 receptor and are attracted to the Netrin ortholog UNC-6 produced by the neurons located within the ventral nerve cord (Culotti and Kolodkin, 1996; Levy-Strumpf and Culotti, 2007). AVM and PVM neurons also express the ROBO ortholog SAX-3 and are repelled ventrally by the Slit ortholog SLT-1 expressed in the dorsal muscle cells (Hao et al., 2001). The transmembrane protein UNC-5 also functions in axon guidance as axons expressing UNC-5 are repelled

from the ventral nerve cord and are directed dorsally toward dorsal muscle cells. It has been demonstrated that axons expressing both UNC-5 and UNC-40/DCC are repelled from the ventral nerve cord and are directed dorsally (Hamelin et al., 1993).

A study by Adler et al. showed that Netrin/UNC-6 and DCC/UNC-40 can also modulate the initiation, maintenance and orientation of axonal growth of the HSN neuron. In wild-type animals, the post-mitotic HSN breaks its spherical symmetry by extending a filopodial leading edge ventrally at L2 and multiple short, ventrally polarized neurites at early L3. By mid L3 stage, a single axon-to-be neurite continues to expand in size and length while others retract. The single ventrally polarized axon turns anteriorly and forms synaptic contacts with the vulva muscles and the VC4 and VC5 motor neurons (Adler et al., 2006). In *unc-6* and *unc-40* mutants, the HSN initiated the break in spherical symmetry at L3 instead of L2 and the ventral polarization of filopodia and transient neurites is lost as neurites extend in random directions (Adler et al., 2006). The Netrin/UNC-6 and its receptor DCC/UNC-40 were shown to control the ventral polarization of the HSN axon by recruiting the lamellipodin protein MIG-10 to the ventral side of the cell body at L2 stage. Consequently, it was proposed that the asymmetric localization of MIG-10 is a result of communication between the Netrin/UNC-6 extracellular cue and the membrane receptor UNC-40/DCC which leads to localized recruitment of PI3K and the production of PIP3. Ventrally localized PIP3 in turn interacts with the PH-domain of MIG-10 and recruits it to the ventral side of the cell (Adler et al., 2006). In addition, MIG-10 has also been shown to bind to the small GTPase Rac1 homolog CED-10 (Chang et al., 2006; Quinn et al., 2006). MIG-10 therefore acts downstream of Netrin/UNC-40 in polarizing HSN axon outgrowth.

1.2.3.2 The Wnt signalling pathway

The Wnt signalling pathway controls a variety of important biological events including cell migration and proliferation, establishment of cell polarity, and stem cells' self renewal capacity (Gao and Chen, 2009). Wnts are soluble morphogens that act as ligands for the seven-pass transmembrane Frizzled (FZ) receptors (Cadigan and Nusse, 1997). The most extensively studied Wnt signalling pathways are the canonical Wnt-β-catenin, the Wnt-Calcium, and the non-canonical Wnt-Planar Cell Polarity (PCP) pathways. The Wnt-β-catenin pathway was the first Wnt signalling pathway discovered and thus sometimes referred to as the canonical Wnt pathway. The Wnt-β-catenin pathway plays important roles in cell differentiation and proliferation and has been implicated in the generation of cancer cells (Bienz, 2005; Cadigan and Nusse, 1997; de la Roche et al., 2008; Macdonald et al., 2007). The binding of Wnt ligands to the seven-pass transmembrane receptor protein FZ and to the co-receptor LDL receptor-related proteins 5 or 6 (LRP5 or LRP6) activates the β-catenin pathway (Endo and Rubin, 2007; He et al., 2004). The WNT/FZ/LRP complex mediates the phosphorylation of the cytoplasmic *Dishevelled* (*dsh*) and initiates disruption of the glycogen synthase kinase-3β (GSK-3β) degradation complex whose degradation target is the cytoplasmic signalling molecule β-catenin (Endo and Rubin, 2007). In the absence of GSK-3β, β-catenin accumulates in the cytosol and enters the nucleus where it interacts with the T-cell factor (TCF)/ lymphoid enhancer factor (LEF) transcription factor complex to start the transcription of WNT target genes (Behrens et al., 1996; Molenaar et al., 1996).

Like the β-catenin pathway, the Wnt-calcium signalling pathway also requires the binding of Wnt to FZ receptor to activate DSH. Activated DSH stimulates production of

intracellular calcium and the increased level of intracellular calcium in turn activates a variety of signalling complexes such as protein kinase C (PKC) and calmodulin kinase II (CamKII) (Endo and Rubin, 2007). The Wnt-calcium pathway is suggested to modulate the motility and invasiveness of cancer cells (Sugimura and Li, 2010).

1.2.3.3 Wnt signalling pathway in *C. elegans* axon guidance

There are five Wnt orthologs in *C. elegans*: CWN-1, CWN-2, EGL-20, LIN-44, and MOM-2. The four FZ *C. elegans* orthologs are LIN-17, CFZ-2, MIG-1, and MOM-5. The Wnts have been shown to play a role in establishing polarity of ALM and PLM mechanosensory neurons (Hilliard and Bargmann, 2006; Pan et al., 2006; Zinovyeva et al., 2008). ALM extend a long process anteriorly and a shorter neurite posteriorly; PLM also extend a long anterior axon and a shorter posterior process. The Wnts cooperate via partial redundancy in regulating ALM neurite polarity as the single *cwn-1, cwn-2,* and *egl-20* mutants display no phenotypic defects but the double mutants *cwn-1;egl-20* and *cwn-1;cwn-2* display an aberrant shorter anterior process and a longer posterior neurite (Hilliard and Bargmann, 2006; Pan et al., 2006). Wnts also function redundantly in controlling the polarity of PLM neurite outgrowth. The polarity of PLM neurites are reversed in *lin-44* mutants whereby the posterior axon becomes the longer process and the anterior axon develops into the shorter axon (Hilliard and Bargmann, 2006). The polarity reversal defect is not observed in *egl-20* mutants but the phenotypic defect is enhanced in the double mutants *lin-44;egl-20* (Hilliard and Bargmann, 2006). EGL-20, CWN-1, and LIN-44 are produced by epidermal and muscle cells in the posterior region of the nematode. Interestingly, the Frizzled receptor LIN-17 is preferentially expressed in the posterior neurite process of the PLM, and LIN-17 asymmetric localization is lost in *lin-44*

mutants, suggesting that externally-expressed Wnts regulate neurite polarity via internally-localized FZ receptor (Hilliard and Bargmann, 2006). Additionally, *wnt* signalling also regulates the anterior-posterior (A/P) directed neurite outgrowth of the GABAergic RMED and RMEV motor neurons. Anteriorly located in the head region, RMED/V neurons extend one process around the nerve ring and another process posteriorly along the dorsal and ventral body axis, respectively. *cwn-2* functions as an attractive cue for posteriorly-directed outgrowth RMED/V axons and genetically interacts with *cfz-2* and *mig-1* (Song et al., 2010).

1.3 The Planar Cell Polarity (PCP) signalling pathway

The study of planar cell polarity began about 25 years ago when Gubb and Garcia-Bellido discovered that the orientation of *Drosophila* cuticle hairs and bristles along the body axis is governed by a small set of genes (Gubb and Garcia-Bellido, 1982). The authors coined the phenomena "tissue polarity". The polarization across the *Drosophila* epithelial cells is now termed Planar Cell Polarity (PCP). However, studies have shown genes in the PCP signalling pathway to be involved not only in *Drosophila* epithelial cells but also in a variety of cell types and movements in both invertebrate and vertebrates. Despite advances in understanding of the pathway, the genetics and mechanisms of the PCP signalling pathway is best understood in *Drosophila*.

1.3.1 PCP in *Drosophila*

1.3.1.1 Epithelial PCP

The cells within the epithelium planes of *Drosophila* wing and the body wall are respectively polarized along the proximal-distal (P/D) and anterior-posterior (A/P) axis

(Goodrich and Strutt, 2011; Seifert and Mlodzik, 2007). The wing epithelial cells generate distally-pointing cuticular hair structures that emerge from the distal end of the cells. Similarly, the thorax epithelial cells project hair structures that protrude from the posterior region and point posteriorly (McNeill, 2010). Gubb and Garcia-Bellido initially showed that *Drosophila frizzled (fz), prickle (pk), multiple wing hair (mwh), spiny legs (sple),* and *inturned (in)* mutants displayed defects in the polarization of the cuticle hair structures along the epithelium planes (Fig. 1A) (Gubb and Garcia-Bellido, 1982). These polarity mutants are now known to act in the PCP pathway.

The PCP pathway is a non-canonical *wnt/frizzled* signalling pathway that is highly conserved across the animal kingdom (Goodrich and Strutt, 2011; Seifert and Mlodzik, 2007). The core components of the PCP signalling pathway can be categorized into membrane and cytoplasmic proteins. The membrane proteins are the seven-pass Frizzled (FZ) receptor, the cadherin protein Flamingo (FMI), and the four-pass PDZ-binding motif-containing protein Van Gogh (VANG); the cytoplasmic proteins consist of Prickle (PK), Dishevelled (DSH), and Diego (DGO). PK contains three LIM domains and one PET domain and exists in multiple isoforms (Lin and Gubb, 2009; Sweede et al., 2008). DSH contains DIX, PDZ and DEP domains, and DGO contains multiple ankyrin repeat domains (Fig. 2). The core PCP genes modulate the polarity of cells in the plane of the *Drosophila* wing epithelium. Mutations in any of these proteins result in orientation defects of wing hairs and formation of multiple ectopic hairs in one single wing cell (Fig. 1A and Fig. 3) (Axelrod, 2009; McNeill, 2010; Seifert and Mlodzik, 2007; Valentine and Collier, 2011). In addition, there is also a subset of tissue-specific effector genes, which are *in, mwh, fuzzy (fy),* and *fritz (frtz)* (Goodrich and Strutt, 2011).

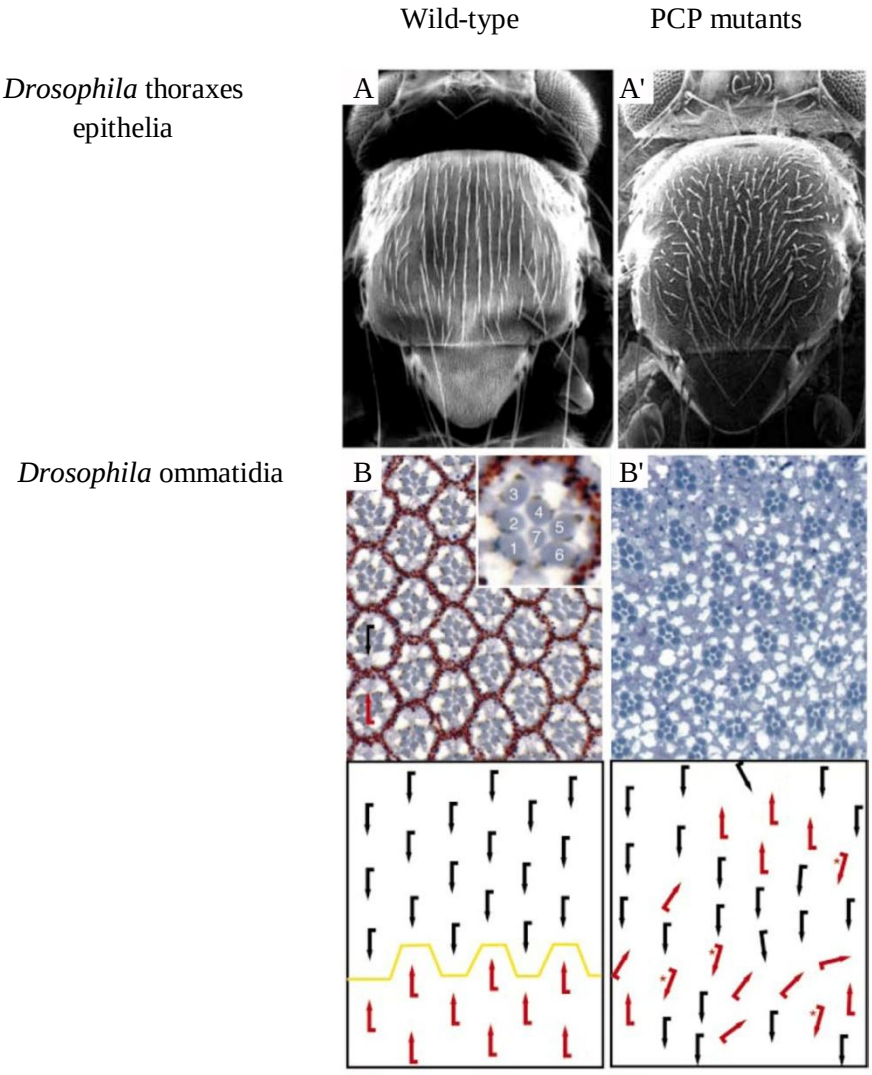

Figure 1. Planar Cell Polarity defects in *Drosophila*. (A,B) Wild-type and (A',B') *Drosophila* PCP mutants. PCP mutants display defective hair (A') and ommatidia (B') orientations. Defective hair orientations occur as a result of incorrect polarization of cells across epithelium plane. Black and red arrows in (B) and (B') represent orientation of individual ommatidium with respect to the equator (yellow line). In PCP mutants (B'), the polarization of R3 and R4 photoreceptors is disrupted, leading to defect in the orientation of individual ommatidium. Images are taken with permission from Wolff and Rubin, 1998 (A,A') and Jenny et al., 2003 (B,B').

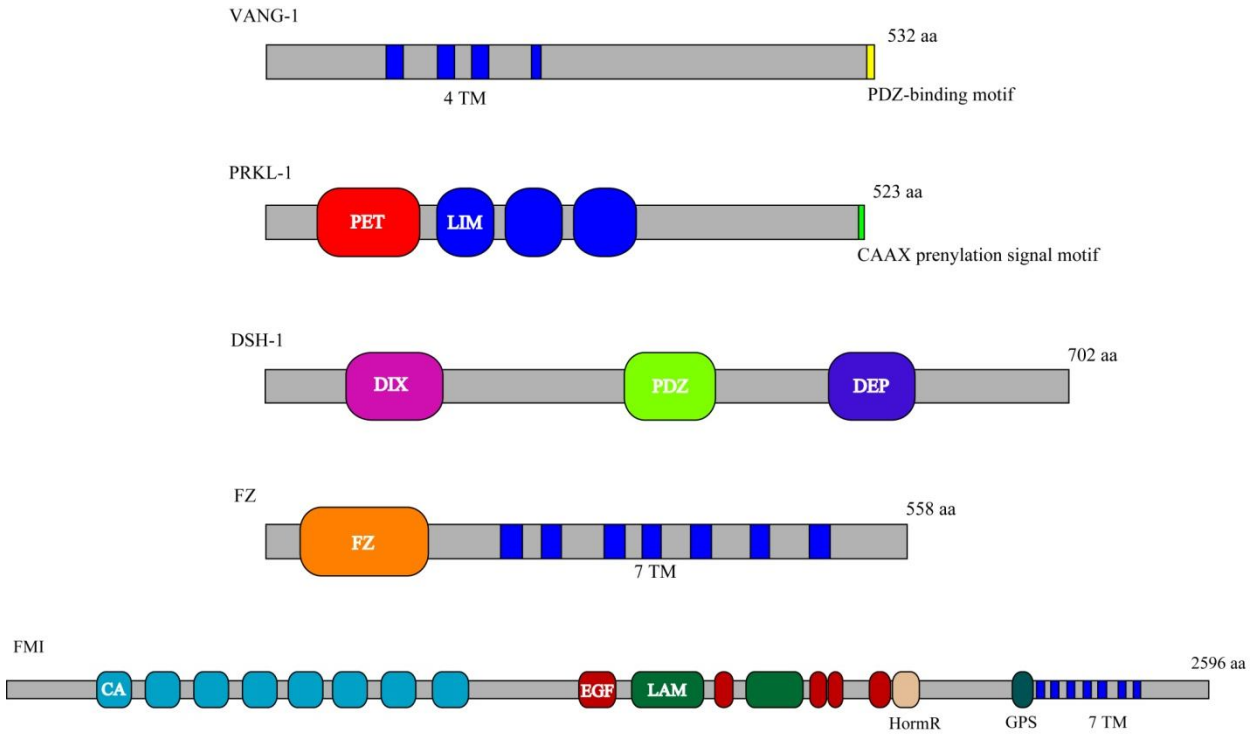

Figure 2. Schematic drawings of *C. elegans* PCP proteins. VANG-1 is a four-pass transmembrane protein containing a PDZ-binding domain at the C-terminal. PRKL-1 is a cytoplasmic protein containing a PET domain, three LIM domains, and a CAAX prenylation signal motif. DSH-1 is a cytoplasmic protein possessing a DIX domain, a PDZ domain, and DEP domain. FZ is a seven-pass transmembrane protein containing an extracellular FZ domain at the N-terminus. FMI is a seven-pass cadherin transmembrane protein containing extracellular cadherin (CA) glycoprotein repeats, epidermal growth factor-like domain (EGF), laminin domains (LAM), a G-protein coupled receptor HormR domain, and G-protein-coupled receptor proteolytic site domain (GPS).

The core PCP genes function both cell and non-cell autonomously. *Drosophila* clonal experiments showed that *fz, vang, pk, dgo,* and *dsh* clones affect polarity within the mutant cells and therefore act cell-autonomously. However, *fz* and *vang* also act non-cell autonomously as mutant *fz* and *vang* clones not only affect the phenotype of the mutant cells but also the phenotype of the surrounding wild-type cells (Wu and Mlodzik, 2009). Therefore, it is likely that *pk, dgo,* and *dsh* act to receive or interpret signals from neighbouring cells whereas *fz* and *vang* function in propagating cell-cell communication signals across the epithelium plane (Wu and Mlodzik, 2009). Wild-type cells distal to the *fz* mutant clones orient their cuticular structures toward the mutant patch. It has been proposed that cells orient their polarity away from high source of FZ and toward region expressing low level of FZ activity (Adler et al., 1997). In contrast, wild-type cells distal to the *vang* mutant clones are not affected; however, wild-type cells proximal to the mutant clones adjust the polarization of hair structures to point away from the mutant clones (Wu and Mlodzik, 2009). Non-cell autonomous functions of *fz* and *vang* are also demonstrated via *gain-of-function* experiments where overexpression of FZ in wild-type wing epithelial cells causes the adjacent cells to point their wing hairs away from the patch overexpressing FZ (Wu and Mlodzik, 2009). Overexpression of VANG brings about the opposite phenotype in which the neighbouring cells orient their wing cuticular structures toward the source of VANG overexpression. The double mutant clone of *fz,vang* shows the same phenotype as *fz* mutant clone, suggesting that FZ may be the primary cell-cell communication cue that regulate epithelium planar polarity (Wu and Mlodzik, 2008; Wu and Mlodzik, 2009). Interestingly, *fmi* mutant clones do not show any cell-autonomous polarity defects within the clones themselves but overexpression of FMI causes non-cell autonomous defects in the neighbouring wild-type cells (Strutt and

Strutt, 2008). The cells distal to the patch of cells overexpressing FMI point their hair toward the source of FMI, suggesting that FZ activity is reduced in the patch of cells overexpressing FMI (Strutt and Strutt, 2008).

The epithelia planar polarity is generated by asymmetric localizations of core PCP proteins. The sequence of localizations is best studied in the developing *Drosophila* wing. All core PCP proteins are initially localized around the apical-lateral cortex (Wu and Mlodzik, 2009). Once the apical polarity is established, the core PCP proteins form opposing complexes along the PD axis. PK and VANG are proximally localized, FZ, DGO and DSH are distally localized, and FMI is both proximally and distally localized; the VANG-PK and FZ-DGO-DSH complexes antagonize each other's activity (Fig. 3). (Goodrich and Strutt, 2011; Vladar et al., 2009). The distal FZ-DGO-DSH complex promotes the generation of hair at the distal end by activating downstream effectors such as RhoA and Rac1 (Gao and Chen, 2009). The proximal PK-VANG complex antagonizes the actin-formation activity of FZ-DGO-DSH by restricting the FZ-DGO-DSH localization to the distal side of the cell (Axelrod, 2009; Tissir and Goffinet, 2010). The antagonistic interaction of the two complexes in the epithelial cells leads to polarized polarity across the epithelium plane (Goodrich and Strutt, 2011; Strutt and Strutt, 2009; Wu and Mlodzik, 2009).

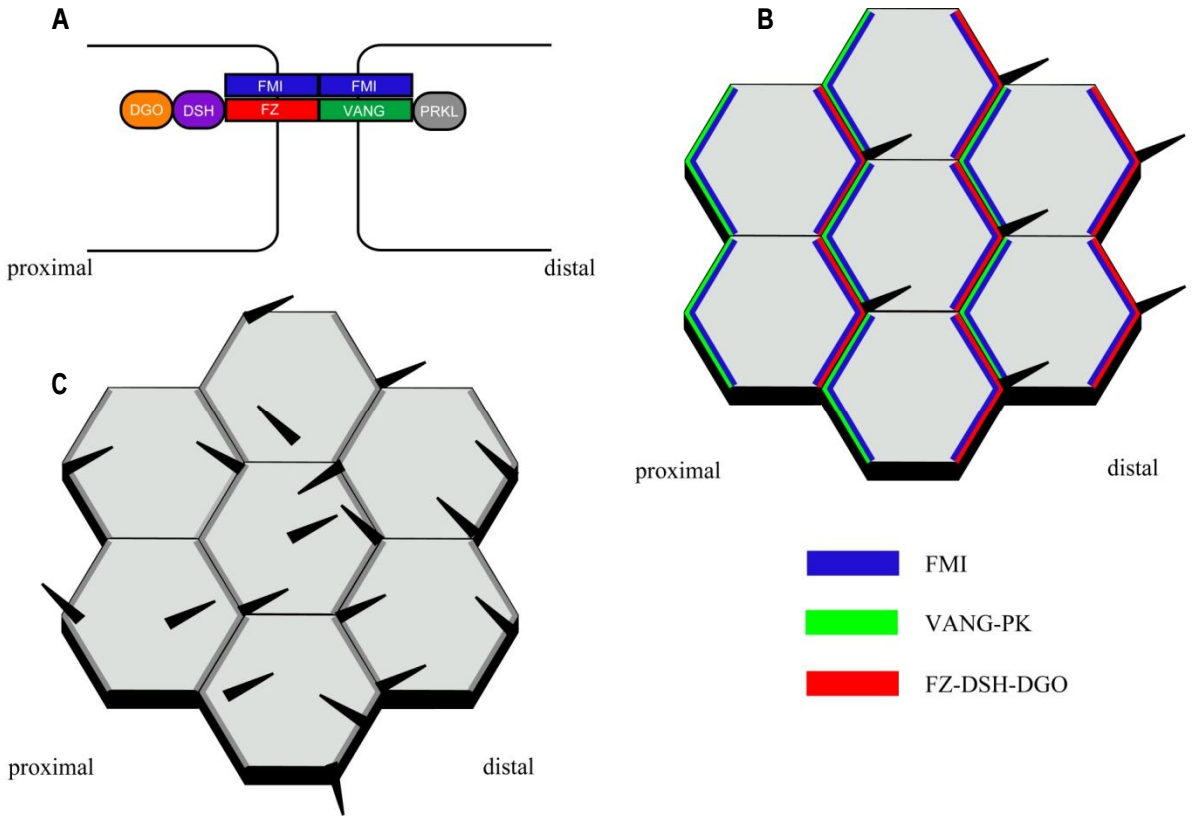

Figure 3. Asymmetric localizations of PCP proteins in *Drosophila* wing epithelium. (A) Schematic representation of apical-lateral localizations of PCP proteins. FMI homotypically interacts with another FMI localized on the adjacent membrane to form FMI-FMI complexes. FZ recruits and interacts with DGO and DSH to form a FZ-DSH-DGO complex on the distal side of the cell membrane. PK is recruited by VANG to the cell membrane and forms PK-VANG complexes on the proximal side of the cell membrane. Planar polarity is established by the asymmetric localization and antagonistic interaction between the FZ-DSH-DGO and VANG-PRKL complexes. (B) Localizations of core PCP proteins across the epithelial plane of *Drosophila* wild-type wing. The cuticular structures protrude from the distal side of the cell and point distally. (C) *Drosophila* PCP mutant wings randomly protrude and point cuticular structures in all directions.

1.3.1.2 Cell fate specification and orientation

The function of PCP signalling pathway is not limited to polarization in the epithelial plane. In the wing cells, PCP genes regulate the cytoskeleton organization and formation of actin-based hair structures. In contrast, PCP genes regulate cell fate specification of photoreceptor cells in the eye. The *Drosophila* eye is composed of a lattice of repeating units called ommatidia. Within each ommatidium reside eight asymmetrically arranged photoreceptor cells (Vladar et al., 2009). The precursors of these photoreceptor cells are initially arranged in a symmetrical fashion along the AP axis. The fate of the photoreceptor R3 and R4 must first be specified before the photoreceptor precursors break the initial symmetry by rotating 90˚ towards the dorsal-ventral equator midline (Goodrich and Strutt, 2011; Vladar et al., 2009). The opposing orientation of the ommatidia along the equator midline and the position of the R3 and R4 in each ommatidium create mirror-image symmetry in which the ommatidia on each side have opposite chirality. Such asymmetric organization subsequently leads to establishment of opposite chirality and orientation between the dorsal and ventral ommatidia (Vladar et al., 2009). In PCP mutants, the ommatidia show defects in the arrangement of the photoreceptors within each ommatidium and in the orientation of ommatidia with respect to the whole eye (Fig. 1B) (Jenny et al., 2003; Jenny et al., 2005; Strutt et al., 2002; Strutt and Strutt, 2008).

Like in the wing cells, PCP proteins are also asymmetrically localized in the photoreceptor cells. However, asymmetric localizations are only observed along the border of R3 and R4 precursor cells, not across the eye epithelium as in the wing (Jenny et al., 2003; Jenny et al., 2005); (Strutt and Strutt, 2009; Vladar et al., 2009). FZ, DSH,

VANG, and PK are initially localized symmetrically along the apical region of R3/R4 boundary, and they subsequently become asymmetrically localized prior to the ommatidia rotation (Vladar et al., 2009). The FZ-DGO-DSH complex is eventually localized on the polar side of R3; the VANG-PK complex is enriched on the equatorial side of R4; and FMI is localized to both sides of the R3/R4 boundary after the completion of ommatidia rotation (Vladar et al., 2009).

1.3.1.3 Oriented cell division

The polarized sensory bristles are derived from the ectodermal sensory organ precursor (SOP) cells through a series of asymmetric divisions. The SOP cells divide along the AP axis to generate anterior and posterior daughter cells. The PCP genes modulate the morphology and orientation of SOP mitotic spindles via interactions between the polarity complexes Dlg-Pins-Gα1 and Baz-Par6-aPKC (Bellaiche et al., 2004; Bellaiche et al., 2001). The VANG-PK complex localizes at the anterior cortex and recruits the Dlg-Pins-Gα1 complex to the anterior region. FZ-DSH complex localizes at the posterior cortex and regulates the localization of the cell-fate determinant Numb. In PCP mutants, SOP cells display randomized mitotic spindle orientations and loss in division asymmetry (Bellaiche et al., 2004; Bellaiche et al., 2001; Gomes et al., 2009).

1.3.1.4 The Fat-Dachsous pathway

The core PCP genes are not the only players regulating the planar polarity of *Drosophila* epithelial cells. Mutations in *fat* (*ft*) and *dachsous* (*ds*) also result in defects in polarity of the wing, eye, and abdominal bristles, and orientation of cell division in the wing and eye disc. Both *ft* and *ds* encode single-pass transmembrane proto-cadherins. *ft* and *ds* form a parallel signalling pathway and can influence the localization of the core

PCP proteins by affecting the polarization of microtubules by which FZ is transported (Harumoto et al., 2010; Shimada et al., 2006). The *ft-ds* pathway and the PCP pathway also share common effectors which are *in*, *fy*, and *frtz* (Goodrich and Strutt, 2011).

In the *Drosophila* wing epithelial cells, FT and DS are localized asymmetrically around the plasma membrane. The polarization of FT and DS is facilitated by the golgi-associated kinase *four-jointed* (*fj*). FJ phosphorylates both FT and DS; however, FJ-mediated phosphorylation of FT increases FT affinity for DS while phosphorylation of DS decreases DS affinity for FT (Brittle et al., 2010). FJ is expressed in graded gradient manner with highest level distally and lowest level proximally (Simon, 2004). FJ cell-autonomously restricts the activity of DS and promotes the activity of FT in the distal regions, resulting in stronger FT-DS interactions proximally (Simon et al., 2010). The graded FT-DS interactions lead to accumulation of the effector protein Dachs (Mao et al., 2006). Similarly, the gradient activity of FT-DS along the polar-equator axis also regulates the polarity of the *Drosophila* wing disc. It is important to note that the *wnt* homolog *wingless* (*wg*) localized at the dorsal and ventral edges of the disc functions to activate DS expression at the dorsal and ventral poles and to restrict the localization of FJ to the equatorial dorsal-ventral midline (Lim et al., 2005).

As loss of FT disrupts the localization of the core PCP proteins, it is speculated that the *ft-ds* pathway may provide gradient information to the core PCP proteins. A comparison between the gradient of FZ and FJ reveals that the two proteins share the same gradient pattern in the *Drosophila* eye disc as both FZ and FJ are localized at the highest concentration along the equatorial D/V pole of the disc (Wu and Mlodzik, 2009). However, in the *Drosophila* wing disc, the FZ gradient activity is opposite the FJ gradient

as FZ is localized at the highest level at the proximal region while FJ is expressed at the highest level at the distal region (Wu and Mlodzik, 2009). However, ubiquitously expressed DS in wing disc can rescue *ds* planar polarity defect, suggesting that *ft-ds* gradient activity is not essential in the regulation of planar polarity (Simon, 2004). Therefore, the gradient determining factor may not be FJ or DS. It is possible that FJ and DS may function to respond to a graded upstream cue. The relationship between the core PCP signalling pathway and the *ft-ds* pathway is largely unknown but they can be viewed as parallel pathways that possibly respond to a common graded upstream cue and can influence each other's activity via shared downstream inputs (Goodrich and Strutt, 2011).

1.3.2 PCP in vertebrates

The role of PCP signalling in regulating the polarity of epithelia is conserved in vertebrates. Many aspects of vertebrate development can be classified as manifestations of coordinated polarized cell movements along the plane of the epithelium. The polarization of sensory hair cells in the organ of Corti and in the vestibular epithelia, the orientation of hair follicles, and the convergent extension (CE) of mesodermal and neuroectodermal cells during gastrulation and neurulation, are all examples of vertebrate planar polarity (Goodrich and Strutt, 2011; Vladar et al., 2009) (Fig. 4A-J). In addition, genes in the PCP pathway also regulate the orientation of renal tube cells division and neurite guidance (Endo and Rubin, 2007; Okuda et al., 2007; Shafer et al., 2011; Tissir and Goffinet, 2010; Yates et al., 2010).

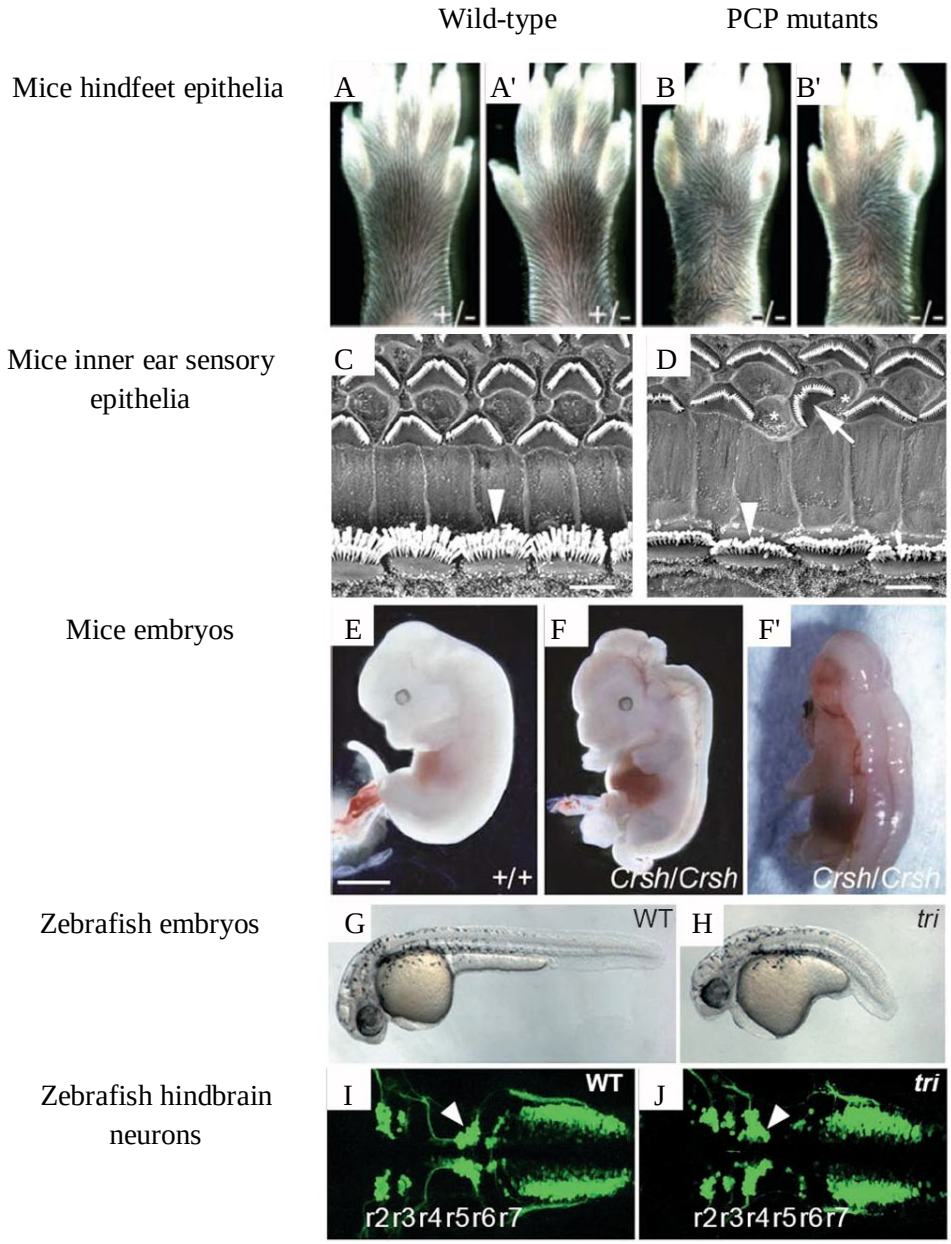

Figure 4. Vertebrate PCP defects. (A, A') wild-type mice hindfeet epithelia (B, B') Mice PCP mutants displaying defective epithelia polarity. (C) Wild-type mice inner ear sensory epithelia and (D) PCP mutants showing misoriented outer hair stereocilia bundles (arrow) and unaffected inner hair bundles (arrowheads). (E) Wild-type mice embryos and (F, F') PCP mutant embryos showing convergent extension defects leading to craniorachischisis. (G,I) Wild-type and (H.J) zebrafish PCP mutants. Zebrafish PCP mutants display defective convergent extension movements, resulting in shortened body axis (H) and neuronal migration defect (J). Arrowheads indicate hindbrain motor neurons migrating from rhombomere 4 to 5 in wild-type (I) and non-migrating neuron in PCP mutants (J). Images are taken with permission from Guo et al., 2004 (A,A',B,B'), Curtin et al., 2003 (C,D,E,F,F'), and Jessen et al., 2002 (G,H,I,J).

1.3.2.1 The polarization of hair follicle cells

Similar to *Drosophila* epithelium plane, mutations in the core PCP genes also disrupt the polarization of mice cuticular structures in both the epithelial cells of the skin and the auditory vestibular epithelia of the inner ear (Fig. 4B,B'). The structure and formation of vertebrate hair is vastly different from *Drosophila* wing hair. *Drosophila* wing hair is composed of a single actin-based extension from an epithelium cell whereas vertebrate hair is generated from a group of cells. In mice, hair formation begins at E14.5 when the placode cells bud from the overlying epithelium and invaginate into the underlying dermis (Devenport and Fuchs, 2008). The invaginating hair germ cells subsequently acquire polarity along the A/P axis as the anterior cells constrict basally and the posterior cells assume columnar shape. The difference in cell morphology along the A/P axis is maintained as the germ cells elongate and establish an anterior-oriented follicle. The protrusion of hair is correlated with the orientation of the follicle as actin filaments and keratin accumulate in the basally-constricted anterior cells (Wang and Nathans, 2007; Warchol and Montcouquiol, 2010).

Clues of PCP involvement in polarization vertebrate hair orientation comes from adult homozygous *fz6* mutants as the mutant mice display a swirly hair pattern reminiscence of PCP defects seen in *Drosophila* epithelial cells. FZ6 functions in establishing the orientation of hair follicles globally across the epithelium plane (Wang et al., 2006b). The mice homologs of *vang* and *fmi*, *vangl2* and *celsr1,* have only recently been implicated in regulating hair polarity as homozygous *vang* and *fmi* mutants are embryonic lethal (Curtin et al., 2003; Torban et al., 2008). Immunostainings of wild-type skin sections show that FZ6, VANGL2 and FMI are enriched at A/P membrane of the

basal epidermis cells and this enrichment is lost in *vang* and *fmi* mutants (Devenport and Fuchs, 2008). In addition, *vangl2* and *celsr1* anterior germ cells fail to constrict basally, resulting in randomly oriented hair follicles. It was also revealed that VANG acts non-cell autonomously as wild-type *vang*+/+ hair follicles surrounded by *vang*-/- epidermal cells display randomized orientation. Moreover, *vangl2* and *celsr1* function interdependently as mutations in *vangl2* or *celsr1* affect each other's A/P localization pattern (Devenport and Fuchs, 2008).

1.3.2.2 The polarization of inner ear sensory cells

PCP signalling also modulates the orientation of inner ear sensory cells in mice. The mammalian inner ear consists of two main types of sensory epithelia: vestibular and auditory. The vestibular system consists of the sensory epithelium in the ampulla of the semi-circular canals known as the crista and the otoliths organs utricle and saccule; the auditory system is made up of the organ of Corti (Wang and Nathans, 2007). Both types of sensory epithelia are highly polarized, projecting one single asymmetrically positioned cilum called kinocilium and bundles of apical microvilli-derived stereocilia. The longest stereocilia are positioned adjacent to the kinocilium and the shorter stereocilia are located away from the kinocilium with the shortest one situated furthest away. The stereocilia bundles and the kinocilium of the crista, utricle, and saccule are arranged in a circular shape. The stereocilia and the kinocilium of the organ of Corti are organized into a V-shaped structure (Wang and Nathans, 2007). Sensory hair cells in *vangl2, celsr1,* the *dsh* orthologs *dvl1;dvl2* and *fz* orthologs *fz3;fz6* double mutants all display incorrect polarity (Fig. 4D) (Greene et al., 1998; Kibar et al., 2001; Lu et al., 2004; Montcouquiol et al., 2003; Murdoch et al., 2001; Torban et al., 2004; Wang et al., 2005b; Wang et al., 2006b;

Wang et al., 2002). Additionally, WNTs may also play a role as overexpression of WNT7a in cultured explants of sensory epithelium from the organ of Corti disrupts orientation of the hair bundles (Dabdoub et al., 2003).

Interestingly, asymmetric localizations have been reported not only in the sensory hair cells but also in the surrounding support cells (Wang et al., 2006b). Mosaic studies reveal that FZ6 and PRKL2 localize at the opposite membrane of the hair cells and such asymmetric localizations are dependent on VANG. A recent study in chick embryo suggests that the localization of VANGL2 in the support cells may modulate the polarity of hair cells (Warchol and Montcouquiol, 2010).

1.3.2.3 Oriented cell movements

Although vertebrates and invertebrates undergo different processes of organogenesis, all animals share basic types of cell movements. One such movement that is central to animal development is convergent extension (CE). CE can be defined as the movement of cells in which they converge into one layer of tissue by intercalating between themselves (Benazeraf and Pourquie, 2008; Goodrich and Strutt, 2011; Ybot-Gonzalez et al., 2007). During gastrulation in vertebrates, embryos elongate and lengthen the mesoderm germ layers in order to prepare for organogenesis (Kuriyama and Mayor, 2008; Vervenne et al., 2008; Wada and Okamoto, 2009a). In zebrafish, the lateral and ventral mesoderm will give rise to blood and connective tissue precursors; the dorsal mesoderm will give rise to the notochord and somites (Dale et al., 2009; Solnica-Krezel, 2006; Tada and Kai, 2009). In avian, reptiles, and mammals, the mesodermal cells migrate through the primitive streak, a thickening of blastomeres caused by the ingression of the presumptive endodermal cells into the blastocoels, the fluid-filled cavity of the

embryo (Chuai and Weijer, 2009; Cooper et al., 2008). The migration order and the positions of mesodermal cells determine the anterior-posterior body axis. The first mesodermal cells to migrate through the primitive streak will be positioned anteriorly and will give rise to the head (Chuai and Weijer, 2009). The later migrating cells will develop into the notochord. The elongation of the mesodermal cells and the subsequent notochord is critical not only in the lengthening of the embryo's anterior-posterior (A/P) body axis, but also in defining the dorsal-ventral (D/V) body axis (Formstone and Mason, 2005b; Gilbert, 2000; Goodrich and Strutt, 2011; Jenny et al., 2003; Ybot-Gonzalez et al., 2007). The movements of CE are driven by the lamellipodia localized at the medio-lateral surface of the mesodermal cells. At the onset of neurulation, the dorsal mesoderm induces the overlying dorsal ectoderm to become neural ectoderm to form the neural plate (Gilbert, 2000). Invaginations within the neural plate create a groove in the middle of the neural plate (Gilbert, 2000). The dorsal regions of the U-shaped neural plate subsequently converge to fuse the neural plate, creating the neural tube (Gilbert, 2000; Kuriyama and Mayor, 2008).

Genes in the PCP signalling pathway have been shown to play a role in modulating convergent extension of both the mesoderm and neural ectoderm in vertebrates (Carreira-Barbosa et al., 2003; Ciruna et al., 2006; Goodrich and Strutt, 2011; Jessen et al., 2002; Montcouquiol et al., 2003; Vervenne et al., 2008; Wallingford and Harland, 2002; Wallingford et al., 2000; Wang et al., 2006a; Ybot-Gonzalez et al., 2007). Disruptions of core PCP genes along with vertebrate-specific genes such as the WNT ligands *wnt5* and *wnt7*, *scribbled* (*scrl*), *disc-large (dlg)* and *protein tyrosine kinase 7* (*ptk7*), and genes considered as PCP effectors in *Drosophila* such as *daam1*, *inturned (in)*

and *fuzzy (fy)* result in shortened body axis along the anterior-posterior axis and neural-tube closure failures (Fig. 4F,F',H). For example in mice, heterozygous *vang* ortholog *loop-tail* (*lp*)+/- mutants display a looped-tail phenotype whereas homozygous *lp-/-* mutants produce open-neural tube phenotype and are embryonic lethal (Kibar et al., 2001). Similarly, mutations in *celsr1* and *ptk7* bring about the same phenotypes (Curtin et al., 2003; Lu et al., 2004). The mice *dsh* and *fz* homologs function redundantly as only double mutants of the *dsh* homologs *dvl1;dvl2* (Wang et al., 2006a) and the *fz* homologs *fz3;fz6* (Wang et al., 2006b; Wang et al., 2002) display an open-neural tube phenotype and shortened body axis. In zebrafish, loss of *vang* homolog *vangl2* and *prickle* homolog *prickle1a (pk1a)*, the *wnt* ligand *wnt11* and the *fz* receptor *fz7* all lead to CE defects (Carreira-Barbosa et al., 2003; Ciruna et al., 2006; Gong et al., 2004; Jessen and Solnica-Krezel, 2004; Jessen et al., 2002; Park and Moon, 2002; Wada and Okamoto, 2009b; Yin et al., 2008). In *Xenopus*, lack of VANG and DSH in *vang* and *dsh* mutants and overexpression of VANG and DSH both lead to defective CE phenotypes (Park and Moon, 2002; Wallingford and Harland, 2002). The WNT ligands WNT5 and WNT11 also play a role in regulating CE of mesoderm cells; however, they do not display the same phenotypes. In both zebrafish and *Xenopus*, loss of *wnt5a* results in misalignment and randomized orientation of cells undergoing CE (Kilian et al., 2003; Wallingford et al., 2001). Migrating cells in zebrafish *wnt11a* mutants, on the other hand, display total loss of lamellipodia and limited mobility (Ulrich et al., 2003). WNT5a and WNT11 do not seem to function redundantly as WNT11 fails to rescue a morpholino-induced WNT5a knockdown phenotype (Schambony and Wedlich, 2007).

A recent study also demonstrates the role of *wnt5a* in establishing PCP in the chondrocytes of the developing limb bud. Gao and colleagues show that a gradient of WNT5a along the proximal-distal (P/D) axis of the limb bud mediates PCP signalling via its interaction with VANGL2 and ROR2. The graded activity of WNT5a phosphorylates VANGL2 in a dosage-dependent manner (Gao et al., 2011). Therefore, WNT5a gradient orients the planar epithelium by controlling activities of VANGL2 and subsequently create asymmetrically PCP signalling along the P/D axis in developing limb bud (Gao et al., 2011).

PCP signalling also controls vertebrate neuronal migration. In zebrafish, the hindbrain nVII facial motor neuron migrates caudally from rhombomere four to rhombomere six. The caudal-directed migration is impaired in *vang* ortholog *trilobite (tri), prickle* ortholog *(pk1b), frizzled* ortholog *fz3a (fz3a), flamingo* ortholog *celsr2,* and *scribble* ortholog *landlocked (llk)* (Fig. 4J) (Bingham et al., 2002; Carreira-Barbosa et al., 2003; Jessen and Solnica-Krezel, 2004; Jessen et al., 2002; Mapp et al., 2010). Genetic mosaic analysis shows that *vangl2, llk , fz3a,* and *celsr2* function non-cell autonomously in regulating the migration of the nVII neuron as wild-type nVII neurons aberrantly migrate radially in mutant embryos (Jessen et al., 2002; Wada et al., 2005; Wada et al., 2006). It is proposed that PCP signalling may function within the underlying neuroepithelium to prevent nVII from radially integrating into the neuroepithelium as the *fz3* nVII neuron fails to radially migrate and integrate into the neuroepithelium (Wada and Okamoto, 2009a). In contrast, wild-type nVII extends processes radially and integrate into the underlying PCP mutant neuroepithelium (Wada and Okamoto, 2009a). Furthermore, Pk appears to play a dual role during nVII migration. In a screen searching

for downstream effectors of zebrafish *hoxb1a*, *prickle1b* (*prk1b*) was identified and is proposed to act cell-autonomously as it is expressed in the migrating neurons. In contrast, *prk1a* is expressed mainly in the neuroepithelium outside of the migrating cells, suggesting that it acts non-cell autonomously (Carreira-Barbosa et al., 2003). It is speculated that *prk1b* and other cell-autonomously acting genes receive and interpret cues from the surrounding neuroepithelium as disruptions in both cell-autonomous and non-cell autonomous genes result in the same phenotype (Rohrschneider et al., 2007; Rohrschneider and Nance, 2009).

PCP signalling also regulates the migration of neural-fold derived neural crest cells. The neural crest cells initiate their migration by moving away from the neuroepithelium sheet and migrating toward each other. The direction of migration is changed as the cells form contact with each other and are directed to migrate away from the cell-cell contact point (Kuriyama and Mayor, 2008). The PCP proteins WNT11, FZ, and DSH have been found to localize at the contacting surface and possibly inhibit lamellipodia formation via DSH-activated RhoA (Shnitsar and Borchers, 2008; Sisson and Topczewski, 2009; Ulrich et al., 2003). The inhibition of lamellipodia along the contacting surface subsequently controls the direction of cell migration (Wada and Okamoto, 2009a).

It is not clear if PCP proteins in migrating cells are asymmetrically localized. Unlike in *Drosophila* where epithelial cells are imbedded within the epithelium plane, cells undergoing CE are in motion and do not establish permanent cell-cell contacts with neighbouring cells. PCP proteins may only localize transiently as cell-cell contacts are shifted from one movement to the next. Localizations of PCP proteins in migrating cells

have been most clearly described in zebrafish dorsal mesoderm where PK and DSH are localized in a punctate manner on the proximal and distal membrane, respectively. The localization of PRKL and DSH are dependent on *vang* ortholog *tri* and on three *wnt* genes: *wnt4, wnt5* (also known as *pipetail, ppt*), and *wnt11* (also known as *silblick, slb*) (Dale et al., 2009; Roszko et al., 2009; Tada and Kai, 2009; Vervenne et al., 2008; Yin et al., 2008). A study suggests that the localizations may be transient as DSH localization is not restricted to the distal region but is rather variable as cells change their shapes during CE (Yin et al., 2008).

1.3.2.4 Asymmetric cell division and ciliogenesis

PCP signalling has recently been implicated in the modulation of vertebrate kidney development. Mutations in *wnt9b*, *vangl2* and the vertebrate *dgo* homolog *inversin* (*invs*) result in Polycystic Kidney Disease (PKD) (McNeill, 2009; Yates et al., 2010). In PKD, multiple cysts ectopically protrude from the nephron and subsequently separate from the nephron and expand. The cysts proliferation is maintained by fluid obtained from the parental nephron (McNeill, 2009). PKD usually leads to kidney failure. It was recently demonstrated that during nephron development, the majority of the kidney epithelial tubule cells divide within 34 degrees of the tubule, resulting in elongation of the thinly-shaped tubules (Fischer et al., 2006). *wnt9b* ligand appears to modulate the tubule development via regulation of asymmetric cell division and CE of tubule cells. In wild-type E15 mice, the diameter of the tubules initially spans an average of 11 cells per tubule. At postnatal day 0, the tubule cells intercalate and the diameter of the tubules is subsequently reduced to an average of four cells per tubule. In *wnt9b* mutants, the tubule cells fail to intercalate and display misoriented cell division and

disorganized cell shapes (Karner et al., 2009). These findings suggest that PCP signalling plays a role in the generation of ectopic cysts in PKD.

Moreover, PCP signalling has been implicated in the generation of the non-motile cilia located on the surface of kidney tubule cells (McNeill, 2009). The clues that PCP is involved in ciliogenesis came from observations of mice and zebrafish lacking Bardet-Beidl Syndrome (BBS) proteins. BBS mutations in *bbs1, bbs4,* and *bbs6* bring about ciliogenesis defects, and misorientation of inner ear sensory hair bundles (Ross et al., 2005). Morpholino knockdown of *bbs4* also leads to CE failures (Ross et al., 2005). BBS4 is localized to the kinocilium and its cellular anchor on the basal body and is essential in ciliogenesis and vesicular transport (Nachury et al., 2007). *bbs4* has also been shown to genetically interact with *vangl2* (Ross et al., 2005). Another protein in the PCP pathway that is localized on the basal body of the kinocilium is Inversin. *inversin (invs)* is the vertebrate homolog of the *Drosophila diego (dgo)*. Mutations in *invs* also lead to PKD phenotype along with PCP defects (Simons et al., 2005). Biochemical studies reveal that INVS binds to DVL and accelerates its degradation in the cytoplasm (Simons et al., 2005).

1.3.2.5 PCP and vertebrate brain development

Many PCP genes are expressed in the vertebrate brain, suggesting that PCP signalling may also regulate multiple aspects of nervous system development other than neuronal migration. In developing mice brains, *frizzled3* (*fz3*) is expressed in the neuronal stem cells (NSC) in the ventricular zones and in post-mitotic neurons (Tissir and Goffinet, 2006). *vangl2* is expressed in NSC and in all neural cells. The *fmi* orthologs *celsr1* and *celsr3* are expressed in NSC and in post-mitotic neurons respectively (Tissir

and Goffinet, 2006). *celsr2*, on the other hand, is expressed in both NSC and post-mitotic neurons and continues to be expressed into adulthood (Tissir and Goffinet, 2006). The homologs of *dsh* are similarly expressed in both NSC and post-mitotic; DVL1 is expressed in NSC and post-mitotic neurons whereas DVL2 and DVL3 are respectively expressed in NSC and post-mitotic neurons (Tissir and Goffinet, 2006). The *pk* orthologs PK1 and PK2 are expressed in post-mitotic neurons in different regions of the brain and maintain expression into adulthood (Okuda et al., 2007; Tissir and Goffinet, 2006). The expressions of PCP genes can therefore be categorized into those that expressed in NSC and those expressed in post-mitotic neurons.

In addition to regulating epithelia cell polarity, oriented cell movements, and asymmetric cell divisions, recent findings have also uncovered a role for PCP genes in regulating axon guidance during brain wiring. Knockout studies in mice targeting *frizzled3 (fz3)* or *celsr3* produced planar polarity defects not only in the inner ear sensory hair bundles and in CE movements but also in axonal tract formation (Lyuksyutova et al., 2003; Zhou et al., 2008). In the mouse spinal cord, Fz3 plays a role in axonal path finding of dorsal neural tube interneurons. *In situ* hybridizations revealed that *fz3* mRNA is expressed in the interneurons and the wnt ligand WNT4 is expressed in the floor plate in a graded fashion with highest concentration at the anterior and lowest at the posterior (Lyuksyutova et al., 2003). In wild-type mice, the interneurons project commissural axons across the floor plate. Upon crossing the floor plate, the axons turn anteriorly towards the brain, following the gradient cue of WNT4 (Lyuksyutova et al., 2003). In *fz3* knockout mice, the commissural neurons randomly turn along AP axis or become arrested after crossing the floor plate (Lyuksyutova et al., 2003).

The activity of *celsr3* implicates a PCP-like pathway that modulates axonal development in vertebrate brain. *celsr3* functions in the forebrain in guiding the thalamocortical and corticothalamic axons. In wild-type mice, the thalamocortical neurons send out axons through the striatum towards the cortical region whereas the corticothalamic and subcerebral neurons extend axons through the striatum towards the thalamic region (Zhou et al., 2008). Thalamocortical, corticothalamic and subcerebral neurons are unable to project axons through the striatum when the activity of CELSR3 in the striatum is reduced (Zhou et al., 2008). Additionally, *celsr3* has been shown to act cell-autonomously. In wild-type mice, the olfactory neurons project commissural axons anteriorly and subsequently connect the olfactory bulbs. Knockout mice lacking celsr3 activity in the olfactory neurons failed to extend commissural axons anteriorly (Zhou et al., 2008). Therefore, *celsr3* is required cell-autonomously at least in olfactory neurons and functions non-cell autonomously in the striatum region to guide commissural axons through the region.

A recent finding has also revealed PCP-like signalling to play a role in guiding the axons of serotonergic (5-HT) and dopaminergic (mdDA) neurons along the AP axis of the brainstem. In wild-type mice, the ascending and descending serotonergic neurons respectively project their axons anteriorly and posteriorly. Similarly, the dopaminergic neurons send out their axons anteriorly. In *fz3, celsr3,* and *vangl2* mutants, the ascending serotonergic neurons aberrantly project their axons posteriorly or laterally and the descending neurons incorrectly send out axons anteriorly (Fenstermaker et al., 2010). The guidance of the dopaminergic axons is also affected in PCP mutant backgrounds as axons are randomly projected in dorsal and caudal directions (Fenstermaker et al., 2010).

Additionally, WNT5a is expressed in gradient in the brainstem and modulates axon guidance of the serotonergic and dopaminergic neurons. It was shown that FZ3 functions as a WNT receptor as cultured dopaminergic neurons from *fz3* mice failed to respond to the exogenous WNT5a and WNT5b cues. Moreover, PCP signalling also regulates the orientation of the cell body. Detailed analysis of wild-type serotonergic neurons demonstrates that wild-type descending 5-HT neurons initially orient the cell body laterally and gradually adjust the orientation along the AP axis during their mediolateral migration. The cell body is fully oriented along the AP axis upon completion of migration. Interestingly, the orientation of the cell body appears to be dependent on the direction of axon guidance. In *fz3* mutants, the aberrant anterior axon guidance of descending 5-HT neurons lead to eventual misorientation of the cell body, suggesting that the directions of projections dictate the orientation of the cell body (Fenstermaker et al., 2010). However, the establishment of orientation of initial neurites projections is still largely undetermined.

1.4 Molecular mechanisms of PCP signalling

1.4.1 The core PCP pathway

In *Drosophila* epithelial cells, the first step in PCP signalling is the recruitment of core PCP proteins toward the apical region of the cells. The PCP proteins symmetrically localize around the adherens junctions and subsequently rearrange their localizations to establish asymmetrical localizations (Goodrich and Strutt, 2011; Wu and Mlodzik, 2009). The formations of FZ/DSH/DGO on the distal side and VANG/PK on the proximal side polarize the epithelial cells along the PD axis. The distal FZ/DSH/DGO complex activates downstream effectors including the cytoskeleton regulator RAC1 to promote

actin-based trichrome formations and the proximal VANG/PK complex acts to inhibit the localization and activity of the FZ/DSH/DGO complex (Shafer et al., 2011; Strutt and Strutt, 2009). The mechanism of the generation of asymmetrical localizations is best studied in *Drosophila* wing epithelial cells. Cells within an epithelium plane must first initiate the apical recruitment and direct the opposing PCP complexes to distal and proximal ends. The asymmetrical localizations in epithelial cells must then establish polarization across the entire epithelium plane. However, the mechanisms that the cells use to polarize the epithelial plane are only coming to light.

It is speculated that the transmembrane proteins FZ, VANG, and FMI initiate the PCP signalling and therefore act upstream of the cytoplasmic DSH, DGO, and PRKL (Wu and Mlodzik, 2008). Mutations in *fz, vang*, and *fmi* affect the initial apical recruitment and eventual localizations of DSH, DGO, and PK (Axelrod, 2001; Bastock et al., 2003; Strutt et al., 2002; Strutt, 2001; Strutt, 2002; Tree et al., 2002) (Chen et al., 2008; Strutt and Strutt, 2007). The localizations of FZ, VANG, and FMI, on the other hand, are not affected in *dsh*, *dgo*, and *pk* mutants (Das et al., 2004). Non-cell autonomous activity of FZ and VANG observed in *Drosophila* epithelia cells further suggests that FZ and VANG play a role intercellularly in propagating the polarity message across the epithelium plane and DSH, DGO, and PK may only act as amplifying factors (Wu and Mlodzik, 2009). Based on the evidence that the trichromes of the wild-type cells distal to the *fz* mutant clones point toward the mutant clones, it is proposed that in *fz* mutant clones, VANG asymmetrical localization is lost due to the absence of the antagonizing FZ complex and instead localizes around the plasma membrane. Wild-type cells distal to the mutant clones respond to the incorrect VANG localization by localizing

FZ along the proximal side of the membrane, resulting in the non-cell autonomous phenotype (Goodrich and Strutt, 2011; Wu and Mlodzik, 2009). Similarly, *fz* overexpression clones also bring about disruption in planar polarity as wild-type cells proximal to the clones orient their hair structures away from the clones overexpressing FZ (Adler et al., 1997; Lawrence et al., 2004). The proximal wild-type cells interpret the excessive localization of FZ by localizing VANG to the distal membrane. The planar polarity of wild-type cells proximal to the *vang* mutant clones also point their hair away from the clones, suggesting that FZ is incorrectly localized around the plasma membrane and the proximal wild-type cells respond by altering the localization of VANG to the distal side (Lawrence et al., 2004; Taylor et al., 1998). The trichromes, therefore, point towards the region of low FZ activity. The non-cell autonomous phenotype of the double *fz, vang* mutant clones mimics the phenotype of *fz* clones, indicating that the surrounding wild-type cells interpret polarity cues from FZ activity (Wu and Mlodzik, 2008).

Symmetrically localized on both distal and proximal sides of the cells, FMI was originally thought of as an anchoring protein for the FZ and VANG complexes. However, recent studies suggested that FMI may play a key role in spreading polarization cues across the field of cells. FMI recruits both FZ and VANG to the apicolateral regions as loss of *fmi* affects FZ and VANG localizations and loss of *fz* and *vang* also affect FMI localization (Bastock et al., 2003; Das et al., 2004; Strutt, 2001). Moreover, clones overexpressing FMI results in non-cell autonomy phenotype similar to *fz* mutant clones (Strutt and Strutt, 2008). FMI is known to interact homophilically with FMI on the plasma membrane of the adjacent cell (Chen et al., 2008). It has been shown that FMI binds to FZ more readily than to VANG and forms FZ-FMI, and the interaction between

FMI and the FZ-FMI complex is more stable than interaction between FZ and the FZ-VANG complex (Strutt and Strutt, 2008). Therefore, FMI in *fz* mutant clones will preferentially bind to FZ-FMI in the distal wild-type cells, resulting in proximal recruitment of FZ-FMI. Similarly in clones overexpressing FMI, the excess FMI preferentially binds to FZ-FMI in the neighbouring wild-type cells and therefore recruit FZ-FMI complex to the proximal sides (Strutt and Strutt, 2009). Furthermore, FMI stabilize FZ and DSH as overexpression of FMI simultaneously increases the stability of FZ and DSH and decreases the stability of VANG and PK at the adherens junction (Strutt and Strutt, 2008). It is proposed that FMI functions to establish initial asymmetry by preferentially binding to FZ within the cell to generate FZ-FMI complexes (Strutt and Strutt, 2009). The FZ-FMI complex subsequently forms an intercellular complex with VANG-FMI in the adjacent cells. In addition, the FZ-FMI complex may aid in recruiting VANG to the proximal membrane of adjacent cells distal to the FZ-FMI complex as FZ has been shown to interact with VANG via its extracellular cysteine-rich domain (Wu and Mlodzik, 2008).

As mutations in *dgo, dsh*, and *pk* only disrupt the polarity of cells within the mutant cells, DGO, DSH, and PK likely function as downstream amplifying factors whose roles are to receive and interpret polarity cues initiated by FZ, VANG, and FMI (McNeill, 2010; Valentine and Collier, 2011; Wu and Mlodzik, 2009). DGO and DSH function intracellularly to exclude PK and inhibit its activity along the distal side. The inhibition of proximal signalling complex by the distal complex is supported by the finding that PRKL physically interacts with DSH and DGO (Jenny et al., 2005). Therefore, the interaction between FZ-FMI and VANG-FMI complexes leads to

recruitment of DSH and DGO to the distal edge and PRKL to the proximal edge. The mutual inhibition of the distal FZ-FMI-DSH-DGO and the proximal VANG-FMI-PRKL creates a feedback loop where the intracellular asymmetry is amplified (Strutt and Strutt, 2009; Tree et al., 2002; Wu and Mlodzik, 2009).

In *Drosophila*, it is currently not known whether there are long-range, global cues that align polarized epithelial cells along the P/D axis of the wing. Although the transmembrane proteins FZ, VANG, and FMI initiate the asymmetrical localization, the polarizing cues that act upstream are not determined. It is proposed that a gradient of FZ may be present across the plane of the epithelium. A graded level of FZ where the FZ activity is highest at the proximal end and lowest at the distal end of the epithelial plane may explain the findings that the hair structures point distally toward low source of FZ activity (Strutt and Strutt, 2009; Wu and Mlodzik, 2009). Wnts ligands have been shown to act as polarizing cues in vertebrate PCP, but their involvement in *Drosophila* PCP has not been demonstrated.

1.4.2 Effectors and outputs of the core PCP pathway

Genes that act downstream of the core PCP genes in regulating the polarity of hair structures in tissue or cell-specific manners are called effectors. Effectors that act in the *Drosophila* wing cells include *fuzzy* (*fy*), *inturned* (*in*), *fritz* (*frtz*), and *multiple hair wing* (*mwh*). These effector proteins co-localize with VANG and PRKL at the proximal end and contribute to actin destabilization proximally (Adler et al., 2004; Strutt and Warrington, 2008). In addition, the small GTPase RhoA and its effectors Drok and Rac function to regulate cytoskeleton dynamics as mutations in genes encoding these proteins lead to formation of multiple trichromes (Chung et al., 2007; Govek et al., 2005;

Schwamborn and Puschel, 2004; Winter et al., 2001; Yoshimura et al., 2006). Therefore, PCP signalling in *Drosophila* epithelium wing cells act to specify the initiation site and polarization of trichrome. In vertebrates, RhoA along with Rac1, Cdc42, Rok, and MyosinII modulate CE during gastrulation (Koster et al., 2010; Roszko et al., 2009; Tada and Kai, 2009) .

RATIONALE AND HYPOTHESIS

While much progress has been accomplished in probing mechanisms responsible for axon specification, little is known about the mechanisms regulating the initial break in neuronal symmetry that leads to the emergence and outgrowth of neurites (Tahirovic and Bradke, 2009). Indeed, the protrusion of filopodia is the first overt sign of polarity in which a neuron breaks morphological symmetry by generating filopodia that are polarized toward specified directions (Ou and Shen, 2010). We utilized the nematode *Caenorhabditis elegans* to explore the genetics and molecular basis of neurite outgrowth in individual neurons *in vivo*.

We used the *Pcat-1::green fluorescent protein (gfp)* transgene to examine the neuronal polarity of the VC4 and VC5 neurons, members of the VC motor neurons. The VC motor neurons are hermaphrodite specific bipolar motor neurons located along the ventral nerve cord. VC1-3, and VC6 extend neurites along the anterior-posterior (AP) axis; the vulva-flanking neurons VC4 and VC5 extend neurites around the vulva along the medial-lateral (ML) axis (Fig. 5). VC1-3, and VC6 are oriented along the anterior-posterior (AP) axis, sending anterior and posterior processes that form synaptic contacts among themselves, the HSN, and the vm2 vulva muscle arms (Waggoner et al., 1998). The vulva-flanking VC4 and VC5 neurons are oriented along the orthogonal left-right (L/R) axis, projecting processes around the vulva and forming synaptic contacts with the vm2 vulva muscles and the HSN (White et al., 1976). In vulvaless mutants, VC4 and VC5 project their processes along the A/P axis instead of the L/R axis, indicating that the vulva is a source of branching and guidance cues (Li and Chalfie, 1990). The processes of VC4 and VC5 are categorized as neurites as they possess both axonal and dendritic

properties (Schafer, 2005). The VC4 and VC5 neurons together with the HSN neuron make up the neuronal circuitry that regulates egg-laying behaviour (Schafer, 2005).

A forward genetic screen identified two alleles of *neurite defective* (*nde*) mutants. *nde-1(zy1)* and *(zy2)* mutants displayed ectopic axons along the AP axis and were mapped to a region on the nematode X chromosome. Through phenotype rescue injection of genomic PCR and plasmids containing *vang-1* cDNA, *nde-1(zy1)* and *nde-1(zy2)* were identified as the *C. elegans* homolog of *Van Gogh*, *vang-1*. *nde-1(zy10)*, an additional allele of *vang-1*, was isolated in forward EMS mutagenesis screens for *nde* mutants. *nde-1(zy1), (zy2),* and *(zy10)* mutants are subsequently referred to as alleles of *vang-1*. All three *vang-1* alleles both display highly penetrant tripolar phenotype. *vang-1* is a highly conserved core member of the non-canonical PCP signalling pathway. Orthologs of *vang-1* are found in *Drosophila* and vertebrates. *vang* orthologs are *Drosophila Van Gogh (vang)*, mice *looptail (lp)* and *vang-like2 (vangl-2),* zebrafish *trilobite (tri)*, *Xenopus Xvang*, and human *vang-like1 (vangl-1)* and *vang-like2 (vangl-2)*. *vang-1* is the only *C. elegans* homolog of *vang*. VANG-1 shares a high degree of sequence identity in the PDZ-binding domain with *Drosophila* and vertebrates and well-conserved similarity in the overall sequence (Fig. 6).

Consequently, mutations in *vang-1* activity could affect the activity of PCP signalling pathway. It has been shown that the activity of PCP signalling pathway in *Drosophila* is mediated by the asymmetric localizations of core PCP proteins. In *Drosophila* epithelia cells, Frizzled (FZ), Dishevelled (DSH), and Diego (DGO) are localized to the distal side of the cells and Van Gogh (VANG), Prickle (PRKL) are localized to the proximal side. Flamingo (FMI) is localized to both the distal and

proximal sides. Therefore, we hypothesize that VANG-1 asymmetrically localizes to the anterior and posterior side of VC4 and VC5 respectively to suppress neurite outgrowth along the anterior-posterior axis through its interaction with other PCP genes.

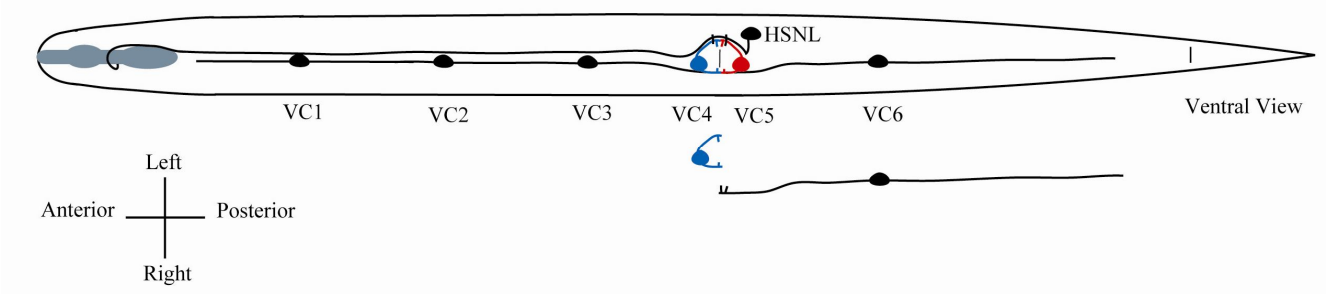

Figure 5. Schematic drawing of adult hermaphrodite *C. elegans* VC motor neurons. VC motor neurons are located along the ventral nerve cord and function to regulate egg-laying activity. VC1, VC2, VC3, and VC6 (darkly shaded circles) project neurites along the anterior-posterior body axis and form synaptic contacts among themselves, and the HSN neuron and the vulva muscles. In contrast, the vulva-flanking VC4 (blue shaded circle) and VC5 (red shaded circle) project neurites along the mediolateral left-right body axis around the vulva and form synaptic contacts with the HSN neuron and the vulva muscles. Anterior is left and left is up.

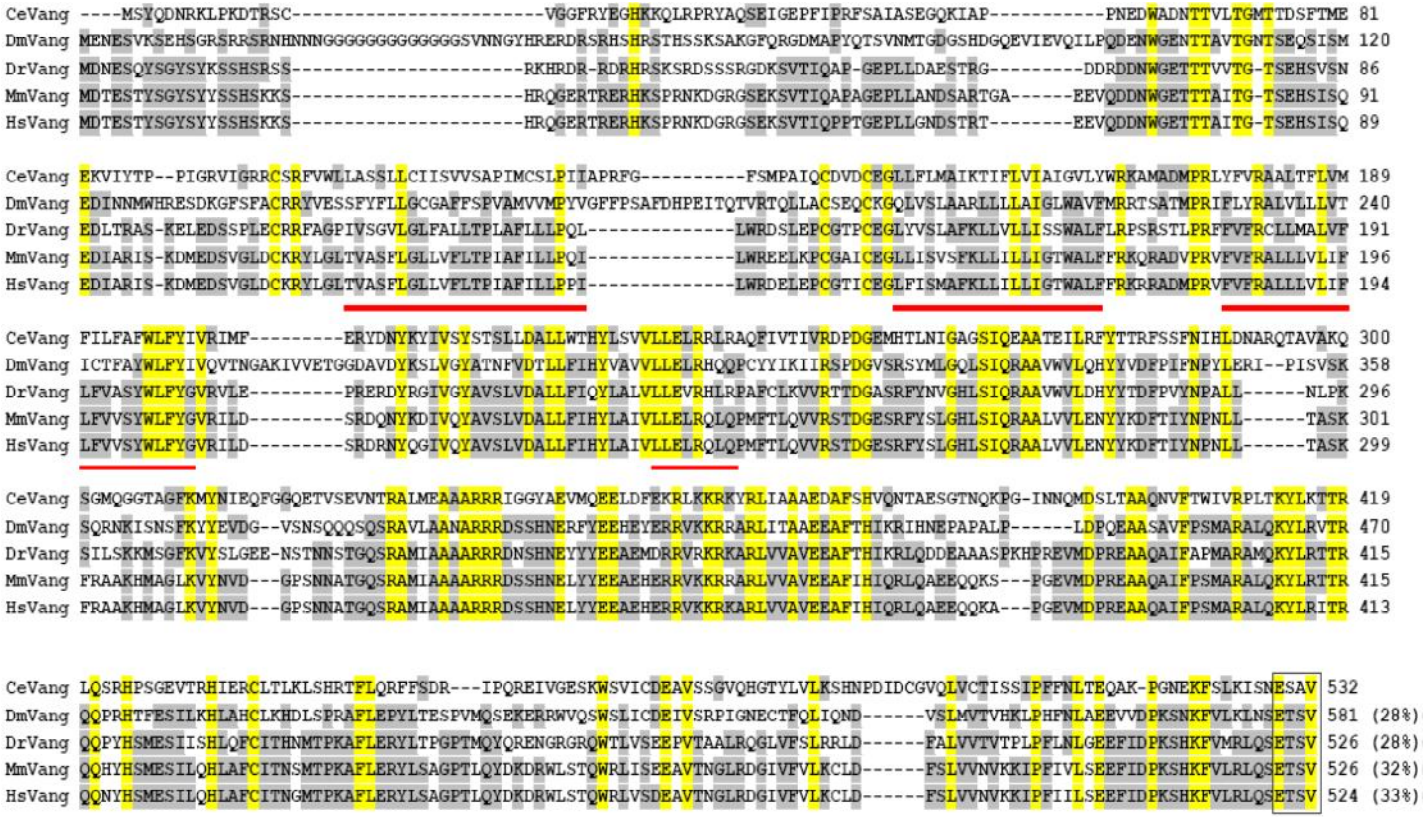

Figure 6. VANG-1 alignment. An alignment of the predicted amino acid sequence of *C. elegans* VANG-1 (Ce) and its *Drosophila* (Dm), zebrafish TRI (Dr), mice (Mm) and human VANGL-2 (Hs) homologs. Conserved and identical amino acids are indicated by grey and yellow shadings respectively. Amino acid sequences underlined in red are the transmembrane domains. The boxed amino acid sequences are the PDZ-binding domain. Percentages represent shared similarity between C. *elegans* VANG-1 and its homologs.

Objectives

I. To isolate and identify new genes involved in modulating VC4 and VC5 neurite outgrowth and orientation via forward mutagenesis genetic screens and candidate gene approach.

II. To characterize the function of *vang-1* in regulating neurite outgrowth and orientation.

III. To investigate the genetic interaction between *vang-1* and other genes in the PCP pathway.

IV. To identify the subcellular localizations of VANG-1, PRKL-1, and DSH-1.

Significance

The non-canonical *wnt*-PCP signalling pathway has been implicated in many aspects of both invertebrates and vertebrate development, from polarizing an epithelium plane to modulating cell movements. This work attempts to uncover novel roles for PCP signalling pathway in modulating neurite orientation and outgrowth. This thesis will provide new insights to the field of neuronal development and will reveal a novel role for PCP signalling in regulating neuronal polarity.

CHAPTER 2

MATERIALS AND METHODS

2.1 Strains

2.1.1 Strains used in the study

Methods for handling, culturing, and genetic manipulations were performed using standard techniques (Brenner, 1974). Worms were maintained on nematode growth medium (NGM) plates streaked with *Escherichia coli OP50* and experiments were performed at 20 ˚C unless otherwise specified. The *C. elegans* N2 Bristol strain was used as wild-type. *vang-1* alleles (*zy1*, *zy2*, and *zy10*) were outcrossed at least two times. The following alleles were obtained from the *C. elegans* Genetic Center unless specified:

Linkage Group (LG) I: *lin-44(n1792)*, *lin-17(n677)*, *mig-1(n687)*, *mom-5(or57)*

LG II: *dsh-1(ok1445),mig-5(tm2639)*

LG IV: *prkl-1(ok3182)*, *egl-20(n585)*

LG V: *fmi-1(tm306)*, *cfz-2(ok1201)*

LG X: *vang-1(tm1422)*, *bar-1(ga80)*

vang-1(zy2), dpy-20(e1282), cyIs4; Ex[8.5kb genomic DNA(5ng μl^{-1}); dpy-20(20ng μl^{-1})]

vang-1(tm1422), cyIs4; Ex[Pvang-1::vang-1(30ng μl^{-1}); Podr-1::dsRed(40ng μl^{-1})

vang-1(tm1422), cyIs4; Ex[Pcat-1::vang-1(30ng μl^{-1}); Podr-1::dsRed(40ng μl^{-1}]

vang-1(tm1422), dpy-20(e1282), cyIs4;Ex[Punc-4::vang-1(40ng μl^{-1}); dpy-20(20ng μ-l^{1})]

vang-1(tm1422), cyIs4; Ex[Punc-4::gfp::vang-1(40ng μl^{-1}); rol-6(35ng μl^{-1}]

vang-1(tm1422), cyIs4; Ex[Punc-4::vang-1(40ng μl^{-1}); Podr-1::dsRed (45ng μl^{-1})]

vang-1(tm1422), cyIs4; Ex[Pajm-1::gfp::vang-1(40ng μl^{-1}); Podr-1::dsRed(45ng μl^{-1})]

vang-1(tm1422), cyIs4; Ex[Punc-129::gfp::vang-1(40ng μl^{-1}); Podr-1::dsRed(45ng ul^{-1})]

vang-1(tm1422), cyIs4; Ex[Pvang-1::gfp::vang-1 (35ng μl^{-1}); Podr-1::dsRed (40ng μl^{-1}); rol-6 (35ng μl^{-1})]

N2; *Ex[Punc-4p::myr::gfp (30ng μl^{-1}); 35 Podr-1::dsRed(35ng μl^{-1}]*

N2; *Ex[Punc-4::gfp::vang-1 (40ng μl^{-1}); Podr-1::dsRed (35ng μl^{-1})*

N2; *Ex[Pvang-1::gfp (40ng μl^{-1}); Podr-1::dsRed (40ng μl^{-1}); lin-11::rfp(20ng μl^{-1})]*

N2; *Ex[Pvang-1::gfp::vang (5ng μl^{-1}); rol-6 (50ng μl^{-1}); Podr-1::dsRed (40ng μl^{-1})]*

N2; *Ex[Punc-4::lin-17::rfp (15ng μl^{-1}); Podr-1::dsRed (35ng μl^{-1})]*

cyIs4[Pcat-1::GFP]

cyIs3[Punc-4::GFP]

zyIs1[Plin-11::RFP]

Is[Punc-4::gfp::vang-1(5ng μl^{-1}); Podr-1::dsRed(45ng μl^{-1})]; Is[lin-11::rfp]

Is[Punc-4::gfp::prkl-1(5ng μl^{-1}); Podr-1::dsRed(45ng μl^{-1})]; Is[lin-11::rfp]

Is[Punc-4::dsh::gfp-1(5ng μl^{-1}); Podr-1::dsRed(45ng μl^{-1})]; Is[lin-11::rfp]

2.1.2 Transgenic animals

The extrachromosomal transgenic lines were generated following standard microinjection techniques (Mello and Fire, 1995; Mello et al., 1991). Young adult animals were suspended in halocarbon oil (Halocarbon Products, River Edge, NJ) placed on air-dried 3% agarose gel pad and were gently put onto the agarose injection pad. A Zeiss Axiovert microscope with 40X objective lens was used to visualize the animals. The injection needle was made using a Sutter P-97 microelectrode needle puller to pull

capillary glass needles. The pulled needle was loaded with pre-mixed injection solutions containing plasmids of interests at concentrations described below. An Eppendorf FemtoJet Microinjector injection system equipped with a micromanipulator was used to inject the plasmids of interest into the gonads of the nematode. After injection, a few drops of M9 solution were added on top of the Halocarbon oil to aid in dislodging the worms from the agarose pad. The worms were recovered and placed onto *E. coli*-seeded NGM plates and allowed to lay F1 progeny. The F1 populations were subsequently inspected for the presence of the coinjection markers. F1 animals that expressed the coinjection markers were individually placed onto *E. coli*-seeded plates to isolate for stable extrachromosomal array lines. The vector pSK was used as a carrier and *dpy-20, rol-6,* or *Podr-1::dsRed* were used as coinjection markers.

The integrated lines were generated using UVP CL-1000 crosslinker to induce breaks in the chromosome (Rieckher et al., 2009). Extrachromosomal arrays are subsequently integrated into the chromosomes during DNA repair processes. Adult transgenic worms carrying extrachromosomal arrays were placed in the UV crosslinker and exposed to UV at energy setting of 325mJ(x100)/cm^2 for 30 seconds. The healthy worms were transferred to a new plate to lay F1 progeny. Approximately 25 F1 animals were transferred to new *E. coli*-seeded plates. Several subsequent generations were screened for homozygous integrants. Once integrated lines have been obtained, integrants were outcrossed twice.

2.1.3 Genotyping

Strains were genotyped using polymerase chain reaction (PCR)-based approach to confirm mutations. Ten to fifteen adult worms were placed in 10 µl worm lysis solution (50mM KCl, 10mM Tris-HCl pH8.2, 2.5mM mgCl2, 0.45% nonidet P-40, 0.45% Tween 20, 0.01% gelatine, 60µg/ml proteinase K) in a PCR tube and were incubated in a PCR machine at 60˚C for 1 hour and then at 95˚C for 15 min. 1.5µl of the lysate was used as DNA template for PCR genotyping. The reaction mix for a 10µl PCR reaction is as followed: 1 µl of 10X PCR buffer, 1µl of 10pmol of each primer, 1µl of 2mM dinucleotide triphosphates, and 0.2µl of *Taq* DNA polymerase). The general PCR conditions were as follows: 94˚C for 1 min, followed by 35 cycles of 94˚C for 30 seconds (sec), 58˚C for 1 min, and 72˚C for 45 sec and 72˚C for 5 min at the end of the cycles. Restriction digest analysis of PCR product was used to confirm the genotype of the mutants. The restriction digest conditions for a 20µl reaction are as follows: 10µl of PCR product, 1 µl of restriction enzyme(s) of interest, and 2µl of restriction enzyme buffer at 37˚C or at a recommended temperature. The primers and restriction enzymes for strains used in the study are listed in Table 1.

2.2 EMS-induced mutagenesis screens

L4 wild-type worms were synchronized and grown on several plates. The plates were washed with approximately 2 ml of M9 buffer (22 mM KH_2PO_4, 22 mM Na_2HPO_4, 85 mM NaCl, and 1 mM $MgSO_4$). The M9 buffer containing the L4 worms was collected into a 15ml falcon tube and the tube was centrifuged at 1000 rpm for 30 seconds (sec) to collect the worms at the bottom of the tube. M9 was aspirated without disturbing the worm pellet at the bottom of the tube. The washing process was repeated. M9 containing

0.05M of ethyl methanesulfonate (EMS), a mutagen, was added to the tube and the worms are suspended in EMS mutagen solution for four hours at room temperature. EMS induces point mutations at the frequency of approximately $1x10^{-4}$ and $5x10^{-4}$ per mutagenized gamete (Anderson, 1995). The EMS solution was removed by washing the worms twice with M9 buffer. The mutagenized worms were then transferred to *E. coli*-seeded plates using sterilized glass Pasteur pipettes. The worms were allowed to recover for approximately 15 minutes (min) and were transferred to new *E. coli*-seeded NGM plates (Brenner, 1974). The mutagenized worms were classified as the P0 generation and allowed to lay eggs for two to three days. Five F1 L4-stage worms were subsequently placed on a new *E. coli*-seeded NGM plate to lay eggs. The plates containing young adult F2 worms were visually screened using a Zeiss AxioplanII microscope for neurite polarity defects.

2.3 Candidate gene approach

2.3.1 Construction of *vang-1* feeding RNAi vector

vang-1 cDNA was removed from an *Pvang-1::vang-1* using restriction enzymes KpnI and PstI and was subcloned into the RNAi vector L4440 (a RNAi-inducible plasmid, a gift from A. Fire). The *vang-1*-containing L4440 vector was transformed into *E. coli* HT115 (DE3) competent cells, an RNase III-deficient strain with IPTG-inducible T7 polymerase activity (Kamath and Ahringer, 2003), and cultured overnight in 100µg/ml ampicillin (AMP)-containing LB media at 37°C. The overnight culture was thinly seeded on NGM plates containing AMP and Isopropyl β-D-1-thiogalactopyranoside (IPTG). IPTG is needed to activate T7 polymerase. The activated T7 polymerase binds to the *vang-1* cDNA-flanking T7 sites on the L4440-feeding vector and subsequently generates

vang-1 dsRNA (Kamath et al., 2003; Kamath et al., 2001). The plates were allowed to dry overnight. RNA-sensitive strain *rrf-3, cyIs4* animals were transferred onto the plates and left for 36 hrs at 22°C to induce RNAi effect. *rrf-3* encodes for an RNA-directed RNA polymerase that inhibits somatic RNAi by suppressing RNAi-stimulated *rrf-1* and *ego-1*; therefore, mutation in *rrf-3* results in RNAi-sensitive worms (Johnson et al., 2005; Simmer et al., 2002). The worms were then individually placed onto NGM-AMP-IPTG plates seeded with dsRNA-containing bacteria and the progeny populations were scored for ectopic AP neurite phenotype.

2.3.2 Candidate gene RNAi knockdown

We obtained a library of approximately 11,500 *C. elegans* full-length open reading frame (ORF) cDNAs clones from Thermo Scientific Open Biosystem (Thermo Scientific, Huntsville, AL, USA). The ORF cDNAs were amplified from full length cDNA and cloned into pL4440-dest-RNAi feeding vector using high throughput-recombination cloning method. The cloned RNAi vectors were subsequently transformed into HT115(DE3) competent cells. The collection of ORF clones were provided in microtiter plates and are stored at -80°C. A total number of 46 genes were targeted for RNAi silencing analysis.

The clones were replicated by placing a sterilized pipette tip into contact with the well containing ORF of gene of interest. The pipette tips were incubated overnight at 37°C in 5ml of LB containing 100µg/ml of AMP. To generate sufficient amount bacteria needed to produce several experimental replicas, 50 µl of the overnight bacterial culture containing dsRNA was further added to 5ml of LB containing 100µg/ml of AMP and incubated at 37°C for 8 hours (hrs). The bacterial culture were directly seeded onto

NGM plates containing 1mM IPTG and 100µg/ml AMP and were left at room temperature overnight to allow induction of IPTG and the subsequent production of dsRNA to take place. Bacteria expressing dsRNA were fed to L4 RNAi-sensitive strains *eri-1,lin-15,cyIs4* to enhance RNAi-silencing effects in the nervous system. Mutation in *eri-1* disrupts an enzymatic function of a ribonuclease that is involved in degrading small interfering RNAs and thus suppressing the process of RNAi (Kennedy et al., 2004). Mutation in *lin-15* results in the expression of germ line-specific genes that make neurons susceptible to RNAi-silencing effects (Schmitz et al., 2007; Sieburth et al., 2005; Wang et al., 2005a). Five F1 worms were transferred to new HT115-seeded, IPTG-containing NGM plates and F2 adult progeny were inspected for RNAi effects. The nematodes were grown at room temperature.

2.4 Sequencing, rescue, and molecular cloning

Mutants displaying tripolar morphology were previously isolated and mapped to a region encoding for B0410.2, the *C. elegans* homolog of *vang-1*, on LGX (A. Colavita unpublished). Additionally, a 10kb genomic fragment containing the B0410.2 ORF's and upstream and downstream sequence was injected into the *vang-1(zy2)* mutants. The primers used to identify and rescue *zy1* and *zy2* mutations can be found in Table 1. Rescuing and expression constructs were made in a pSK plasmid vector (Stratagene, Santa Clara, CA, USA). The following plasmids were generated using standard cloning techniques (Fire et al., 1990):

Pvang-1::vang-1 and *gfp::vang-1*

vang-1 cDNA was amplified from yk211g1 (a gift from Y. Kohara) and subcloned into the pSK vector. A *vang-1* genomic fragment containing two introns and the 3'UTR

was amplified from genomic DNA, digested with SacI, and cloned into the *vang-1* cDNA-containing pSK vector. A 3kb sequence upstream of the start codon was amplified from genomic DNA, digested with restriction enzymes PstI and SalI and inserted upstream of the atg start codon. GFP cassette was amplified from pPD95.77 and cloned upstream of the ATG start codon of *vang-1* to generate *GFP::vang-1*.

Pcat-1::gfp::vang-1

The promoter region of *cat-1* was amplified from an existing *Pcat-1::yfp* plasmid and cloned upstream of *vang-1* cDNA to generate *Pcat-1::vang-1*. A GFP cassette from PD95.77 was PCR amplified, digested with BamHI, and subcloned into the BamHI site of *Pcat-1::vang-1* to generate *Pcat-1::gfp::vang-1*.

Punc-4p::gfp::vang-1

The promoter region of *unc-4* was removed from construct *Punc-4::bam-1* by restriction digest with Pst and BamHI and subcloned immediately upstream of *vang-1* cDNA. A GFP cassette from PD95.77 was PCR amplified, digested by BamHI, and subcloned into the BamHI site of *Punc-4::vang-1* to generate *Punc-4::gfp::vang-1*.

Pajm-1::gfp::vang-1

The promoter region of *ajm-1* was amplified from an existing *Pajm-1*-containing plasmid, digested by PstI and XbaI, and subcloned upstream of *gfp::vang-1* to generate *Pajm-1::gfp::vang-1*.

Punc-129::gfp::vang-1

The promoter region of *unc-129* was amplified from genomic DNA, digested with PstI and XbaI, and subcloned upstream of *gfp::vang-1* to generate *Punc-129::gfp::vang-1*.

Punc-4::myr::gfp

myr motif was tagged was amplified from pPD95.77. The *myr::gfp* PCR product was digested with AgeI and XhoI and cloned into the pPD95.77 vector. *Punc-4* was removed from *Punc-4::vang-1* using restriction enzymes PstI and XbaI and cloned into the *myr::gfp* vector to generate *Punc-4::myr::gfp*.

Pvang-1::gfp

A 3kb upstream of the start codon was amplified from genomic DNA, digested with SalI and PstI and subcloned into gfp-containing pSK vector upstream of gfp cassette.

Pvang-1::gfp::vang-1

The construct was prepared via yeast homologous recombination using the Gene CATCHR cloning procedure (Sassi et al., 2005). An approximately 9.9 kb genomic fragment containing *vang-1* exon and intron genomic regions was amplified and combined from the YAC Y7110. A GFP cassette was inserted upstream of the ATG start codons of *vang-1* to create *Pvang-1::gfp::vang-1* translational fusion.

The generated plasmid constructs were transformed using the following procedures. 2µl of plasmids was added to an eppendorf tube containing 40µl of DH5α competent cells and placed on ice for 30 min. The constructs and the competent cells were heat-shocked at 42˚C for 45 sec and were immediately placed on ice for 2 min. 1 ml of Luria-Bertani (LB) solution (5g of yeast extract, 10g of tryptone, 10g of NaCl per

L) was added to the eppendorf tube and the tube was incubated at 37˚C in a shaking incubator for 1 hour (hr). QIAprep Spin Miniprep Kit was used to extract DNA plasmids from the transformed bacteria (Qiagen Inc., Toronto, ON). Restriction enzyme analysis was used to assess the sequence of the extracted DNA plasmids.

2.5 Fluorescence microscopy and confocal imaging

Worms were placed on glass slide mounted with a 2% agarose pad and immobilized using 10 mM levamisole (Sigma) in M9 solution. Epifluorescence images were taken using Zeiss AxioplanII with a 63X objective lens. Stacks of VC4 and VC5 neurons images with an interval of 0.250 μM between each stack were collapsed into a single image using AxioVision software version 4.8. A Zeiss LSM 510 confocal microscope was used to obtain images of fluorescently tagged fusion proteins. Stacks of VC neurons images taken under a 63X lens were collapsed into a single image. Worms were staged with respect to developmental stages as described (Kenyon, 1988; Riddle et al., 1997). L4-stage and adult animals were used for imaging and quantification, unless otherwise specified.

2.6 Phenotypic analysis

2.6.1 VC4 and VC5 neurite polarity

Animals expressing *cyIs4 [Pcat-1::gfp]* and *cyIs3 [Punc-4::gfp]* were scored for VC4 and VC5 neurite polarity defects. In adult worms, an anterior-posterior directed neurite was scored as an ectopic neurite if the length of the neurite is equal to or greater than the length of the mediolateral directed neurite. In L4 animals, for an anterior-posterior directed neurite to be quantified as an ectopic neurite, the length of neurite had

to be equal to or greater than the length of the soma cell body. Neurons with two neurites projected along LR axis and a single neurite extended along the AP axis is classified as having tripolar morphology. Neurons with two neurites projected along the AP axis were classified as bipolar and neurons projected a single axon along the AP axis were classified as unipolar.

2.6.2 DA, DB, VD, and DD motor neurons

Animals expressing *Punc-129::gfp* and *Punc-25::gfp* were scored for DA, DB and VD, DD commissural guidance defects, respectively. The dorsally guided trajectories of commissural axons were scored as defective if the axons failed to reach the dorsal nerve cord or are misguided anteriorly or posteriorly prior to reaching the dorsal nerve cord. An animal displaying one or more misrouted axons was counted as n of one.

2.6.3 HSN and the mechanosensory AVM, ALM, PLM, and AVM neurons

Animals expressing *Punc-86::gfp* and *Pmec-4::gfp* were scored for HSN and AVM, ALM, PLM, and AVM neurons axon guidance and outgrowth defects, respectively. The neurons were scored as defective if the anteriorly guided axons are prematurely terminated prior to reaching the pharyngeal bulb, misguided, displayed ectopic neurites or reversal in neuronal polarity. An animal showing one or more defective axons was considered as n of one.

2.7 Quantification of sub-cellular localization

For quantitative analysis of VANG-1::GFP, PRKL-1::GFP, and DSH-1::GFP localization, stacks of VC4 neuron images with an interval of 0.250 μM between each image were collapsed into a single image using AxioVision software version 4.8. To

calculate the posterior/anterior intensity ratio, AxioVision measurement tool was used to draw a vertical line along the LR axis across the middle of the cell body to divide the perimeter of the cell into two equal posterior and anterior halves. Line-scan intensity plots were drawn clockwise around the cell periphery to measure the intensity of GFP signal of the pixels. The average of GFP intensity readings of the posterior and anterior halves was taken and the posterior/anterior ratio was calculated as the average intensity readings of the posterior half of the perimeter divided by the average intensity readings of the anterior half.

.

2.8 Statistical Analysis.

Data are reported as mean ± standard error of the mean of at least three independent experiments, unless specified. n indicates total observations. Statistical analysis was carried out by ANOVA using PRISM (Version 5.0 GraphPad, San Diego, CA, USA) software. Differences between strains were determined by the Bonferroni's *post hoc* test. P values of $P<0.05$ were considered significant.

CHAPTER 3

RESULTS

3.1 *nde-1* shows VC4 and VC5 polarity defects

cyIs4[Pcat-1::gfp] was used to visualize VC4 and VC5 neurons. VC4/5 extend two processes along the left-right (L/R) axis (Fig. 7A). Two alleles of ***n****eurite-****de****fective (nde)* mutants were identified serendipitously in a screen for VC4/5 neurite branching defects by A. Colavita and M. Tessier-Lavigne (unpublished results). *nde-1(zy1)* and *nde-1(zy2)* mutants displayed highly penetrant VC4 and VC5 tripolar neurite polarity defects possessing ectopic neurites that extend along the anterior-posterior (A/P) axis in addition to the normal left-right (L/R) projected neurites (Fig. 7B,C). The length of the A/P ectopic neurites is equal to the length of the normally projected L/R neurites. *nde-1* mutants also showed low penetrance of A/P directed bipolar phenotypes in which VC4/5 neurons project two neurites along the A/P axis (Fig. 7C). In addition, a mild monopolar phenotype in which VC4 and VC5 neurons project one single A/P directed neurite was also detected in *nde-1* mutants (Fig. 7D). With the exception of these phenotypes, no other VC4 and VC5 neurite abnormalities such as axon guidance or branching defects were observed.

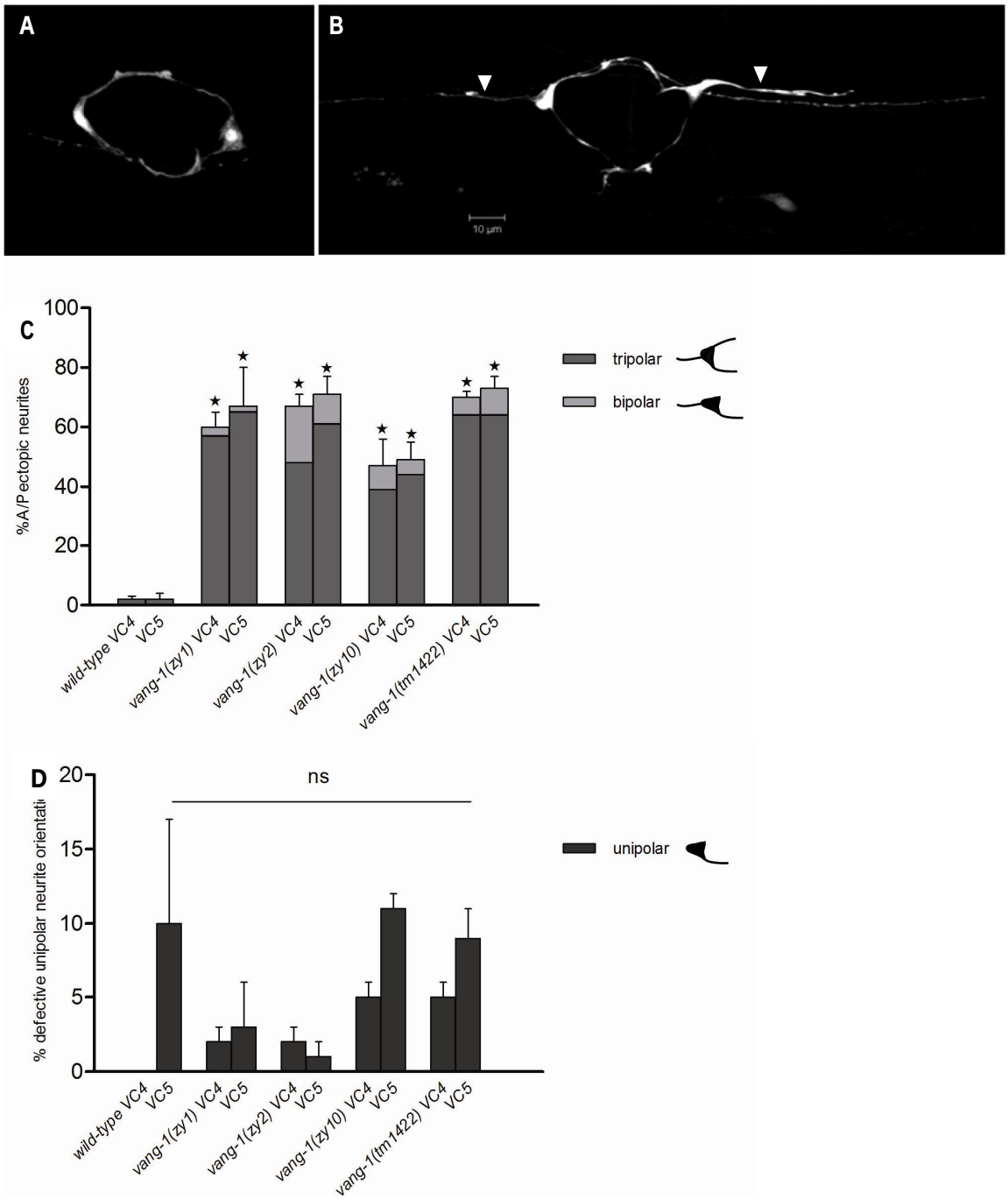

Figure 7. Penetrance of *vang-1(zy1), (zy2), (zy10),* and *(tm1422)* alleles. Ventral view of (A) wild-type VC4 and VC5 expressing *cyIs4 (Pcat-1::gfp)* and (B) *vang-1(tm1422) cyIs4* mutant. *vang-1(tm1422)* displays ectopic neurites oriented along the anterior-posterior (A/P) axis (arrowheads). (C) *vang-1* ectopic A/P neurites are highly penetrant in both VC4 and VC5. (D) *vang-1* mutants also display a statistically non-significant unipolar phenotype compared to wild-type. The representative drawings are of VC4 in ventral view. n >90 in all strains, error bars represent standard error of the mean, ns indicates non-significant statistically, *$p<0.05$ compared to wild-type using analysis of variance and Bonferroni's multiple comparison post hoc test.

3.2 *nde-1* encodes the worm orthologue of *Van Gogh*

Mutations in *nde-1(zy1)* and *(zy2)* were mapped to a region between *unc-2* and *lin-18* near the gene B0410.2/*vang-1*, the *C. elegans* homolog of *Van Gogh*, on chromosome X. Since *Van Gogh* regulates polarity in *Drosophila* epithelial cells, *vang-1* appeared as a likely candidate to encode for *nde-1(zy1)* and *(zy2)*. To confirm the identity of *nde-1* mutants, a 10kb PCR fragment encoding *vang-1* was injected into the mutants to test the PCR fragments' rescuing ability. The PCR fragment rescued the *nde-1(zy1)* and *nde-1(zy2)* ectopic neurite phenotypes, indicating that the *nde-1* ectopic A/P directed neurite phenotype is caused by mutations within the *vang-1* gene sequence (Fig. 8). Plasmids containing 3kb upstream of the *vang-1* atg start codon and the *vang-1* cDNA also rescued *nde-1* aberrant A/P directed ectopic neurites, confirming *nde-1(zy1)* and *(zy2)* as alleles of *vang-1* (Fig. 9). *nde-1* was consequently renamed *vang-1*.

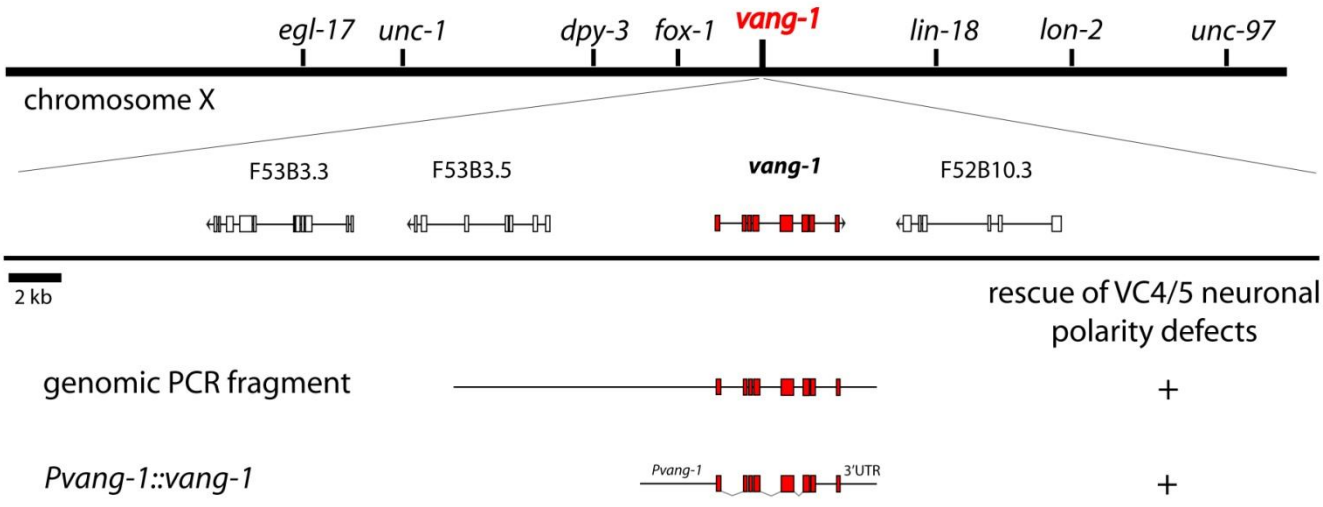

Figure 8. Positional cloning of *vang-1*. Genomic region on chromosome X containing the *vang-1* gene. PCR fragment containing *vang-1* gene and *Pvang-1::vang-1* containing *vang-1* cDNA rescued VC4/5 neuronal polarity defects.

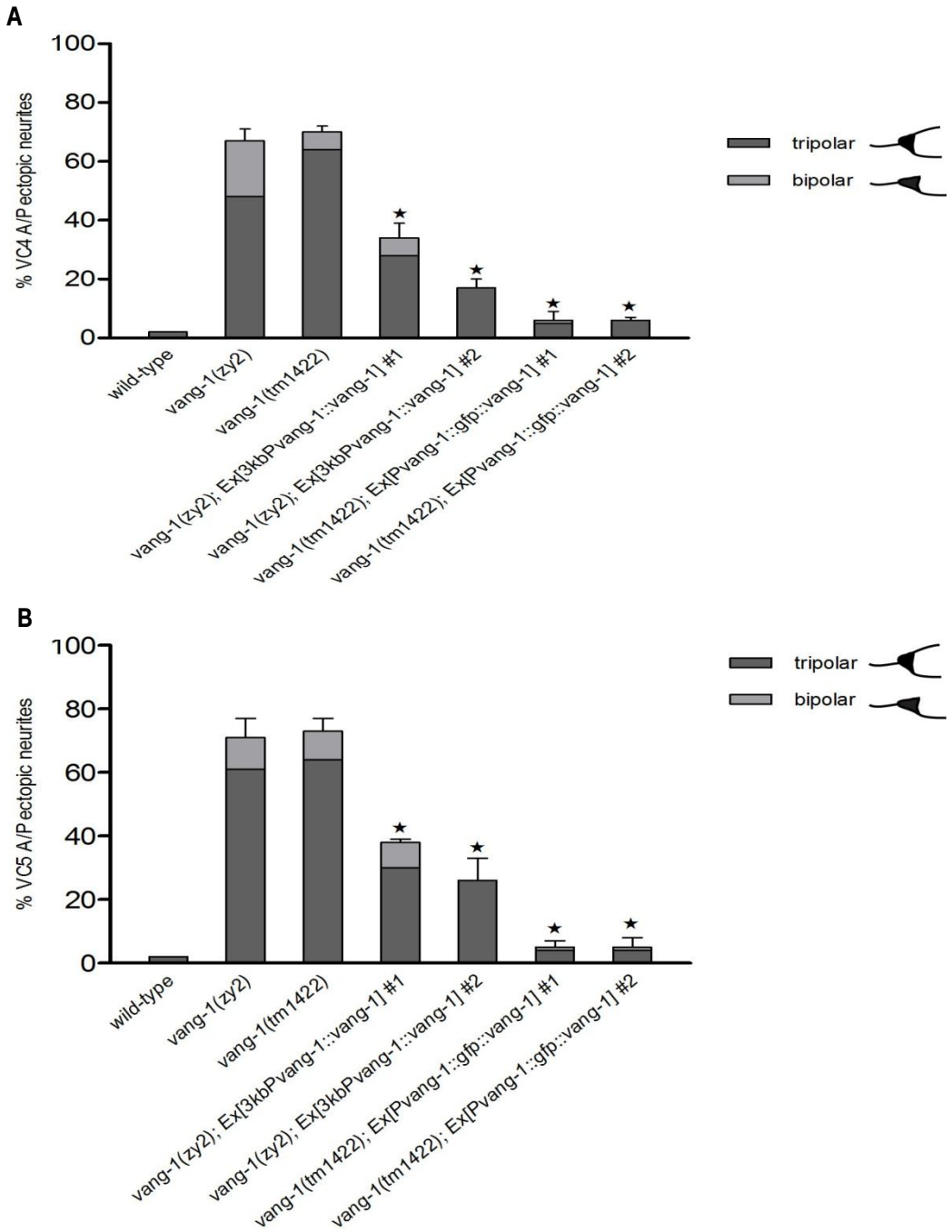

Figure 9. Rescue of *vang-1* Anterior/Posterior ectopic neurites. Phenotype of VC4 (A) and VC5 (B) *vang-1(zy2), vang-1(tm1422), vang-1(zy2)* carrying *Pvang-1::vang-1*, and *vang-1(tm1422)* expressing *Pvang-1::gfp::vang-1*. Two independent extra-chromosomal lines of *Pvang-1::vang-1* and *Pvang-1::gfp::vang-1* are shown. Dark grey indicates tripolar morphology where VC4 and VC5 display two neurites projected along the left-right axis and an ectopic neurite projected along the anterior-posterior axis. Light grey indicates a bipolar morphology in which VC4 and VC5 project two neurites along the anterior-posterior axis. n>50 in all strains and lines, error bars indicate standard error of the mean, *$p<0.05$ compared to *vang-1(zy2)* and *vang-1(tm1422)* using analysis of variance and Bonferroni's multiple comparison post hoc test.

vang-1 is the sole *C. elegans* homolog of *Van Gogh*, a core member of the PCP signalling pathway. *C. elegans* VANG-1 shares 28, 28, and 32% identity with *Drosophila*, zebrafish, and mouse VANG orthologs respectively, and 33% similarity to human VANG (Fig. 6). *vang-1* encodes a predicted four-pass transmembrane protein of 532 amino acids containing a highly conserved C-terminus PDZ-binding domain (50% identity to *Drosophila*, zebrafish, mice, and human) (Fig. 6). DNA sequencing of *vang-1(zy1)* and *vang-1(zy2)* mutants revealed molecular lesions underlying the neuronal polarity defects. *vang-1(zy1)* carries a point mutation in the splice acceptor site of the first intron of the gene; *vang-1(zy2)* has a point mutation in the sixth exon of the gene that substitutes G to A in the codon for tryptophane 406 and is predicted to result in a premature stop codon that possibly generates a truncated protein lacking the C-terminal PDZ-domain-binding motif (Fig. 10). *vang-1(zy10)* is a point mutation in the splice acceptor site of the second intron (Fig. 10). *vang-1(tm1422)* is a deletion allele lacking the second through fourth exon (Fig. 10), and was provided by S. Mitani from Tokyo Women's University. *vang-1(tm1422)* mutants also display VC4/5 A/P directed ectopic neurites with a similar level of penetrance (VC4 69 ± 2%) as *vang-1(zy2)* (VC4 66 ± 4%) (Fig. 7). *vang-1(tm1422)* is predicted to produce a truncated VANG-1 not containing the first three transmembrane domains.

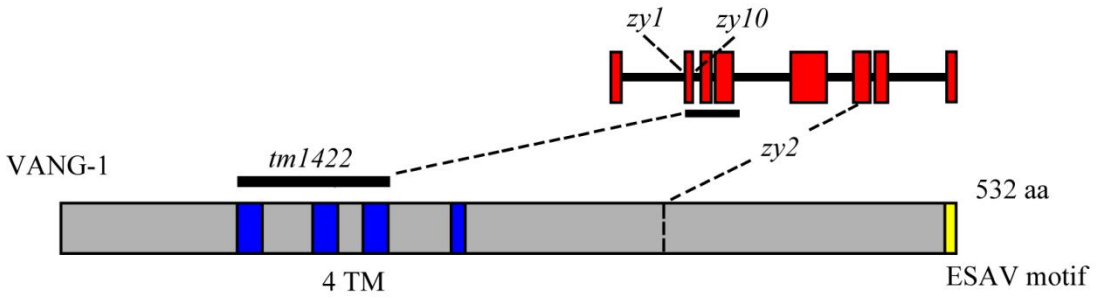

Figure 10. VANG-1 structure and mutations. *vang-1(zy1)* and *vang-1(zy10)* are point mutations in the non-coding intron regions; *vang-1(zy2)* is a point mutation in the coding exon 6 region that replaces W406 with a stop codon. *vang-1(tm1422)* is a deletion allele that is predicted to encode a truncated protein lacking the first three transmembrane domains.

3.3 VANG-1 is involved in maintaining neuronal polarity

To gain insight into when VC4 and VC5 polarity defects are first observed, we examined *vang-1(tm1422)* mutants from the early L4 stage to adulthood. The reporter *cyIs3 (Punc-4::gfp)* was used to visualize VC4 and VC5 neurons in early L4 as *cyIs4 (Pcat-1::gfp)* is not expressed until late L4. We observed an increase in A/P directed neurites in adult *vang-1(tm1422)* worms compared to early L4 animals (Fig. 11). Additionally, stage-specific observations of individual *vang-1(tm1422)* mutants at early L4 revealed that the same animals displayed higher penetrance of ectopic A/P directed neurites once the animals reached adulthood (Fig. 12). These observations demonstrate that *vang-1* is needed to maintain correct neurite polarization.

3.4 Mutations in *vang-1* do not affect other axonal outgrowth and orientation of other classes of neurons

To determine whether mutations in *vang-1* affect the development of other neurons, various neuronal GFP reporter lines were crossed into *vang-1(tm1422)* mutants to probe for neurite outgrowth and guidance defects. The ventral cord DA, DB, DD, and VD motor neurons and the egg-laying regulating HSN motor neurons were examined for dorsal/ventral (D/V) guidance defects. The mechanosensory ALM, AVM, PLM, and PVM neurons were examined for anterior/posterior (A/P) guidance defects (Fig. 13). *vang-1(tm1422)* mutants expressing P*unc-129::gfp* did not show any defects in the dorsally-directed guidance of the DA and DB commissures. *vang-1(tm1422)* mutants expressing P*unc-25::gfp* did not show neurite outgrowth and guidance defects in the D/V-directed outgrowth of DD and VD axons. The anterior-directed axon outgrowths of the mechanosensory neurons ALM, AVM, PLM, and PVM were not disrupted in *vang-*

1(tm1422) carrying *Pmec-4::gfp*. The neurite outgrowth and guidance of the unipolar ventrally-directed HSN neurons were also not affected in *vang-1(tm1422)* expressing *Punc-86::gfp*. To investigate the neuronal polarity of other members of VC motor neurons, *Pida-1::gfp*, a reporter transgene marking all VC motor neurons, was crossed into *vang-1(tm1422)* mutants. *vang-1(tm1422),Pida-1::gfp,* showed that VC1-3 and VC6 neurons were not affected by mutations in the *vang-1* gene (Fig. 13). Similar to *vang-1(zy1), vang-1(zy2),* and *vang-1(tm1422)* expressing *cyIs4* (*Pcat-1::gfp*), *vang-1(tm1422),Pida-1::gfp* also showed VC4/5 A/P-directed ectopic neurite phenotype.

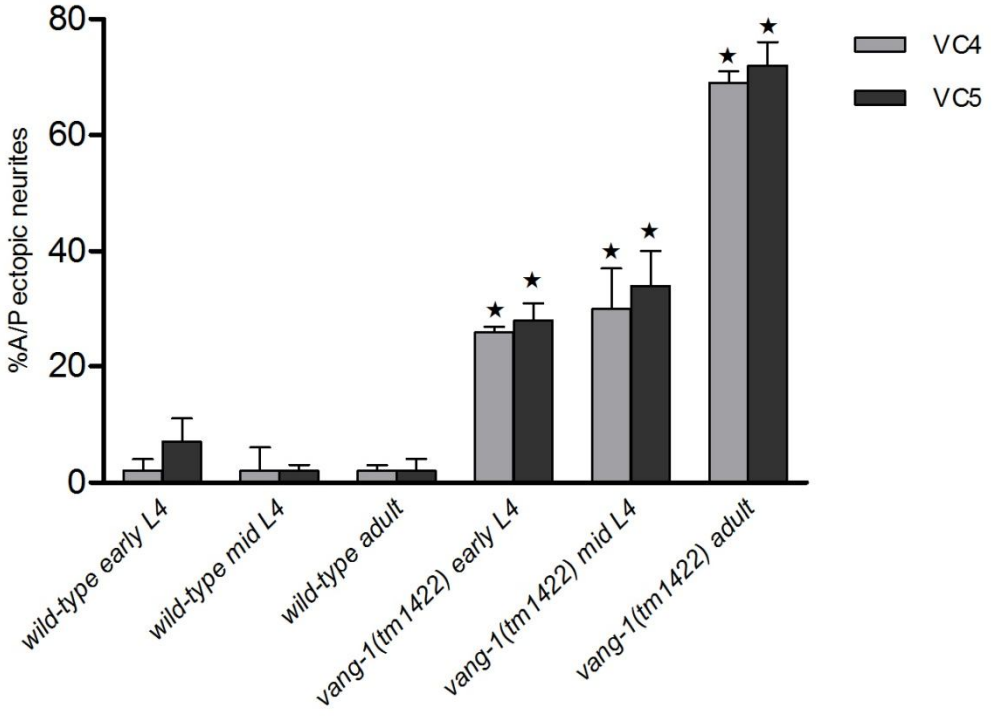

Figure 11. Penetrance of A/P ectopic neurites in early L4, mid L4, and adult *vang-1(tm1422)* mutants. Animals in the early L4 stage were visualized using the *cyIs3 (Punc-4::gfp)* reporter as *cyIs4 (Pcat-1::gfp)* is active from mid L4 stage and onward. Mid L4 and adult animals were scored using *cyIs4* instead of *cyIs3* as neurites from VC1, VC2, VC3, and VC6 and the GFP expression in the ventral nerve cord obscured clear viewing of A/P ectopic neurites. n> 100 in all strains, errors bars represent standard error of the mean; *$p<0.05$ compared to wild-type using one-way analysis of variance Bonferroni's multiple comparison test.

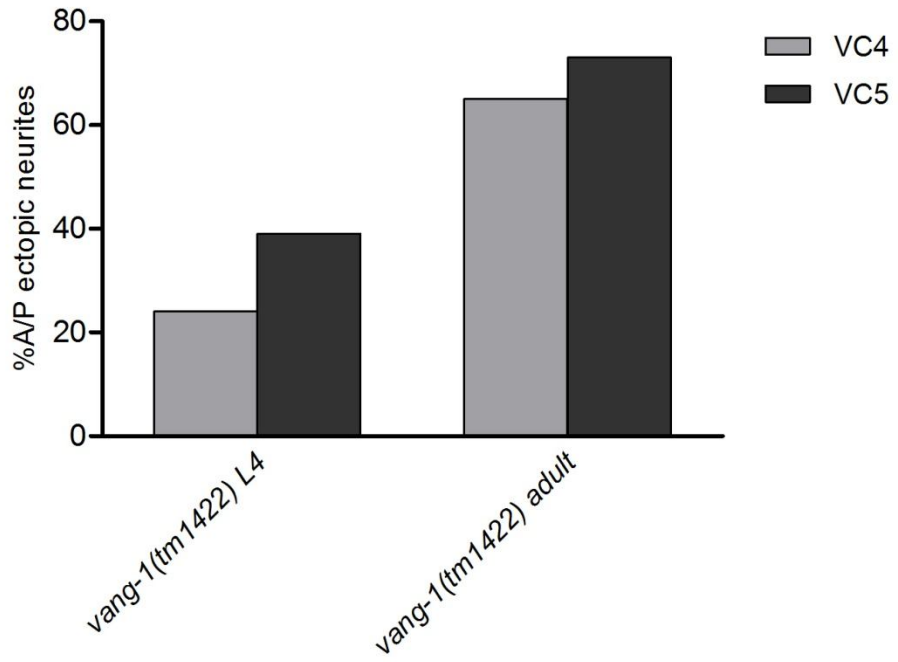

Figure 12. Observation of individual *vang-1(tm1422)* mutants. Animals were individually observed at early L4 (46 hours post hatching) and at adulthood (56 hours post hatching). The majority of L4 worms initially displayed wild-type bipolar phenotype and progressively developed ectopic axons as they entered adulthood. VC4 (n=17) and VC5 (n=18) neurons were scored.

Reporter plasmid	wild-type	*vang-1(tm1422)*
Punc-129::gfp 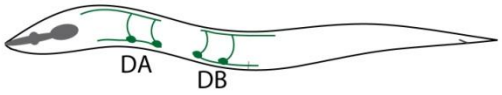	0%	0%
Punc-25::gfp 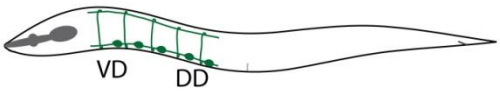	0%	0%
Punc-86::gfp 	0%	0%
Pmec-4::gfp 	0%	0%
Pida-1::gfp 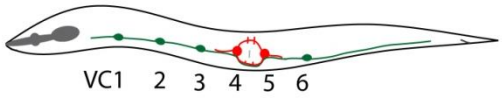	2% ± 2	85% ± 4

Figure 13. Observations of various neurons in *vang-1(tm1422)* mutants. Animals containing various reporter lines used in visualizing specific neurons were crossed into mutant *vang-1(tm1422)*. *Punc-129::gfp* was used to visualize DA and DB neurons. *Punc-25::gfp* was used to visualize VD and DD neurons. *Punc-86::gfp* was employed to illuminate the HSN neurons. *Pmec-4::gfp* was used to inspect the mechanosensory neurons ALM, AVM, PLM, and PVM. *Pida-1::gfp* was used to visualize the six VC motor neurons. % indicates defects in neurite outgrowth, guidance, and orientation. *vang-1(tm1422)*, *Pida-1::gfp* only showed orientation defects in VC4 and VC5. n>50 animals in all strains, anterior is to the left; posterior is to the right. All drawings except *Pida-1::gfp* represent the lateral view; *Pida-1::gfp* shows the ventral view.

3.5 *vang-1* transcriptional expression pattern

To investigate where *vang-1* mRNA is transcribed during VC4 and VC5 neurite outgrowth, we fused the promoter region 3kb upstream of the *vang-1* atg start codon to *green fluorescent protein* (*gfp*) to generate *Pvang-1::gfp* (Fig. 14A). *Pvang-1::gfp* was injected into wild-type animals along with co-expression marker *Plin-11::rfp*, a VC1-6 neuronal reporter. *lin-11* encodes a LIM domain transcription factor that is expressed in VC motor neurons; therefore, *lin-11* expression can be used to identify VC neurons. Since VC neurons extend neurites during the L4 stage and maintain polarity of neurite outgrowth into adulthood, we thus examined the *Pvang-1::gfp* expression in L4 and adult animals. *vang-1* transcriptional activity was found in the HSN neuron, the ventral nerve cord neurons including DA, DB, and VC, and the developing uterine cells, and the vulva muscle and vulval epithelial cells in L4 (Fig. 14B and Fig.15). GFP expression was also observed in several unidentified neurons in the head and the tail regions. In adult animals, *Pvang-1::gfp* expression pattern does not alter from *vang-1* transcriptional expression seen in L4 animals as we observed the same GFP expression pattern as L4 worms (Fig. 14C).

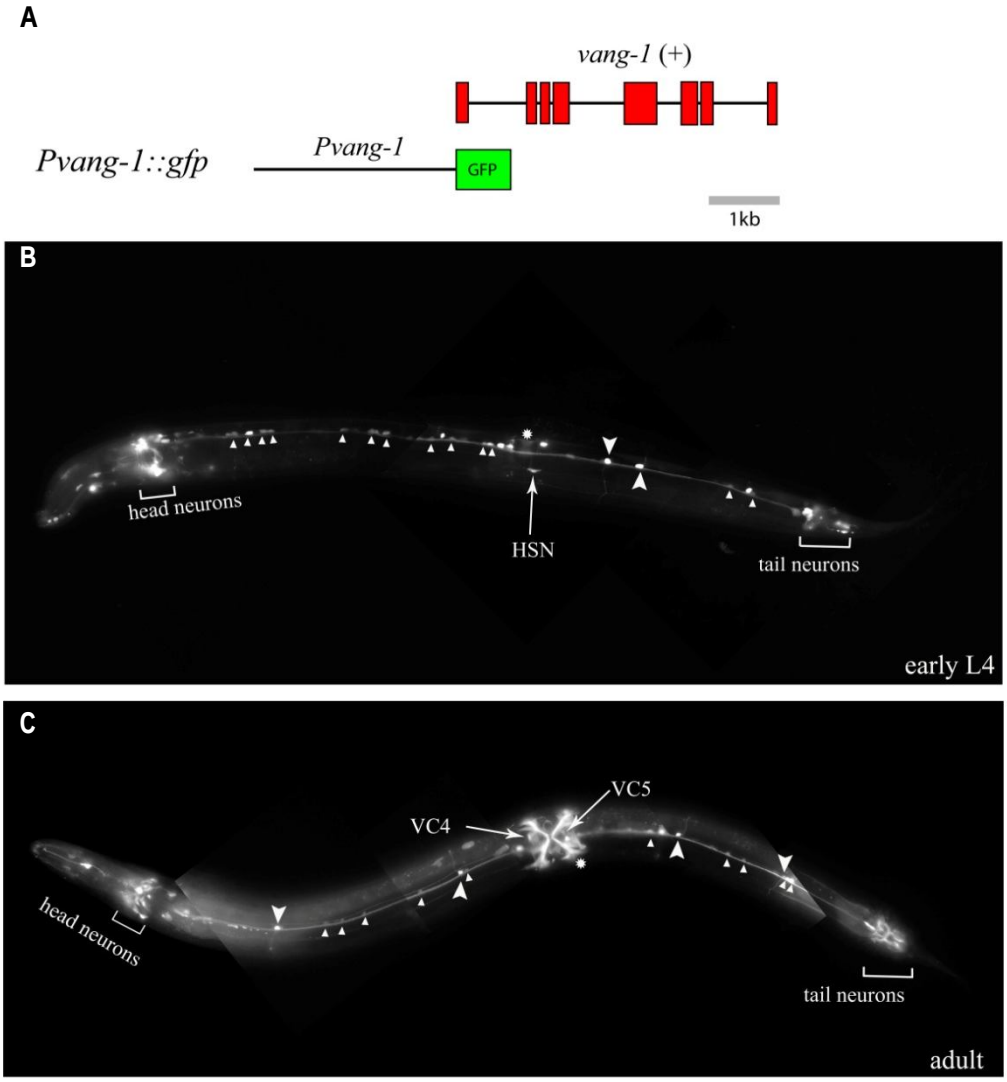

Figure 14. Expression of *Pvang-1::gfp*. (A) A schematic representation of a transcriptional reporter containing 3kb of sequence upstream of *vang-1* tagged with *green fluorescent protein (gfp).* (B) *Pvang-1::gfp* is expressed in unidentified head and tail neurons during early L4 stage. *Pvang-1::gfp* is also visible in ventral nerve cord neurons (small arrowheads), the HSN neuron, and the DA and DB neurons (big arrowheads). (C) In adult animals, *Pvang-1::gfp* is expressed in unidentified head and tail neurons, ventral nerve cord neurons (small arrowheads), DA and DB neurons (big arrowheads) in addition to uterine cells, and vulva muscle and epithelial cells (asterisk).

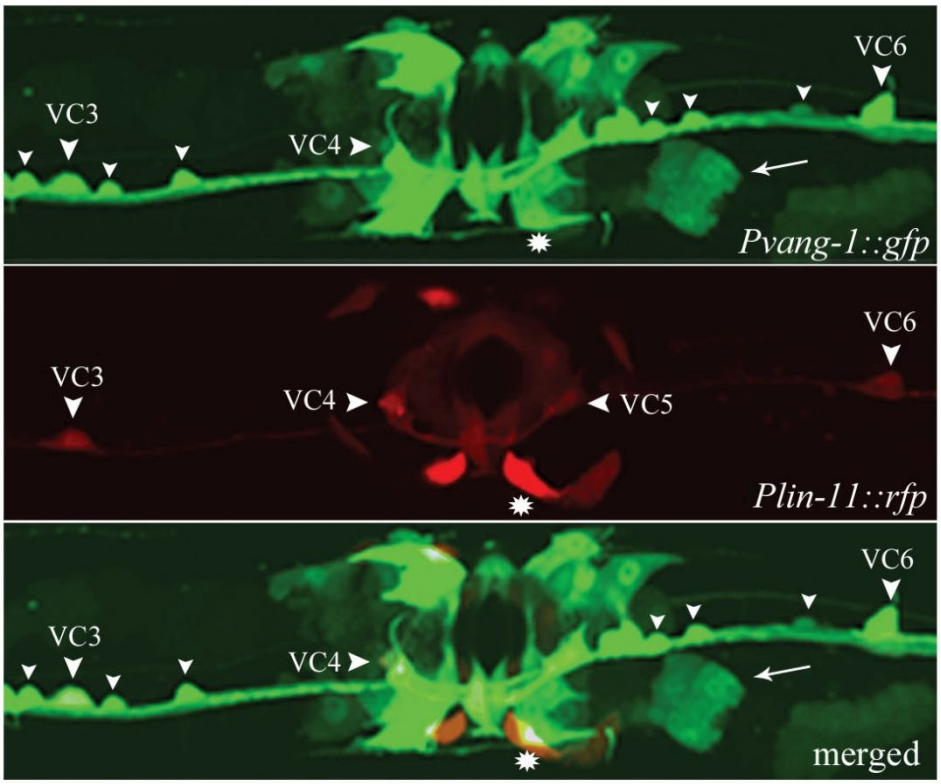

Figure 15. *vang-1* transcriptional activity in VC neurons during the period of neurite outgrowth. Ventral view of transgenic wild-type animals expressing *Pvang-1::gfp* and *Plin-11::rfp*. (A) *Pvang-1::gfp* is visible in uterine and vulva muscle cells (asterisk), developing uterus (arrow), the VC motor neurons (big arrowheads), and unidentified ventral nerve cord neurons (small arrowheads) in L4 animals. (B) *Plin-11::rfp* was used to identify VC neurons. (C) Merged *Pvang-1::gfp* and *Plin-11::rfp* images.

3.6 *vang-1* translational expression

To visualize where VANG-1 is translated and expressed, we generated an N-terminal GFP translational fusion containing 5kb upstream, all introns and exons and 3kb downstream of *vang-1* DNA (Fig. 16A). To test the functionality of *Pvang-1::gfp:vang-1*, we injected *Pvang-1:gfp::vang-1* into *vang-1(tm1422)* mutants. The GFP-VANG-1 fusion was functional as it rescued the A/P directed neurite outgrowth (Fig. 9). The *Pvang-1::gfp::vang-1* translational fusion was injected into wild-type worms along with the VC neurons reporter marker *Plin-11::rfp*. In L4 animals, GFP-VANG-1 was found expressed in neurons in the head and the tail region, the vulva epithelia cells, the gonads, and the spermatheca (Fig. 16B). We also observed expression of *Pvang-1::gfp::vang-1* around the plasma membrane of VC4 and VC5 neurons (Fig. 17). Similarly, in adult animals, GFP-VANG-1 was also expressed in the gonads, the spermatheca, vulva muscle and epithelia cells. In the majority of animals investigated, we observed weak expression of GFP-VANG-1 around the plasma membrane of all six VC motor neurons (Fig. 18). In addition, we did not detect obvious GFP-VANG-1 localization asymmetries around the plasma membranes of VC neurons.

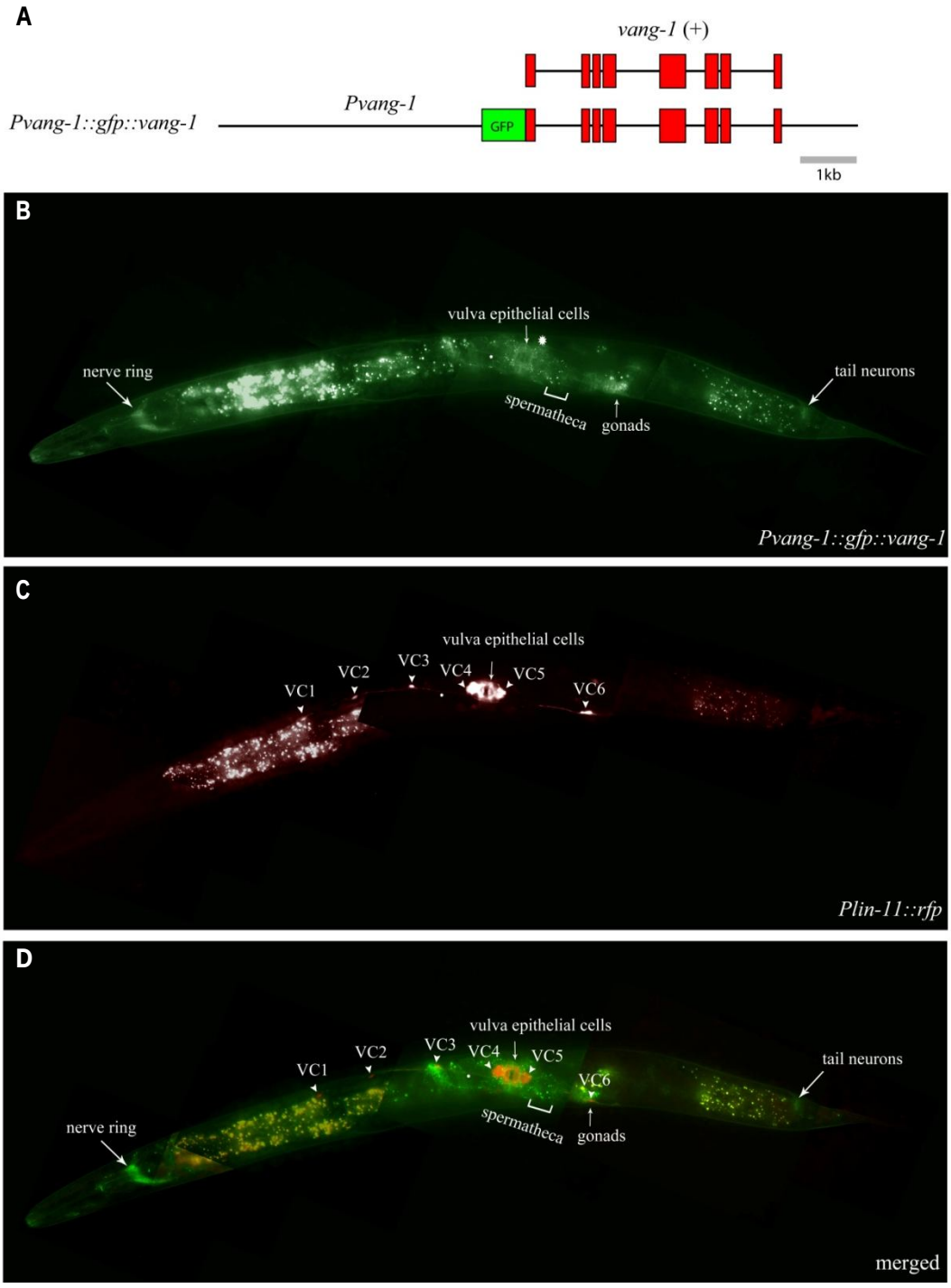

Figure 16. *Pvang-1::gfp::vang*-1 activity during the period of neurite outgrowth. (A) A translational GFP::VANG-1 fusion protein containing 5 kb of sequence upstream of *vang-1* tagged with *gfp* at the N-terminal immediately upstream of *vang-1* atg start codon and *vang-1* genomic DNA. (B) GFP::VANG-1 is expressed in unidentified head and tail neurons, vulva epithelia cells (asterisk), the developing gonads and spermatheca. (C) The co-injection marker *Plin-11::rfp* was used to identify VC1-6 neurons. (D) Merged image of *Pvang-1::gfp::vang-1* and *Plin-11::rfp* showed that GFP::VANG-1 expression in VC neurons is generally difficult to detect due to GFP expression from the surrounding vulva epithelia cells.

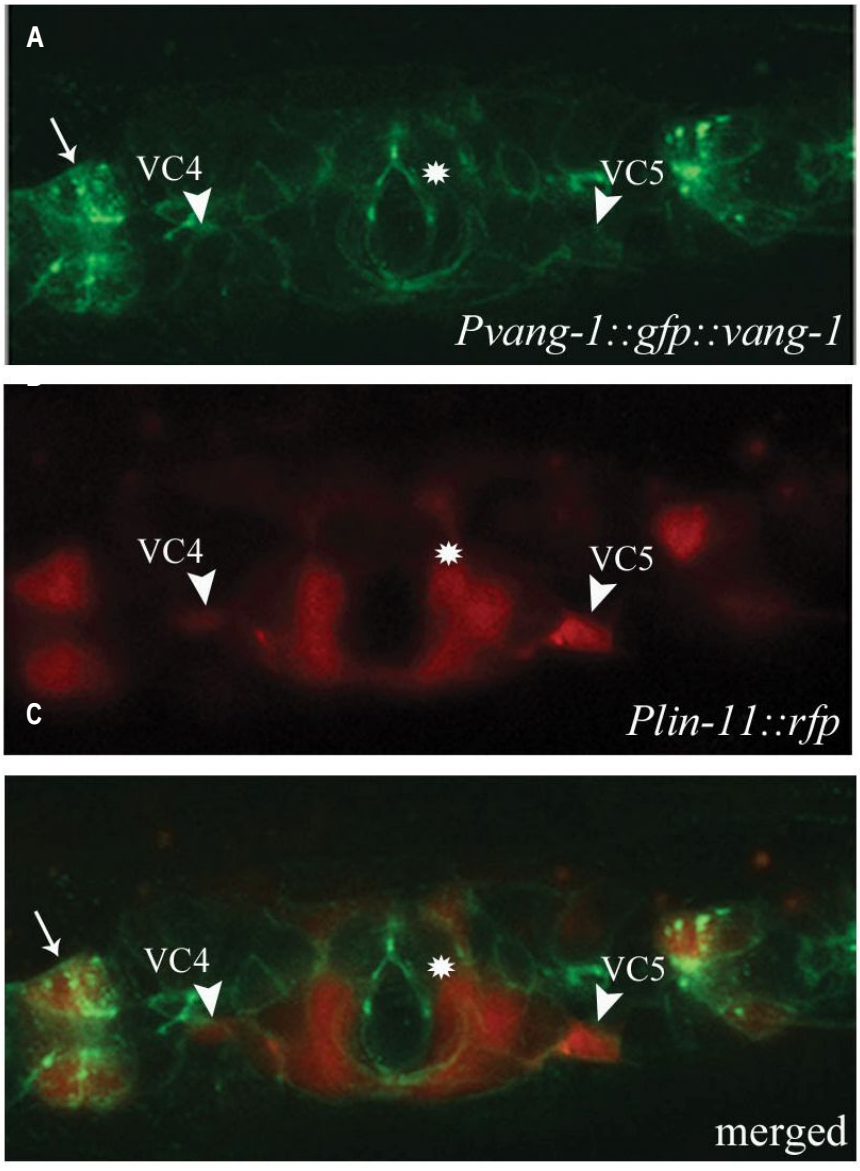

Figure 17. *Pvang-1::gfp::vang-1* expression in VC neurons at the period of neurite extension. (A) GFP::VANG-1 is expressed in vulva epithelia cells (asterisk) and the developing spernatheca (arrow) in L4 animals. (B) The co-injection marker *Plin-11::rfp* is expressed in VC4 and VC5. (C) Merged image of *Pvang-1::gfp::vang-1* and *Plin-11::rfp* showed that VANG-1::GFP is expressed around the plasma membrane in VC5.

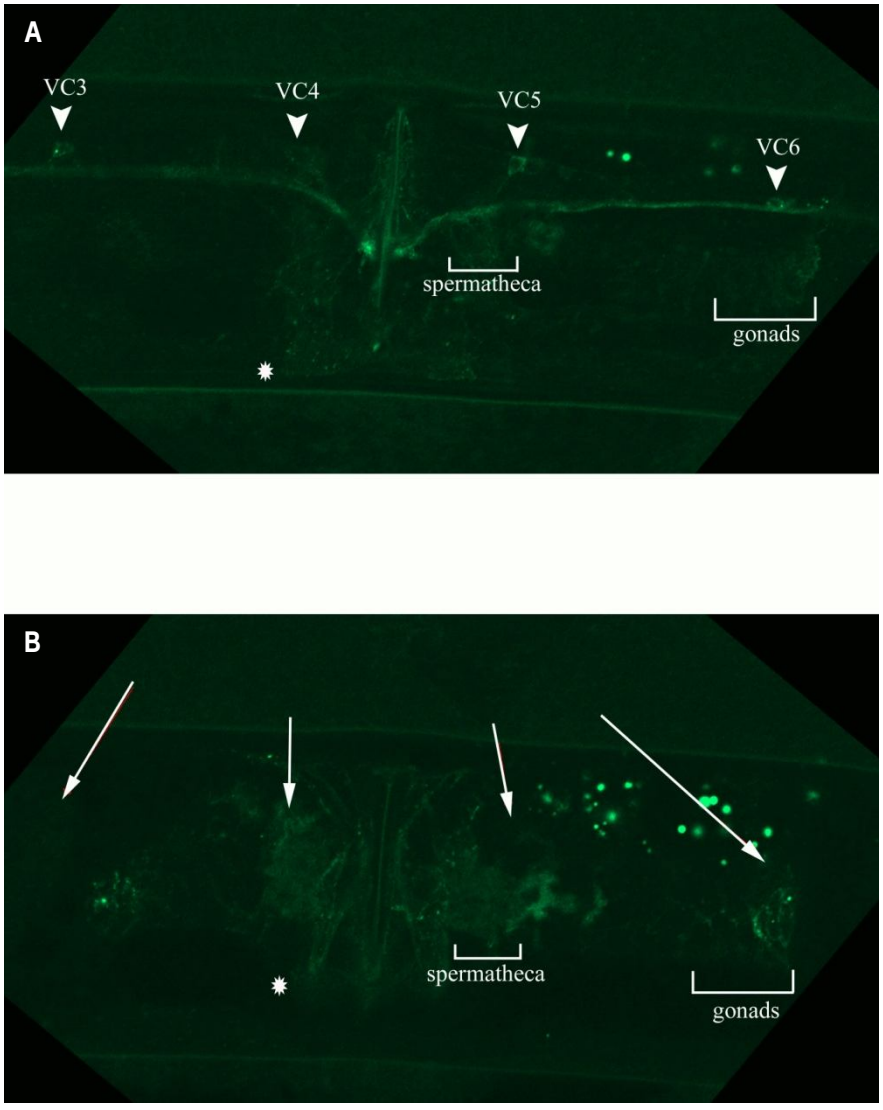

Figure 18. ***Pvang-1::gfp::vang-1*** **activity in VC neurons in adulthood.** **(**A) A single plane snap shot of adult wild-type animal expressing GFP::VANG-1 in VC3-6. (B) A single plane image of the same animal at different body plane showing expression in the spermatheca and the gonads. Arrows indicate positions of VC3-6 and asterisks indicate epithelial cells.

3.7 Expression of *vang-1* in VC neurons and vulva hypodermal cells can rescue neurite outgrowth defects

To test whether VANG-1 acts cell autonomously in VC4 and VC5 to regulate neuronal polarity, *vang-1* was expressed under neuronal or epithelial promoters in *vang-1(tm1422)* mutants. *cat-1* and *unc-4* promoters were used to drive *vang-1* expression in VC neurons as well as other neurons in the head and the ventral nerve cord, and *ajm-1* promoter was used to drive the expression of *vang-1* in the borders of all epithelial cells. In VC neurons, the *cat-1* promoter is activated at the L4 stage and the *unc-4* promoter is activated earlier at the L3 stage. We found that the expression of VANG-1 in VC4 and VC5 and by *Pcat-1::vang-1* did not rescue *vang-1* A/P directed ectopic neurite defects (VC4 53% ± 12, n=110) (Fig. 19 and Table 1) . By contrast, *Punc-4::vang-1* expressing VANG-1 in all six VC motor neuron showed significant rescue (VC4 28% ± 8, n=102) compared to *vang-1(tm1422)* (VC4 69% ± 2, n=543). It is important to note that the *unc-4* promoter is also expressed in DA and VA ventral cord motor neurons (Lickteig et al., 2001). Therefore, to address the possibility that *vang-1* acts cell-autonomously in ventral nerve cord neurons other than VC1-6, we used the promoter of *unc-129* to drive the expression of *vang-1* in DA and DB neurons. *vang-1(tm1422)* animals carrying *Punc-129::gfp::vang-1* were not rescued for *vang-1* neurite polarity defects (VC4 64% ± 5, n=155). We examined transgenic *vang-1(tm1422)* animals expressing *Pajm-1::gfp::vang-1* in all epithelial cells, including the vulva cells, and found that the A/P ectopic neurite phenotype was significantly rescued (VC4 35% ± 2, n=105) compared to *vang-1(tm1422)* (VC4 69% ± 2, n=543) (Fig. 19 and Table 1).

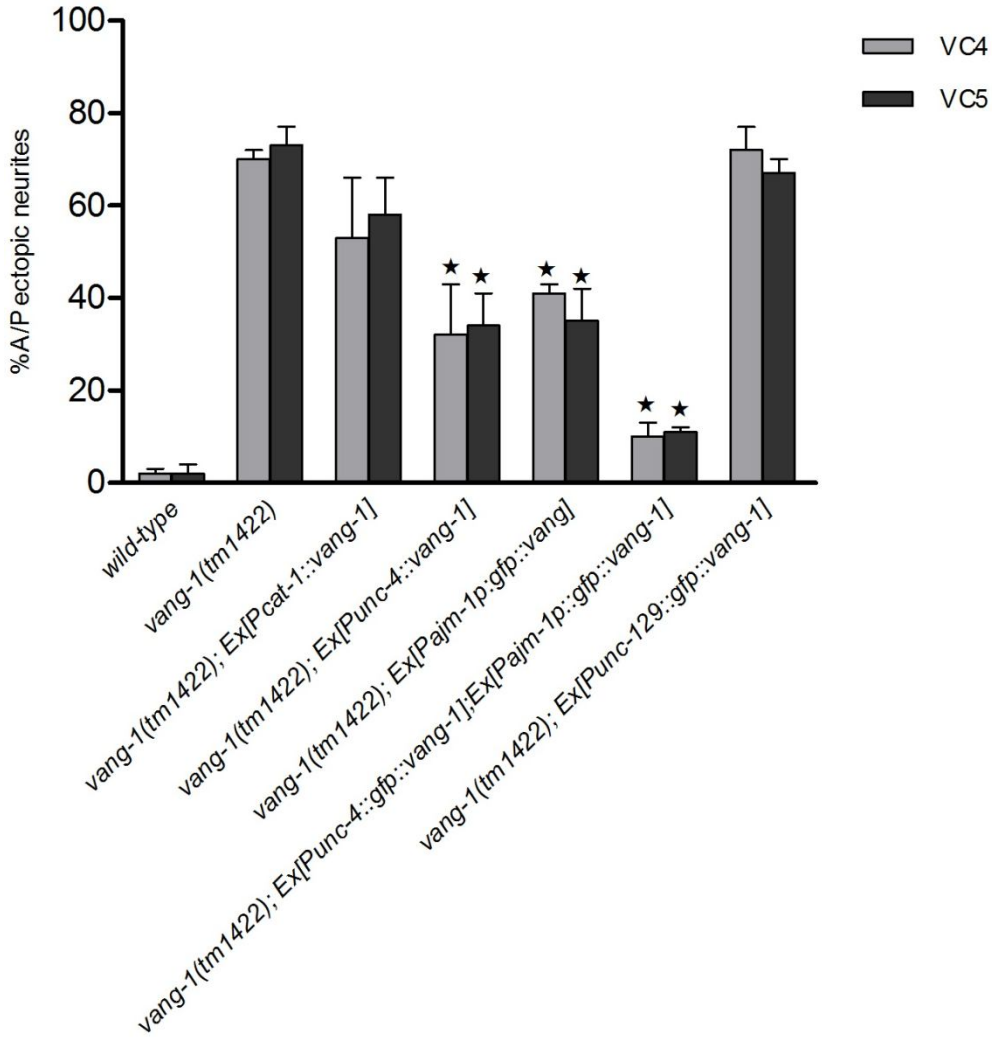

Figure 19. Cell-specific rescue of *vang-1(tm1422)* mutants. *vang-1* acts both cell in VC neurons and non-cell autonomously from epithelial cells. *Pcat-1::vang-1* and *Punc-4::vang-1* drive the expression of *vang-1* in VC4 and VC5 and all VC neurons respectively, and as well as other head and ventral cord neurons. *Pajm-1::gfp::vang-1* expresses VANG-1 in all epithelial cells and *Punc-129::gfp::vang-1* expresses VANG-1 in DA and DB ventral nerve cord neurons. One extrachromosomal line out of 4 obtained lines is shown for all lines. n>80 in all strains, error bars represent standard error of the mean, *$p<0.05$ compared to *vang-1(tm1422)* using analysis of variance and Bonferroni's multiple comparison post hoc test.

Transgene	VC4 (% of defects)			VC5 (% of defects)		
	tripolar	**bipolar**	**unipolar**	**tripolar**	**bipolar**	**unipolar**
vang-1(tm1422)	64 ± 3	6 ± 2	5 ± 1	63 ± 6	9 ± 2	9 ± 2
Ex[Pcat-1::vang-1]1	53 ± 13	0 ± 0	3 ± 3	58 ± 9	7 ± 2	0 ± 0
Ex[Pcat-1::vang-1]2	50 ± 18	7 ± 5	4 ± 4	52 ± 5	7 ± 0	3 ± 1
*Ex[Punc-4::vang-1]1**	27 ± 9	5 ± 2	4 ± 2	24 ± 4	12 ± 3	5 ± 2
*Ex[Punc-4::vang-1]2**	28 ± 8	2 ± 2	8 ± 3	33 ± 6	7 ± 2	10 ± 4
*Ex[Pajm-1::gfp::vang-1]1**	35 ± 3	6 ± 4	4 ± 2	32 ± 7	3 ± 1	5 ± 2
*Ex[Pajm-1::gfp::vang-1]2**	42 ± 3	12 ± 4	4 ± 2	25 ± 5	5 ± 0	0 ± 0
*Ex[Punc-4::gfp::vang-1], [Pajm-1::gfp::vang-1]1**	10 ± 3	0 ± 0	4 ± 1	10 ± 1	1 ± 0	3 ± 1
*Ex[Punc-4::gfp::vang-1], [Pajm-1::gfp::vang-1]2**	15 ± 3	3 ± 1	0 ± 0	13 ± 2	5 ± 2	3 ± 1
Ex[Punc-129::gfp::vang-1]1	60 ± 2	10 ± 2	5 ± 2	53 ± 1	8 ± 2	6 ± 1
Ex[Punc-129::gfp::vang-1]2	63 ± 6	10 ± 2	3 ± 1	56 ± 3	11 ± 3	4 ± 0

Table 1. Selected cell-specific extrachromosomal lines used in *vang-1* rescue experiments. All lines of *Punc-4::vang-1*, *Pajm-1::gfp::vang-1*, and *Punc-4::gfp::vang-1* and *Pajm-1::gfp::vang-1* rescued *vang-1(tm1422)* A/P ectopic neurites. n> 100, ± indicates standard error of the mean, *p<0.05 compared to *vang-1(tm1422)* using analysis of variance and Bonferroni's multiple comparison post hoc test.

However, the rescue of neurite polarity defects by *Punc-4::vang-1* and *Pajm-1::gfp::vang-1* were not as strong as *Pvang-1::gfp::vang-1*, suggesting that simultaneous expression of VANG-1 in both VC neurons and epithelial cells may be required to achieve more complete rescue of *vang-1* defects. Therefore, we asked if combined expression of *vang-1* in VC neurons and the epithelia cells would result in more efficient rescue than either *vang-1* expressed in VC4 neurons or in the epithelia cells alone. We generated transgenic *vang-1(tm1422)* animals carrying *Punc-4::gfp::vang-1* and *Pajm-1::gfp::vang-1* and found that the combined expression of *vang-1* in VC neurons and the epithelia cells strongly rescued *vang-1* neurite polarity defects (VC4 10% ± 3, n=143) compared to single expression of *Punc-4::gfp::vang-1* (VC4 28% ± 8, n=102) or *Pajm-1::gfp::vang-1* (VC4 35% ± 2, n=105) alone (Fig. 19 and Table 1). These results indicate that VANG-1 acts cell autonomously in VC4 and VC5 and non-cell autonomously from the epithelial cells. *vang-1* neurite polarity defects were rescued by *Punc-4::gfp::vang-1* but not by *Pcat-1::gfp::vang-1* suggesting that cell-autonomous activity of *vang-1* is needed at the early L4 stage.

3.8 A candidate approach identifies *pk* and *dsh* homologs as regulators of neuronal polarity

As *vang-1* is a core member of the non-canonical wnt-PCP signalling pathway, we undertook a candidate gene approach to determine if *C. elegans* orthologs of other core PCP genes are involved in regulating neuronal polarity. In *Drosophila*, the core PCP components include the Wnt ligand receptor transmembrane proteins Frizzled (FZ), the Cadherin family seven-pass transmembrane protein Flamingo (FMI), the four-pass transmembrane protein Van Gogh (VANG), the cytoplasmic multi-domain protein Dishevelled (DSH), the Ankyrin repeat protein Diego (DGO), and the LIM domain

protein Prickle (PK). In *C. elegans*, there are five *wnt* homologs (*cwn-1*, *cwn-2*, *lin-44*, *egl-20*, *mom-2*), four *fz* homologs (*lin-17*, *mig-1*, *mom-5*, *cfz-2*), three *dsh-1* homologs (*dsh-1*, *dsh-2*, *mig-5*), and single homologs of *pk* (*prkl-1*) and *fmi* (*fmi-1*). We used a candidate approach to identify neurite polarity mutants with a *vang-1*-like VC4 and VC5 polarity phenotype. To assess loss of *fz*, *dsh*, and *pk* ortholog activity, we undertook RNAi-induced silencing to knockdown the functions of candidate genes. Genes known to modulate axon specification and genes predicted to interact with the *vang-1* PDZ-binding domain were also selected for the RNAi-silencing analysis to uncover new neuronal polarity-regulating pathway components.

To test for the efficacy of gene knockdown by dsRNA, we introduced the *vang-1* cDNA into dsRNA-inducible vector L4440 and transformed the *vang-1*-containing L4440 vector into *E. coli* strain OP50. The vector containing-bacteria was fed to *rrf-3;cyIs4[Pcat-1::gfp]*. *rrf-3* background was used to enhance the effectiveness of RNAi as RRF-3 is an endogenous inhibitor of the RNAi-mediated processes (Grishok, 2005; Simmer et al., 2002). Non-RNAi treated *rrf-3;cyIs4* animals displayed a low percentage of A/P ectopic neurites (6% ± 6, n>100) that is not statistically significant compared to wild-type *cyIs4* animals (3% ± 1, n>100). *rrf-3;cyIs4* fed with *vang-1*-containing L4440 vectors had a significant level of A/P directed ectopic neurites (31% ± 11, n>100) (Table 2.1), indicating that feeding dsRNA encoding candidate genes is a viable option in determining whether the genes of interest modulate neurite outgrowth and orientation. In addition to *rrf-3*, we also employed an *eri-1,lin-15,cyIs4* background to increase the effectiveness of RNAi knockdown in neurons. *eri-1* encodes an endogenous ribonuclease RNAi inhibitor that degrades small interfering RNAs (siRNA) (Kennedy et al., 2004;

Timmons, 2004). *lin-15* encodes a retinoblastoma tumour suppressor and mutations in *lin-15* cause somatic cells to express germline-specific genes that through an unknown mechanism enhance RNAi effects (Sieburth et al., 2005; Wang et al., 2005a). Simultaneous mutations in *eri-1* and *lin-15* have been shown to synergistically enhance the efficiency of RNAi silencing in neurons (Sieburth et al., 2005; Wang et al., 2005a).

A library of *C. elegans* ORF cDNA clones (Open Systems biology, Huntsville, AL, USA) was obtained to circumvent the need to individually clone the target gene cDNAs into dsRNA-inducible vectors. The HE115 DH5α bacteria containing dsRNA-inducible cDNA clones of interest were cultured, induced, and fed to RNAi-sensitive mutant strains *rrf-3, cyIs4* (Fig. 20). We screened a total of 46 genes (Table 2.1 and 2.2) using the protocol outlined by Kamath et al (Kamath and Ahringer, 2003; Kamath et al., 2003). We found that animals fed with Wnts *cwn-1, cwn-2, lin-44, mom-2,* and *egl-20* dsRNA did not display significant neurite polarity defects. However, animals fed with *cwn-1* and *cwn-2* dsRNA exhibited delayed development and animals fed with *egl-20* dsRNA were sterile. These latter observations indicate that RNAi silencing is effective. RNAi knockdown of individual Fz *lin-17, mig-1, mom-5,* or *cfz-2* also did not show a significant A/P directed neurite outgrowth phenotype. RNAi knockdown of *prkl-1* and *dsh-1,* on the other hand, led to significant emergence of A/P directed ectopic neurites (91% ± 2 and 74% ± 10, respectively, n>100) compared to non-RNAi treated *eri-1,lin-15,cyIs4* animals (16% ± 1, n>100) (Table 2.1). We observed no significant neurite polarity defects in our analysis of other candidate genes such as the PAR polarity gene *par-1* (11% ± 3), the Formin actin-regulating homolog *daam-1* (4% ± 1), and the PDZ-domain containing adherens junction gene *let-413* (17% ± 2) (Table 2.2).

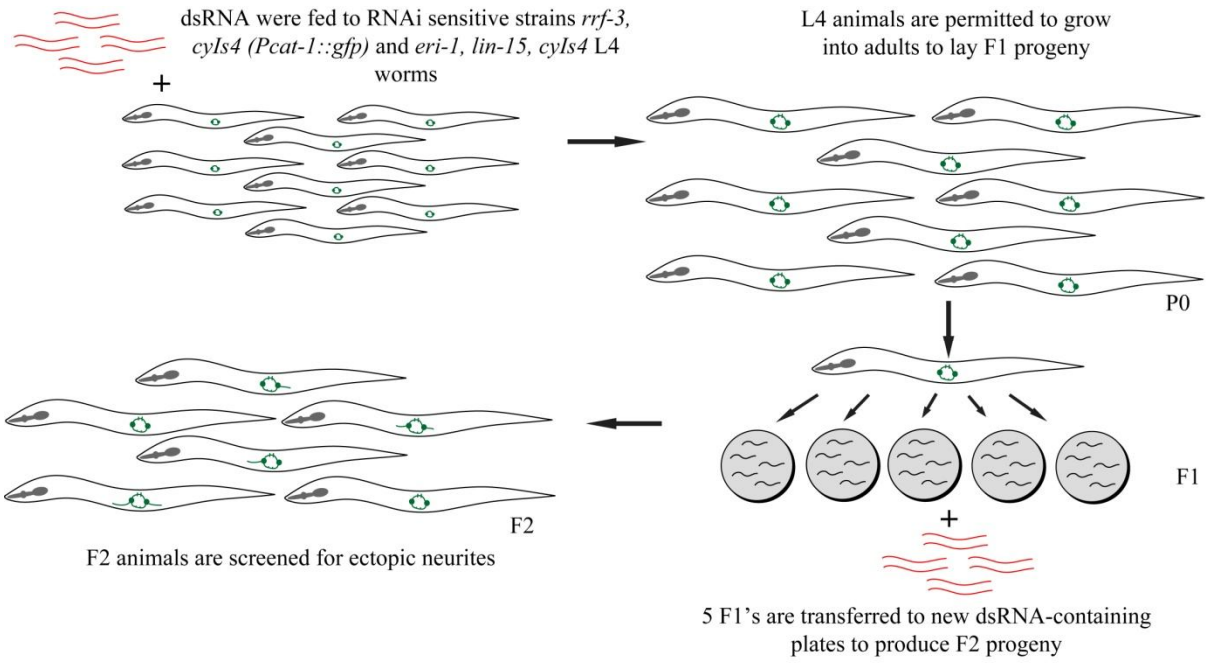

Figure 20. Candidate gene approach for identifying genes involved in VC4 and VC5 neurite outgrowth. *E. coli* containing dsRNA of selected genes were grown and fed to L4-stage RNAi sensitive strains *rrf-3,cyIs4* and *eri-1,lin-15,cyIs4* animals for 36-40 hr at 22˚C. Five animals were plated onto plates seeded with the same *E. coli* expressing dsRNA of the gene of interest and were allowed to lay eggs for 24 hr at 22˚C. RNAi-silencing effects were observed in F2 progeny for neuron polarity defects.

Protein Family	Gene	Molecular feature and biological function in *C. elegans*	Strain Genotype	
			rrf-3, cyIs4	***eri-1, lin-15, cyIs4***
Control	– L4440	wild-type animals fed with bacteria containing no L4440 vectors	3 ± 3	–
	rrf-3, cyIs4	*rrf-3* encodes for an RNA-directed RNA polymerase that inhibits somatic RNAi	6 ± 6	–
	eri-1, lin-15, cyIs4	eri-1 encodes for ribonuclease involved in degrading small interfering RNAs; lin-15 encodes for a transcription factor involved in cell fate specification	–	16 ± 1
Wnt ligands	*cwn-1*	required in cell-fate specification; functions redundantly with *egl-20* in ALM axon guidance	0 ± 0	9 ± 3
	cwn-2	functions in nerve ring development, functions redundantly with *mom-2* and *lin-44* in vulva patternting and axon guidance	0 ± 0	6 ± 2
	lin-44	required in asymmetric cell divisions and in vulval development; functions redundantly with *egl-20* in HSN migration	0 ± 0	7 ± 2
	mom-2	functions in enderdomal induction; acts redundantly with *cwn-2* to regulate vulva patterning	4 ± 0	2 ± 2
	egl-20	regulates the migration of QL and QR and acts redundantly with *cwn-1* in regulating ALM polarity	0 ± 0	9 ± 3
Fz receptors	*mig-1*	required for migration of the QL neuroblast and functions redundantly with *mom-5*, *lin-17*, and *cfz-2* to regulate HSN migration	nd	11 ± 0
	mom-5	regulates embryonic and neuronal asymmetric cell division; acts redundantly with *mig-1* to regulate HSN migration	nd	7 ± 4
	lin-17	functions in specifying the polarity of asymmetric cell divisions and in development of vulva, somatic gonad, and tail; acts redundantly with *mig-1* to regulate HSN migration	nd	18 ± 3
	cfz-2	functions redundantly with *mom-5* to regulate cell migration	nd	8 ± 2
Van gogh	*vang-1*	a four-pass transmembrane protein possessing a PDZ-domain binding site; regulates intestinal tube formation	38 ± 11*	13 ± 3
Dishevelled	*mig-5*	required in embryonic cell migration, cell-fate specification, and spindle orientation; functions redundantly with *dsh-1* and *dsh-2*	17 ± 5	nd
	dsh-1	functions in EMS blastomere endoderm specification	23 ± 2*	74 ± 10**
	dsh-2	interacts with *mig-5* to regulate embryonic endoderm specification, spindle orientation, asymmetric cell division, and cell-fate specification;	6 ± 0	23 ± 2
Prickle	*prkl-1*	a LIM-domain containing cytosolic protein; weakly regulates asymmetric cell division	nd	91 ± 2**
Flamingo	*fmi-1*	a seven-pass cadherin transmembrane protein; required for asymmetric cell division, axon guidance and synapse formation	6 ± 2	nd

Table 2.1: Core PCP genes selected for candidate gene approach RNAi-silencing. Numbers represent % of ectopic A/P neurite. Animals display >25% of A/P ectopic neurites are considered positive (+). dsRNA were fed to both *rrf-3,cyIs4* and *eri-1,lin-15,cyIs4* mutants. n>200, *p<0.05 compared to non-RNAi treated *rrf-3, cyIs4* animals; **p<0.05 compared to non-RNAi treated *eri-1,lin-15,cyIs4* animals

Protein Family	Gene	Molecular feature and biological function in *C. elegans*	Strain Genotype	
			rrf-3, cyIs4	***eri-1, lin-15, cyIs4***
PAR	*par-1*	a membrane-associated protein involved in establishing early embryo polarity	0 ± 0	11 ± 3
	par-6	A PDZ-domain containing protein that interacts with *par-1* to establish polarity of early embryo	larval arrest	larval arrest
Cadherin	*jac-1*	a component of the cadherin-catenin complex; positively promotes association between the actin cytoskeleton and the cadherin-catenin	2 ± 2	10 ± 3
MAGUK	C50F2.8	no known function	5 ± 2	9 ± 3
	lin-2	functions to specify LET-23, an Epidermal growth factor receptor, to the plasma membrane	nd	3 ± 1
	F44D12.1	no known function	nd	12 ± 1
	tag-117	functions as a postsynaptic folding-like protein	nd	9 ± 2
MAP Kinase	*mom-4*	a MAP kinase kinase kinase-related protein; functions to regulate the β-wnt-regulated division of EMS daughter cells	4 ± 1	9 ± 3
	lit-1	a serine threonine protein kinase; interacts with mom-4 to regulate division of EMS daugther cells	embryonic lethal	embryonic lethal
Formins	*daam-1*	a CIP4-binding proteins; interacts with Rho GTPases, CIP4 and Src to regulate actin dynamic	nd	4 ± 1
Syntaxin	*tom-1*	a cytosolic syntaxin-binding protein involved in exocytosis of synaptic vesicles; a homolog of *Drosophila lethal(2) giant larvae*	nd	3 ± 1
PDZ-motif	*ptp-1*	functions in adhering cytoplasmic proteins to the plasma membrane	7 ± 4	23 ± 1
	let-413	a basolateral membrane protein; functions in assembling adherens junctions	3 ± 3	17 ± 2
	mics-1	a mitochrondrial scaffolding protein	3 ± 0	11 ± 1
	cnk-1	a multi-domain adaptor protein that acts to promote Raf activation	1 ± 1	13 ± 3
	pxf-1	a PDZ-guanine nucleotide exchange factor; interacts with Ras-like GTPases to maintain epithelial integrity	4 ± 2	7 ± 2
	F25H2.2	a sorting nexin protein 27 involved in endosomal functions	nd	9 ± 3
	C25G4.6	a PDZ-containing protein that functions in spermatogenesis and meiotic sperm segragation	6 ± 0	20 ± 6
	C01B7.5	no known function	3 ± 1	7 ± 1
	C50D2.3	no known function	9 ± 1	17 ± 4
	ZK849.2	no known function	6 ± 6	12 ± 4
	C53B4.4	no known function	nd	6 ± 0
	F45E4.3	a PDZ-containing and Ca2+-binding domains protein; may play a role in the function of neuromuscular system	4 ± 1	7 ± 2
	W03F11.6	an actin filament binding protein; may regulate myosin contraction during gastrulation	8 ± 3	4 ± 1
	C35D10.2	a GAIP (Gα-interacting protein)-binding protein; may regulate mitochondrial activity	5 ± 5	6 ± 6
	Y55B1BR.4	no known function	4 ± 2	9 ± 2
	C45G9.7	no known function	nd	6 ± 3
	T19B10.5	no known function	nd	17 ± 1
	C50D2.3	no known function	7 ± 2	12 ± 3
	T21G5.4	no known function	nd	10 ± 6
	Y57G11C.22	an atypical Protein Kinase C involved embryogenesis progression	nd	4 ± 2
	Y42H9AR.1	a Golgi reassembly stacking protein; may function in germline cytokinesis	nd	3 ± 2
	shn-1	a homolog of Shank, a postsynaptic scaffolding protein; functions to regulate Ca^{2+}-signaling with IP_3 receptor	nd	8 ± 2
	C46H11.6	no known function	nd	1 ± 1
	ZK1321.4	no known function	nd	6 ± 4
	C09G1.4	no known function	nd	6 ± 2
	H06H21.9	no known function	nd	14 ± 2
	F40F9.3	no known function	nd	6 ± 1
	Y38C1AB.4	no known function	nd	8 ± 2
	F44D12.4	no known function	nd	12 ± 1
Zn finger	C28H8.9	no known function	nd	10 ± 4

Table 2.2: Selected non-PCP genes in candidate gene approach RNAi-silencing. dsRNA were fed to both *rrf-3,cyIs4* and *eri-1,lin-15,cyIs4* mutants. Numbers represent % of ectopic A/P neurite. n>200.

To confirm our RNAi-induced loss of function findings, we crossed in the *cyIs4 [Pcat-1::gfp]* reporter transgene into available genetic mutants to examine VC4 and VC5 neuronal polarity. *prkl-1(ok3182)* and *dsh-1(ok1445)* are deletion alleles that were kindly provided by the *C. elegans* knockout consortium. *prkl-1(ok3182)* is a deletion allele that is predicted to encode a truncated protein and therefore should represent a strong *loss-of-function* allele. *dsh-1(ok1445)* presents a hypomorphic deletion allele (Song et al., 2010). In addition, our group also conducted a non-complementation screen over a chromosomal deficiency (nDf41) that deletes the sole *pk* homolog *prkl-1* and identified *zy11*, a new allele of *prkl-1* (Sanchez-Alvarez et al., 2011). *prkl-1(zy11)* is a point mutation allele that results in a premature stop codon in 102Q. *prkl-1(zy11)* and *prkl-1(ok3182)* animals displayed higher level of A/P ectopic neurites than *vang-1(tm1422)* mutants. *dsh-1(ok1445)* mutants showed penetrance of ectopic A/P directed neurites comparable to *vang-1(tm1422)* (Fig. 21). These observations validate the findings from RNAi-silencing experiments and implicate *prkl-1* and *dsh-1* in the regulation of VC4/5 neuronal polarity.

Our examination of the *fz* mutants *lin-17(n677)*, *mig-1(n687)*, *mom-5(or57)*, and *cfz-2(ok1201)* showed that *mig-1*, *mom-5*, and *cfz-2* do not display defective neuronal polarity (Table 3). *lin-17(n677)* mutants suppressed the expression of *cat-1* in VC4 and VC5 neurons. Interestingly, *cat-1* expression was also silenced in *wnt/lin-44(n1792)* and *bar-1(ga80)/β-catenin* mutants. Taken together, these findings suggest that the canonical wnt signalling pathway controls *cat-1* expression and may play a role in VC4 and VC5 cell fate specification. The transgene *cyIs3[Punc-4::gfp]* was used as an alternative reporter to visualize VC4 and VC5 in *lin-17(n677)* and *bar-1(ga80)*. *cyIs3* drives the expression of GFP in all VC motor neurons and neurons in the ventral nerve cord. Only

L4 *cyIs3* animals were scored as the GFP expression in the ventral nerve cord and VC1-3 and VC6 neurites often obscured visualization of VC4/5 A/P ectopic neurites in adults. *lin-17(n677),cyIs3* (VC4 2% ± 1, n=132) and *bar-1(ga80),cyIs3* (VC4 5% ± 1, n=76) did not display significant neurite polarity defects compared to wild-type (VC4 2% ± 1, n=236) (Table 3).

Frizzled genes have been shown to function redundantly in *C. elegans* axon guidance (Hilliard and Bargmann, 2006; Pan et al., 2006). To determine whether Frizzleds act in a redundant fashion, we generated double mutant strains of *mig-1(n687),lin-17(n677),cyIs3; cfz-2(ok1210),mig-1(n687),cyIs4; lin-17(n677),cfz-2(ok1210),cyIs3* and the triple mutant strains *of mig-1(n687),lin-17(n677),cfz-2(ok1210),cyIs3*. We did not observe neurite polarity defects in the double and triple mutants (Table 3). In addition, we also generated *eri-1,lin-15,lin-17,cyIs3* and introduced dsRNA of the remaining three *fz* homologs to the *eri-1,lin-15,lin-17,cyIs3* mutants. The animals displayed a variety of developmental defects such as uncoordinated movements and protruding vulva but we did not observe a significant number of A/P directed neurites. Taken together, these findings suggest that no particular *fz* homolog functions as a modulator of neurite outgrowth and orientation. However, *lin-17*-induced silencing of *cat-1* expression in VC4 and VC5 could be influenced by alteration of VC4 and VC5 cell fate specification. Moreover, the difficulty of generating quadruple mutant *lin-17(n677),mig-1(n687),mom-5(or57),cfz-2(ok1201)* due to *mom-5(or57)* mutation that results in embryonic lethality makes the investigation of *fz*s involvement in neurite outgrowth incomplete. These findings suggest extensive redundancy among Frizzleds as a possibility.

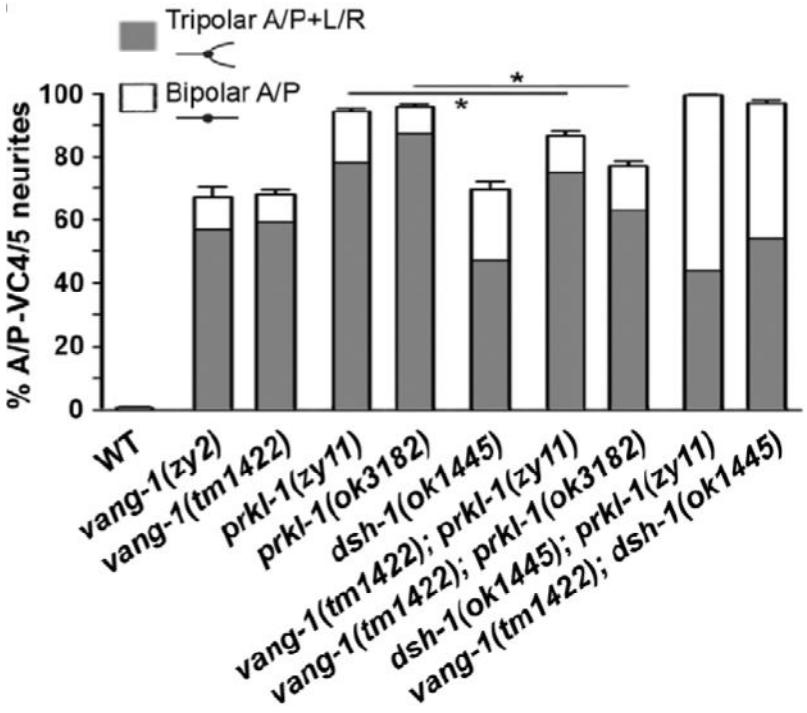

Figure 21. A PCP-like pathway that includes *vang-1, prkl-1,* and *dsh-1* restricts nascent neurite formation to a specific tissue axis. Quantification of VC4/5 polarity defects in *vang-1, prkl-1,* and *dsh-1* single and double mutants, n>250. Error bars represent standard error of proportion, *p,0.01, χ^2.

	VC4 neurite orientation				VC5 neurite orientation			
	Tripolar	Bipolar	Unipolar		Tripolar	Bipolar	Unipolar	
Genotype	%	%	%	n	%	%	%	n
Wild type	2	0	1	236	2	0	12	236
Van Gogh								
vang-1(tm1422) L4	21	4	24	208	21	3	13	211
vang-1(tm1422)	62	6	5	543	61	10	8	541
Wnts								
egl-20(n585)	2	2	2	45	3	4	9	46
vang-1(tm1422);egl-20(n585)	65	16	3	89	55	13	2	92
Frizzled								
cfz-2(ok1220)	4	0	0	310	5	1	21	309
lin-17(n677)	2	5	39	132	2	7	47	137
mig-1(n687)	6	1	1	71	4	6	27	70
mom-5(or57)	0	0	9	23	0	4	17	24
Frizzled double mutants								
cfz-2(ok1220); lin-17(n677)	5	0	31	69	13	0	35	56
cfz-2(ok1220); mig-1(n687)	2	1	12	126	0	1	22	129
mig-1(n687); lin-17(n677)	7	0	43	79	20	3	42	64
***vang-1;fz* double mutants**								
vang-1(tm1422);cfz-2(ok1220)	68	0	3	61	67	4	16	62
vang-1(tm1422);lin-17(n677) L4	20	10	10	121	15	9	6	129
vang-1(tm1422);mig-1(n6870	81	7	2	78	67	13	10	72
Dishevelled								
mom-5(or57)	0	0	9	23	0	4	17	24
β-catenin								
bar-1(ga80)	5	0	9	76	5	0	3	69
vang-1(tm1422);bar-1(ga80)	51	6	18	51	45	13	17	53

Table 3: Neurite orientation in various PCP genetic backgrounds. Neurite orientation was scored in adult animals grown at 20˚C. Protrusions that are of equal length or longer than the endogenous VC4 posteriorly-directed protrusions or VC5 anteriorly-directed protrusions are scored as neurite misorientations. CAT-1::GFP is used to visualize VC4 and VC5 neurons in adult animals; UNC-4::GFP is used to visualize neurons in early L4 stage. Only animals with no vulva defects are scored. *lin-17(n677)* and *bar-1(ga80)* suppressed *Pcat-1::gfp* expression; therefore, *Punc-4::gfp* was used to visualize VC4 and VC5 neurons. Only VC4 neurons of early L4 *lin-17(n677)* animals were scored. *These animals are progeny of *dpy-5 mom-5/nt2* parents and are *dpy-5 mom-5* homozygous. " indicates not statistically significant as revealed by paired t-test analysis with $p>0.05$.

3.9 *vang-1* genetically interacts with *prkl-1* to regulate VC4 and VC5 neurite orientation

RNAi silencing of *prkl-1* and *prkl-1(zy11)* and *prkl-1(ok3138)* mutants showed that loss of *prkl-1* activity lead to the *vang-1*-like emergence of A/P directed neurites. Based on known interactions between *Van Gogh* and *Prickle* in *Drosophila* in which VANG recruits and binds to PK to regulate epithelial planar polarity (Bastock et al., 2003; Strutt and Strutt, 2007), we asked whether *vang-1* and *prkl-1* function in the same common pathway. To investigate the genetic interactions between *vang-1* and *prkl-1*, we generated *vang-1(tm1422); prkl-1(ok3138)* double mutants. We reasoned that if two genes act in the same pathway, the phenotypic penetrance in the double mutants should not exceed the level of the strongest *lof* mutant. However, if two genes act in parallel pathways, loss of activity in both genes would be expected to increase the penetrance. We found that the penetrance of VC4/5 A/P ectopic neurites in *vang-1(tm1422); prkl-1(ok3138)* double mutants (VC4 85% ± 4, n= 165) does not exceed the penetrance of single *prkl-1(ok3138)* mutant (VC4 97% ± 1, n= 145). This finding illustrates that loss of *vang-1* activity does not enhance the severity of *prkl-1* A/P directed neurite phenotype, and therefore suggests *vang-1* and *prkl-1* interact genetically in the same pathway to prevent emergence of ectopic neurites (Fig. 22).

In *Drosophila* epithelial wing cells, the complex of FZ-DSH antagonizes the activity and localization of VANG-PK complex (Bastock et al., 2003; Goodrich and Strutt, 2011; Strutt, 2001; Strutt and Strutt, 2009). In addition, in *Drosophila* wing and abdominal epithelial cells, *fz* genetically and physically interacts with *vang* (Lawrence et al., 2004; Wu and Mlodzik, 2008). Therefore, we generated *vang-1* and *fz* double mutants *vang-1(tm1422),mig-1(n687)*; *vang-1(tm1422),cfz-2(ok1210)*; and *vang-*

1(tm1422),lin-17(n677) to investigate whether *vang-1* genetically interacts with *fz* genes. *vang-1(tm1422),mig-1(n687)* (VC4 87% ± 8, n=78) and *vang-1(tm1422),cfz-2(ok1210)* (VC4 68% ± 2, n=61) displayed similar penetrance of A/P directed neurite outgrowth defects as *vang-1(tm1422)* (VC4 69% ± 2, n=543) (Table 3). We also observed *vang-1(tm1422),lin-17(n677)* double mutants at L4 stage and found the penetrance of the double mutants (VC4 28% ± 6, n=121) to be similar to *vang-1(tm1422),cyIs3* L4 (VC4 25% ± 1, n= 208) animals (Table 3). These findings suggest that *vang-1* does not genetically interact with the three *fz* homologs examined.

3.10 Overexpression of *vang-1* results in ectopic A/P neurite

We showed that loss of *vang-1* activity results in ectopic A/P directed neurites, suggesting that *vang-1* is required to maintain correct neurite orientation via suppression of ectopic neurite outgrowth. Therefore, we asked whether overexpression of *vang-1* would lead to a suppression of VC4 and VC5 L/R oriented neurite formation. We used the *unc-4* promoter to drive the expression of *vang-1* in VC neurons in wild-type *cyIs4* animals. We found that overexpression of *vang-1* mimics the *loss-of-function* (*lof*) *vang-1* phenotype in 23-24% of VC4 neurons (n=77-96) and 27-28% of VC5 neurons (n=79-99) (Fig. 23A). This result suggests that the appropriate dose of *vang-1* activity in VC4 and VC5 neurons is necessary to maintain neurite outgrowth. Our finding of *vang-1* overexpression-induced *lof* phenotype is consistent with *vang-1* overexpression studies reported in *Drosophila* and vertebrate models (Jessen et al., 2002; Park and Moon, 2002; Wallingford et al., 2001). Interestingly, overexpression of *vang-1* in the vulva-distant VC6 neurons did not result in neurite polarity defects (1-2%, n=100-113) (Fig 23B).

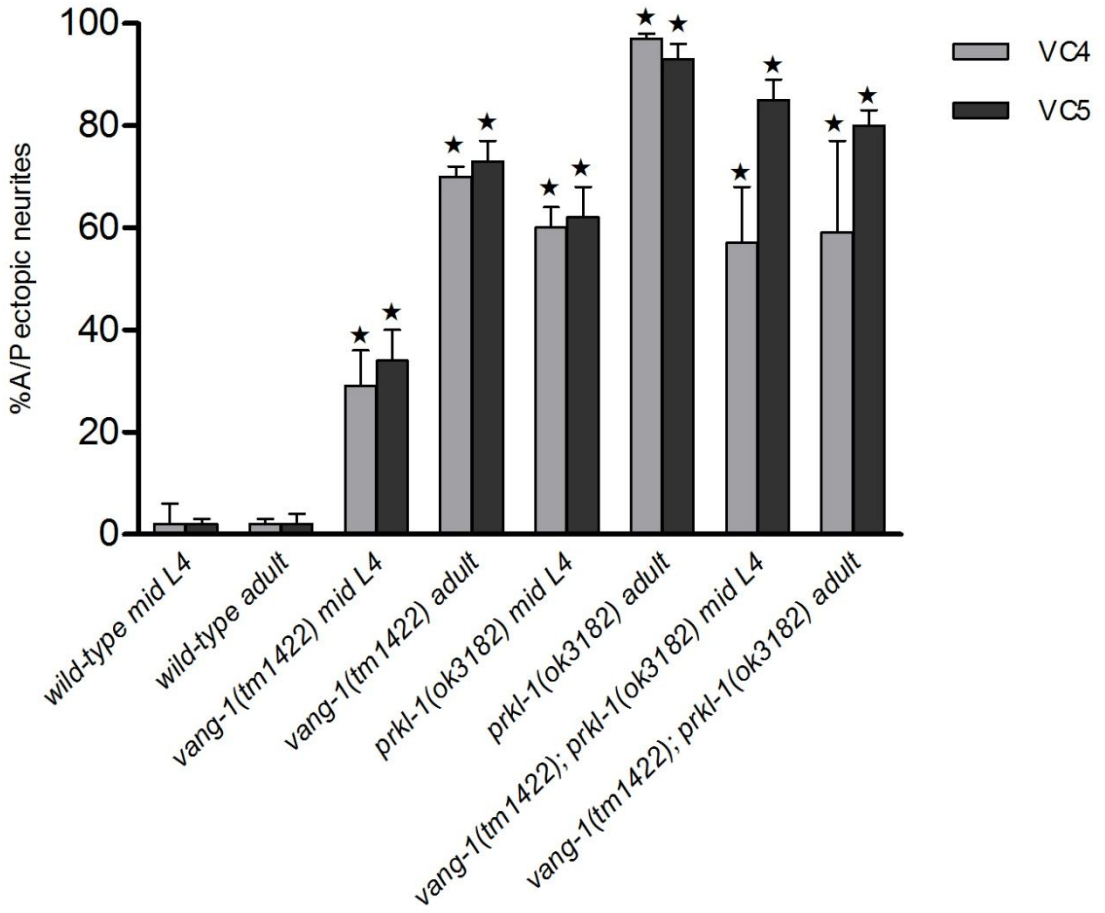

Figure 22. Penetrance of anterior-posterior neurites in *prkl-1(ok3138)* single mutants and *prkl-1(zy11);vang-1(tm1422)* double mutants from early L4 to adulthood. The penetrance of the *vang-1(tm1422);prkl-1(ok3138)* double mutant does not exceed the penetrance of the *prkl-1(ok3138)* single mutant. n>100 in all strains, errors bars indicate standard error of the mean; *p<0.05 compared to wild-type using one-way analysis of variance Bonferroni's multiple comparison test.

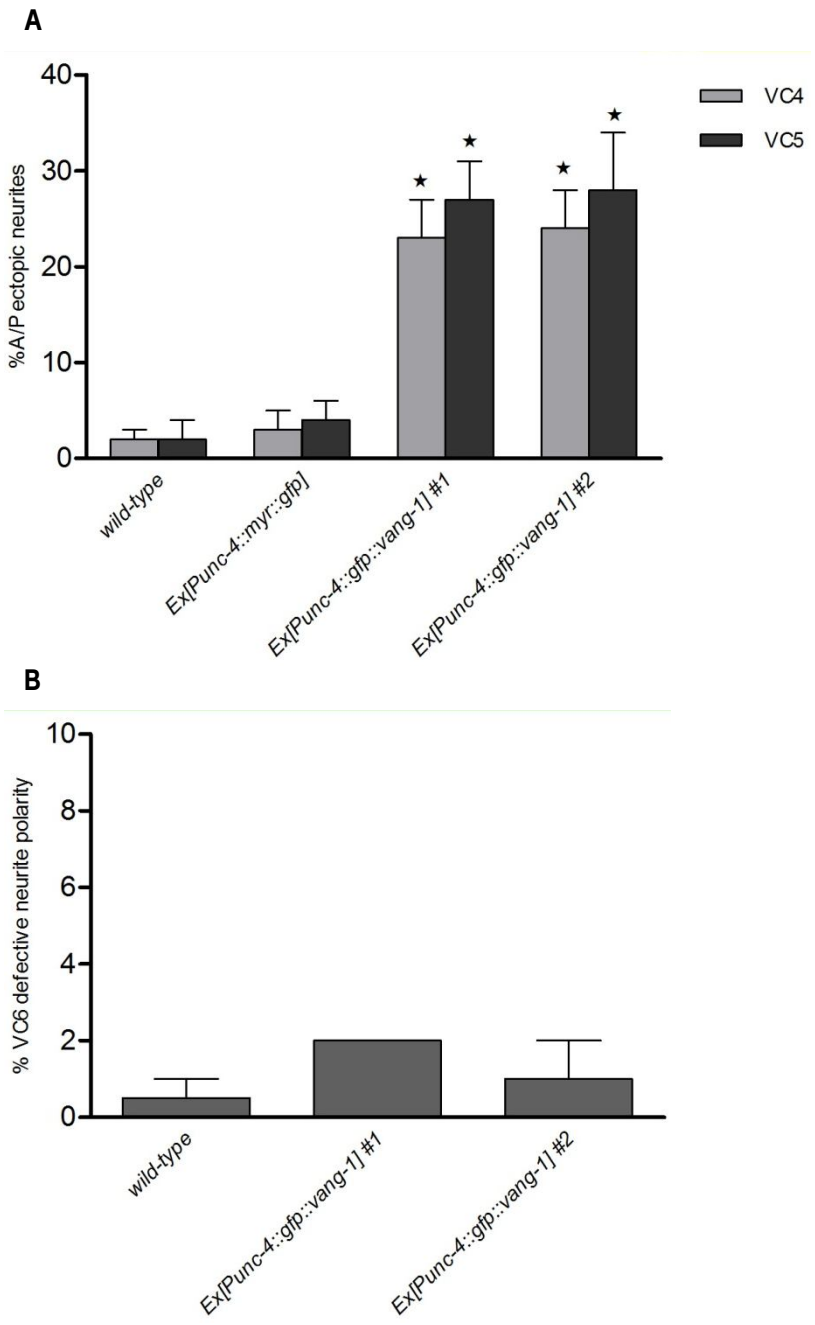

Figure 23. Overexpression of VANG-1. *Punc-4::gfp::vang-1* was expressed in wild-type, *cyIs4* animals. Wild-type animals expressing *Punc-4::myr::gfp*, a translational plasmid expressing myristoylated GFP, were used as control. (A) A gain-of-function phenotype seen in VC 4 and VC5 resembles the loss-of-function A/P ectopic neurite in two independent extra-chromosomal lines. (B) The overexpression of VANG-1 did not affect the orientation of VC6. n>70 in all strains, error bars represent standard error of the mean, *p<0.05 compared to wild-type using analysis of variance and Bonferroni's multiple comparison post hoc test.

3.11 VANG-1, PRKL-1 and DSH-1 are localized symmetrically around the plasma membrane of VC4 somas in wild-type and mutant backgrounds

We previously showed that VANG-1 is expressed in VC motor neurons and vulval epithelial cells and *vang-1* acts both cell and non-cell autonomously (Fig. 17-19). Therefore, we wanted to further examine where VANG-1 is localized in VC4 and VC5 neurons. One possibility is that VANG-1 might be localized in the protrusion site opposite the vulva cells as VANG-1 functions to suppress A/P directed neurite outgrowth. To clearly visualize the subcellular localization of VANG-1, we used the *unc-4* promoter to drive the expression of GFP::VANG-1 fusions in the VC neurons during the late L3 stage as it is the developmental stage in which neurite formations were first observed. *Punc-4::gfp::vang-1* rescues *vang-1* polarity defects and is therefore functional and can be used as a substitute for endogenously expressed VANG-1 in studying VANG-1 localization. *Punc-4::gfp::vang-1* and *Plin-11::rfp* were integrated into wild-type animals.

Given the transmembrane nature of VANG, it is not unexpected that expression of GFP-VANG-1 showed GFP localization around the plasma membrane (Fig 24A-C). GFP-VANG-1 appeared to be expressed symmetrically and uniformly around the plasma membrane. In addition, we detected no obvious signs of GFP-VANG-1 enrichment at the membrane region opposite the vulva cells or on the neurite leading edge protrusion sites. To accurately determine the localization symmetry of GFP-VANG-1 expression, we undertook a quantitative image analysis of anterior and posterior membrane of VC4 neurons expressing GFP-VANG-1. A line-scan plot measuring the intensity of GFP expression was drawn around the periphery of cells and the anterior-posterior intensity ratio (IR) was calculated with an IR ratio between 1.2 and 0.8 considered as symmetrical

(Fig. 25). IR ratio greater than 1.2 indicates asymmetrical localization with greater GFP intensity along the posterior membrane and IR ration less than 0.8 implies greater GFP expression along the anterior membrane. Quantification of the GFP-VANG-1 signal showed symmetry in anterior and posterior localization (88% IR 1.2-0.8, n=16) (Fig. 26). Our findings suggest that, unlike *Drosophila* epithelium planar polarity, asymmetric localization of VANG-1 is not required to regulate neuronal polarity. To determine whether the localization of VANG-1 is dependent on *prkl-1*, we crossed the integrated *Punc-4::gfp::vang-1* transgene into *prkl-1(ok3182)*. Interestingly, the localization pattern of GFP-VANG-1 did not appear to be significantly affected in the *prkl-1(ok3138)* mutant background (Fig 24D-F). GFP-VANG-1 remained symmetrically distributed in a uniform manner in the majority of *prkl-1(ok3182)* mutants (89% IR 1.2-0.8, n=18) (Fig. 26).

We next asked where PRKL-1 and DSH-1 are localized during the period of neurite outgrowth. We used genome integrated *Punc-4::gfp::prkl-1* and *Punc-4::gfp::dsh-1* to examine the localization of PRKL-1 and DSH-1. We found that GFP-PRKL-1 is also symmetrically localized around the plasma membrane (82% IR 1.2-0.8, n=32) (Fig. 26 and Fig. 27A-C). Unlike GFP-VANG-1, GFP-PRKL-1 is localized in a punctate pattern. Similarly, GFP-DSH-1 also formed puncta and appeared to be symmetrically localized along the cell membrane (92% IR 1.2-0.8, n=13) (Fig. 26 and Fig. 28A-C). The membrane localization of GFP-PRKL-1 and GFP-DSH-1 suggest that PRKL-1 and DSH-1 are recruited to the plasma membrane.

To investigate whether the localization of PRKL-1 and DSH-1 are dependent on each other and/or VANG-1, we crossed *Punc-4::gfp::prkl-1* into *vang-1(tm1422)* and *dsh-1(ok1445)* mutant and *Punc-4::gfp::dsh-1* into *vang-1(tm1422)* background. The

expression pattern of GFP-PRKL-1 was not significantly altered in *vang-1(tm1422)* (80% IR 1.2-0.8, n=26) (Fig. 26 and Fig. 27D-F) and *dsh-1(ok1445)* (90% IR 1.2-0.8, n=21) (Fig. 26 and Fig. 27G-I) background as GFP-PRKL-1 puncta remained evenly localized along the anterior and posterior region of the cell membrane. The localization of GFP-DSH-1 in *vang-1(tm1422)* also did not substantially change (90% IR 1.2-0.8, n=20) compared to wild-type animals (Fig. 26 and Fig. 28D-F). These results suggest that localization of VANG-1, PRKL-1, and DSH-1 may not be dependent on each other's activity.

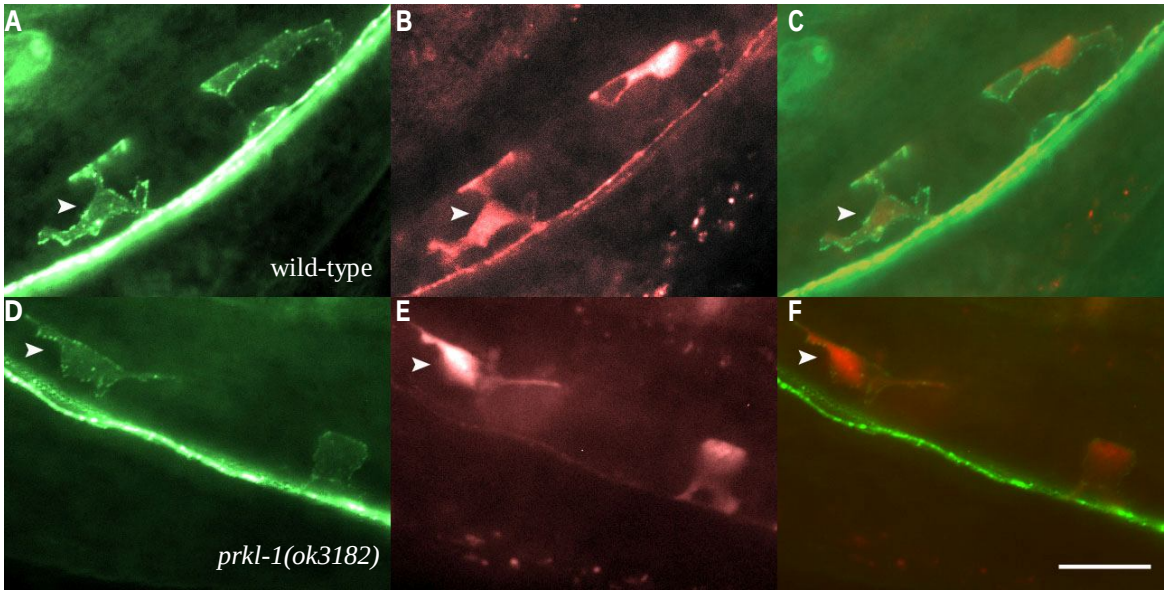

Figure 24. VANG-1-GFP fusions in VC neurons are localized to the plasma membrane during neuritogenesis. Representative images of GFP-tagged VANG-1 in VC4 and VC5 neurons during late L3. GFP-fusion proteins were expressed transgenically from *Punc-4* promoters. LIN-11::RFP was used to label the cytoplasm of VC neurons (B and E). VANG-1::GFP is localized uniformly around the plasma membrane of VC4 (A-C) and the localization pattern retains its symmetry in *prkl-1(ok3182)* mutants (D-F). Arrowheads denote VC4 and scale bar represents 10 μm.

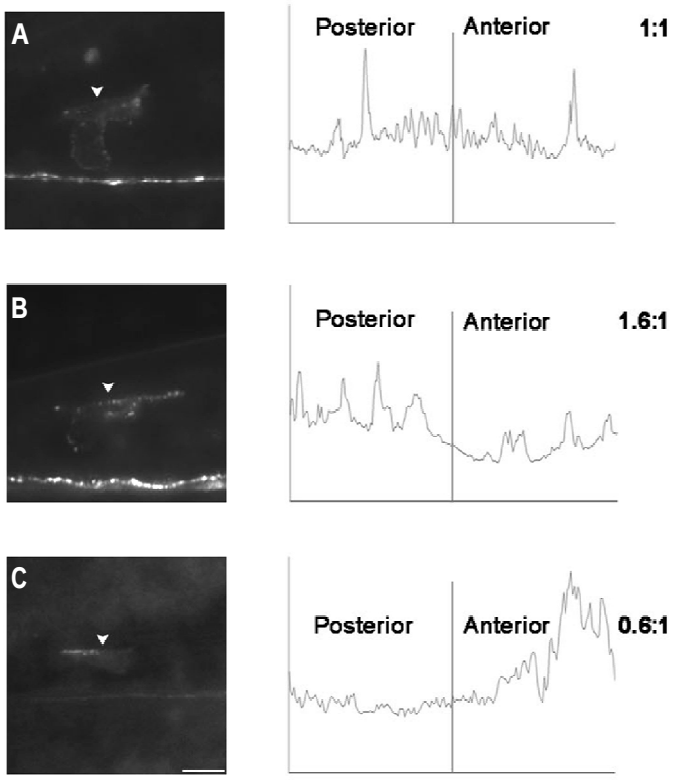

Figure 25. Representative pictures of symmetric and asymmetric localizations of VANG-1::GFP and PRKL-1::GFP. *unc-4p::gfp::vang-1* expression in wild-type animals (A&B). VANG-1::GFP is localized symmetrically around the plasma membrane of VC4 (A). A small percentage of animals (Fig. 26) display asymmetric VANG-1::GFP localization along the posterior side of the plasma membrane of VC4 (B). *unc-4p::gfp::prkl-1* expression in *vang-1(tm1422)* mutants (C). Symmetrical localization of PRKL-1::GFP is disturbed in a small percentage of *vang-1(tm1422)* mutants displaying more PRKL-1::GFP expression along the anterior side of the plasma membrane (C). The graphs represent line-scan intensity readings of the GFP expression around the cell plasma membrane starting from the arrowhead in clockwise directions; the Y axis represents the arbitrary GFP intensity reading and the X axis indicates the position of each GFP reading along the periphery of the cell.

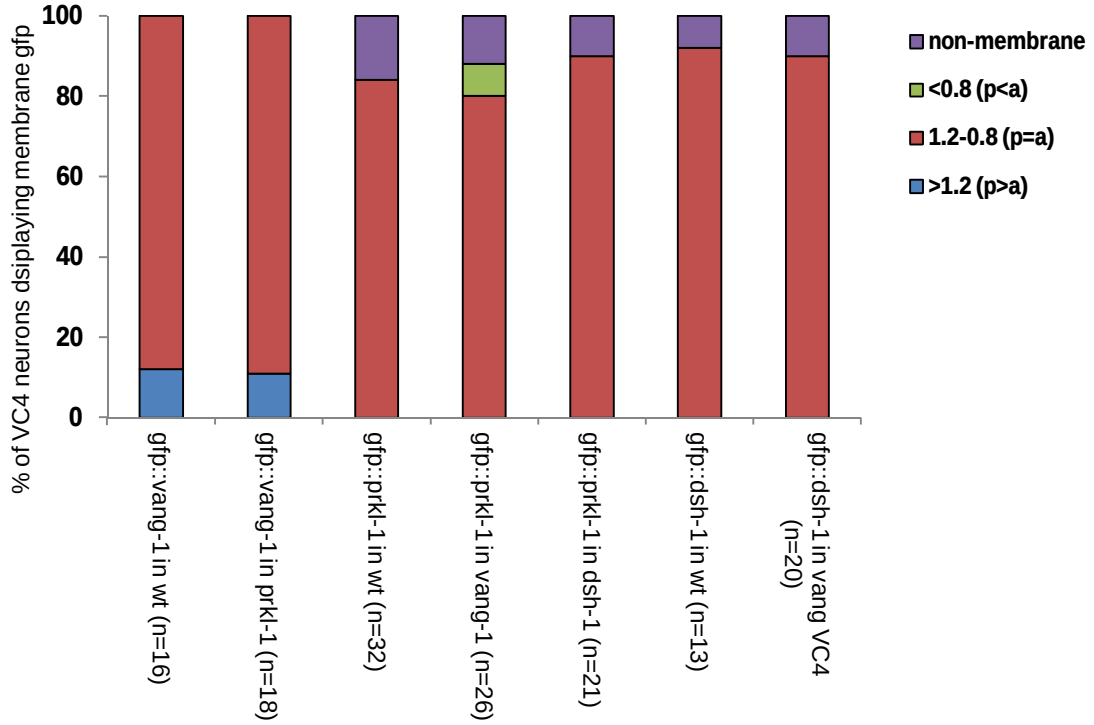

Figure 26. Percentage of average VC4 dorsal to ventral intensity ratio of each genotype. GFP::VANG-1,GFP::PRKL-1, GFP::DSH are localized symmetrically around the plasma membrane and the localization patterns are not affected in mutant backgrounds. To calculate the posterior/anterior intensity ratio, using the AxioVision measurement tool, a line was drawn vertically along the LR axis across the middle of the cell body to divide the perimeter of the cell into two equal lengths. Another line was drawn around the cell periphery to measure the intensity of GFP signal of the pixels. The cell's average value of posterior intensity readings were divided by the average value of anterior readings to obtain the posterior/anterior ratio. Posterior/anterior ratios between 1.2 and 0.8 are considered to represent symmetric localizations.

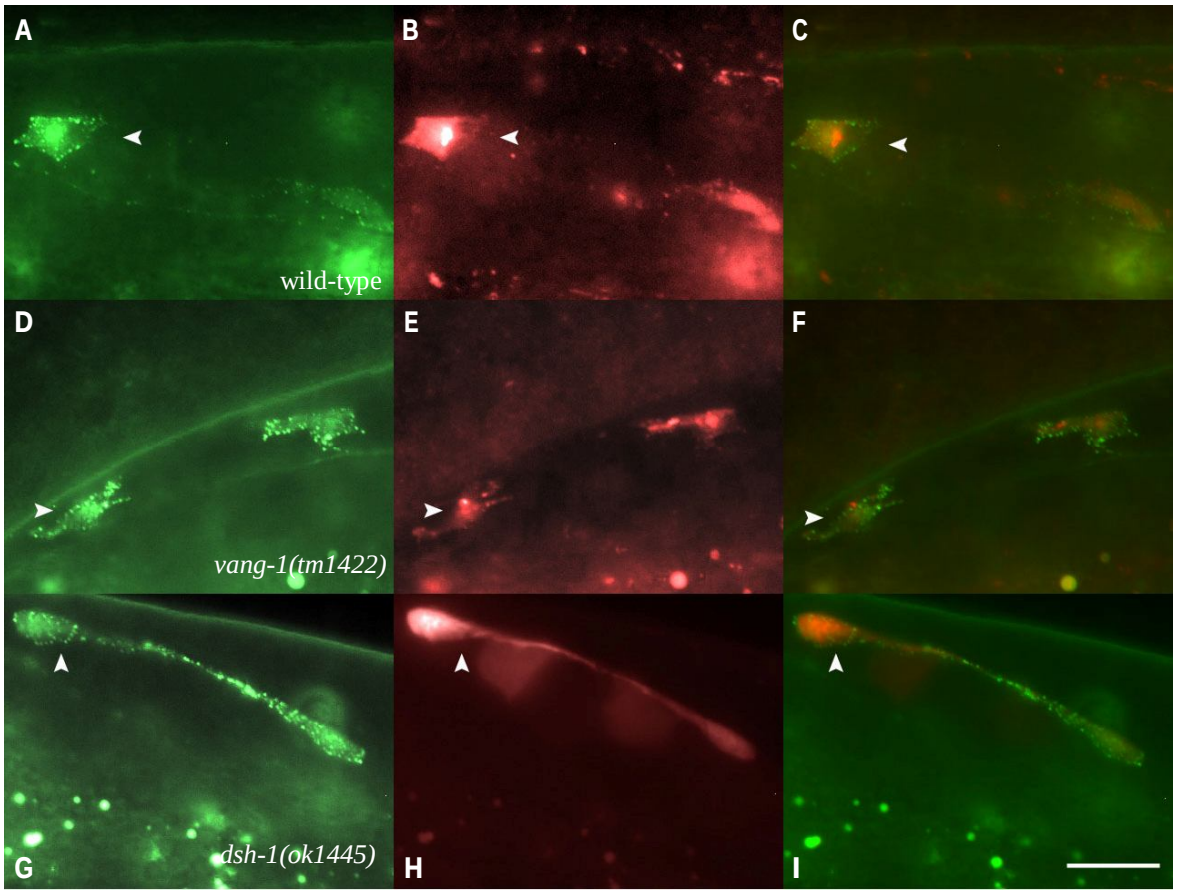

Figure 27. PRKL-1-GFP fusions in VC neurons are localized to the plasma membrane during neuritogenesis. Representative images of PRKL-1::GFP in VC4 and VC5 neurons during late L3. PRKL-1::GFP fusion proteins were expressed transgenically from *Punc-4* promoters. LIN-11::RFP was used to label the cytoplasm of VC neurons (B, E, and H). PRKL-1::GFP is evenly localized in punctate manners in the cytoplasm and around the plasma membrane in wild-type animals (A-C). Localization of PRKL-1::GFP is not affected in *vang-1(tm1422)* (D-F) and *dsh-1(ok1445)* mutants (D-I). Arrowheads denote VC4 and scale bar represents 10 μm.

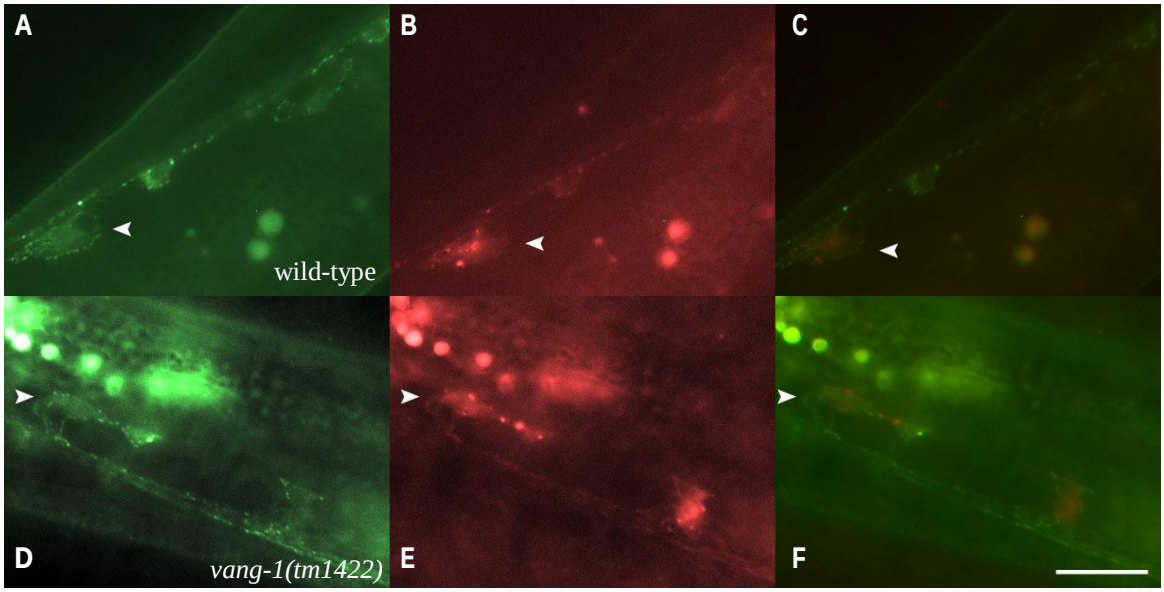

Figure 28. DSH-1-GFP fusions in VC neurons are localized to the plasma membrane during neuritogenesis. Representative images of GFP-tagged DSH-1 in VC4 and VC5 neurons during late L3. DSH-1:: GFP fusion proteins were expressed transgenically from *Punc-4* promoters. LIN-11::RFP was used to label the cytoplasm of VC neurons (B and E). DSH-1::GFP is localized around the plasma membrane of VC4 and VC5 neurons in wild-type (A-C) and *vang-1(tm1422)* (D-F) animals. Arrowheads denote VC4 and scale bar represents 10 μm.

3.12 A forward genetic screen identified alleles of *vang-1, prkl-1,* and *dsh-1* as regulators of neurite outgrowth

To identify new components in the *vang-1/prkl-1* pathway with *vang-1*-like defects, we performed a forward genetic screen covering approximately 15,000 genomes for VC4 and VC5 neurite outgrowth mutants (Fig. 29A). We recovered a total of 12 *nde* mutants and through genetic mapping and complementation tests, placed them into four complementation groups (Fig. 29B). All of the mutants showed the *vang-1*-like phenotype as they displayed an ectopic A/P directed neurite. No obvious axon guidance and branching defects were observed. Neurite polarity defective phenotype rescue with PCR fragments and DNA sequencing revealed that the *nde-2(zy17), (zy18),* and *(zy19)* mutants are alleles of *prkl-1* and *nde-3(zy12)* is an allele of *dsh-1*. The identity of the remaining alleles of *nde-4* and *nde-5* mutants is not known.

A

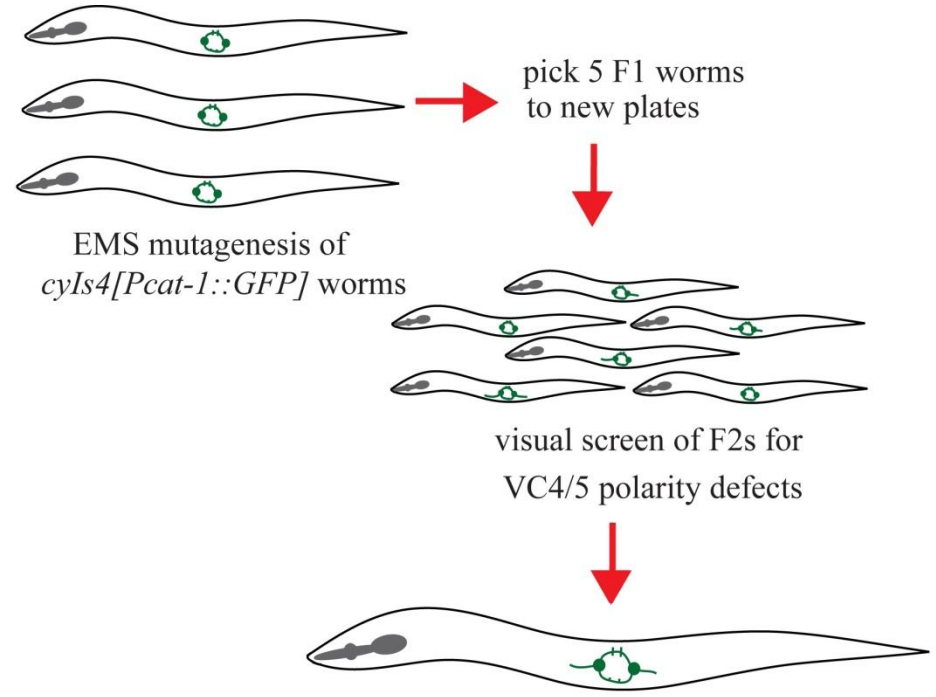

B

gene	# alleles	alleles	Closest homologues (*Drosophila*) (mouse)
vang-1/nde-1	3	***zy1, zy2, zy10***	Van Gogh VANGL1-2
prkl-1/nde-2	3	***zy17, zy18, zy19***	Prickle PRICKLE1-2
dsh-1/nde-3	1	***zy12***	Disheveled DVL1-3
nde-4	6	***zy7, zy20, zy21 zy22, zy23, zt24***	unknown
nde-5	2	***zy25, zy26***	unknown

Figure 29. Forward genetic screen for identifying VC4 and VC5 neurite outgrowth mutants. (A) wild-type cyIs4 animals were subject to mutagenesis by ethyl methanesulfonate (EMS) to induce point mutations in the genome. F2 progeny were visually screened for VC4 and VC5 neurite polarity defects. (B) A total of fifteen *neurite-defective* (*nde*) mutant alleles were assigned to five complementation groups. Three alleles of *vang* and *pk* homologs and one allele of *dsh* homolog were identified.

CHAPTER 4

DISCUSSION

4.1 VANG-1 suppresses growth cone formation along the A/P axis

Planar cell polarity is defined as the coordinated orientation and polarization of cells and cellular structures along a specified body axis (Vladar et al., 2009). The orientation of the VC motor neurons can therefore be considered as a form of planar cell polarity. VC1-3, and VC6 project their neurites along the A/P axis while the vulva flanking VC4 and VC5 neurons extend their neurites around the L/R axis of the vulva. We showed that VC4 and VC5 ectopic A/P directed neurite defects in *vang-1* mutants become more severe as the animals develop from L4 to adulthood. The increase in polarity defects indicates that *vang-1* is involved in maintaining neuronal polarity by blocking ectopic neurite outgrowth from the early L4 stage onward into adulthood.

Observation of neuritogenesis from the time of lamellipodial/filopodial protrusions conducted by our group revealed that beginning in late L3, all six VC neurons initially polarize and extend neurites bilaterally along the A/P axis. As the animals progress by early-mid L4 stage, VC1, VC2, VC3, and VC6 neurons extend their neurites along the A/P axis. VC4 and VC5 neurons, in contrast, start to alter their polarity from bilateral to unilateral A/P directed toward the developing vulva. By late L4 stage, the unilateral A/P projection bifurcates into two neurites enveloping the vulva along the L/R axis. *vang-1(tm1422)* mutants, not unlike wild-type animals, initially polarize VC4 and VC5 nascent neurite outgrowths along the A/P axis at early L4 stage. By mid L4 stage, *vang-1(tm1422)* mutants also polarize neurites toward the developing vulva. However,

by late L4 stage, neuronal polarity failed to be maintained as *vang-1(tm1422)* animals displayed the emergence of A/P directed ectopic neurite outgrowths. In vertebrates, the PCP-dependent directed neuronal migration defects observed is largely the result of failure in polarization and stabilization of filopodia/lamellipodia protrusions (Jessen et al., 2002). Therefore, the emergence of A/P ectopic neurites can be seen as defects in polarization of the filopodia/lamellipodia protrusion at the leading edge. Here, we show that *vang-1* also confers directionality to neurons not in the form of directed migration but rather in the form of maintaining neuronal polarity by suppressing neurite emergence along the A/P body axis.

It is known that *Van Gogh* interacts with other core PCP genes to regulate *Drosophila* epithelium polarity. Our candidate gene approach revealed that *prkl-1* and *dsh-1* play a role in controlling the polarization of neurite outgrowth. Similar to *vang-1*, the investigation of neuritogenesis in *prkl-1* and *dsh-1* mutants also demonstrated that *prkl-1* and *dsh-1* function to maintain L/R neurite polarization. While loss of *prkl-1* does not significantly affect the L/R neurite guidance, loss of *dsh-1* results in a relatively higher penetrance of bipolar A/P neurite polarity defects compared to *vang-1* and *prkl-1* mutants, suggesting that *dsh-1* may also play a role in L/R neurite guidance.

It is intriguing that loss of *vang-1* and *prkl-1* do not disturb the initial polarization of nascent neurite growth cone toward the vulva and the subsequent guidance of bifurcated L/R oriented neurites around the vulva. Therefore, it is possible that VC4 and VC5 neurons use mechanisms independent of *vang-1* and *prkl-1* to regulate the polarity of L/R oriented neurites. Several findings have demonstrated that the vulva acts as guidepost cells for developing neurons. VC4 and VC5 in vulvaless mutants orient and

project their neurites along the A/P axis, suggesting that the presence of the vulva is required for L/R neurite polarization (Li and Chalfie, 1990). In addition, UNC-6/Netrin cues secreted by the vulva precursor cells (VPC's) have been shown to interact with the UNC-40 receptor present in the developing growth cone of the HSN neurons to polarize the ventrally-directed axonal outgrowth (Adler et al., 2006; Asakura et al., 2007). Thus, VC4 and VC5 could sense vulva-derived L/R polarization cues via an unidentified pathway that is independent of *vang-1* and *prkl-1*. Taken together, in the absence of *vang-1* and *prkl-1*, VC4 and VC5 are responsive to both vulva-derived cues and to A/P polarization cues that would normally be silenced by *vang-1* and *prkl-1*-dependent signalling pathway.

Recent studies have provided better insights into the molecular mechanisms of *Van Gogh* in neuronal development. *Drosophila* WNT5a and Van Gogh have been shown to regulate axon guidance of Mushroom Body neurons in a partially redundant manner with FZ (Shimizu et al., 2011). In addition, a recent study has shown that the mouse *vangl2* homolog positively regulates WNT5a-activated PCP signalling at the tips of commissural axon growth cones to control axon guidance (Shafer et al., 2011). While these studies suggest that interactions between WNTs, FZs and Van Gogh are involved in neuronal development, our analysis of *wnt*s and *fz*s demonstrated that their role in VC4/5 polarity remains to be conclusively determined. There are five *wnt* (*cwn-1*, *cwn-2*, *egl-20*, *lin-44*, *mom-2*) and four *fz* homologs (*lin-17*, *mig-1*, *cfz-2*, *mom-5*) in *C. elegans*. We showed that, individually, *wnt*s *lin-44* and *egl-20* and *fz*s *lin-17*, *mig-1*, *cfz-2*, *mom-5* do not regulate VC4/5 polarity. However, it is possible that *wnt*s may function redundantly as we have not investigated the phenotype of different combinations of *wnt* mutations.

Our analysis of the double *lin-1,mig-1* and *lin-17,cfz-2* mutants, and triple *lin-17,mig-1,cfz-2* provided evidence that *lin-17*, *mig-1*, and *cfz-2* are not involved and do not function redundantly in regulating neuronal polarity. However, some of the double mutants display vulva defects and in addition, *lin-17* mutation affects VC4 and VC5 cell fate specification. Since the VC4 and VC5 neurons likely respond to vulva-derived cues and the severity of ectopic neurite defects increases with time, the presence of defective vulva and change of cell fate specification make it difficult to accurately assess neurite polarity in the double and triple mutants.

4.2 VANG-1 acts autonomously and non-autonomously to mediate neurite orientation

Our cell-specific rescue experiments indicate that VANG-1 acts cell-autonomously within VC4 and VC5 neurons and also non-cell autonomously in the surrounding vulva epithelial cells. One of the hallmark characteristics of PCP genes is that some genes act both cell-autonomously and non-cell-autonomously (Goodrich and Strutt, 2011; Vladar et al., 2009). In *Drosophila*, *fz* and *vang* act both cell and non-cell-autonomously, whereas *dsh*, *pk*, and *diego* (*dgo*) function only cell-autonomously (Wu and Mlodzik, 2009). Studies on the migrating zebrafish hindbrain motor neurons showed that non-cell-autonomous activity of *fz* homolog *fz3a* and *fmi* homologs *celsr1a, celsr1b,* and *celsr2* from the neuroepithelium and cell and non-cell-autonomous function of *Van Gogh* homolog *tri* are required to prevent neurons from aberrantly migrating radially toward the ventricle and integrating into the neuroepithelium (Formstone and Mason, 2005a; Jessen et al., 2002; Wada et al., 2006). Homologs of *pk*, on the other hand, function in distinct manners. *pk1a* functions non-cell-autonomously within

neuroepithelium whereas *pk1b* acts cell-autonomously within the migrating hindbrain motor neurons (Carreira-Barbosa et al., 2003; Rohrschneider et al., 2007).

The partial rescue of neuronal polarity defects by cell and non-cell-autonomously expressed VANG-1 indicates that VANG-1 activity resides within VC4 and VC5 neurons and the epithelial cells, including the vulva hypodermal cells. Indeed, VANG-1 is expressed in the VPCs and regulates the orientation of the VPCs (Green et al., 2008). It is thus possible that VANG-1 could be one of the vulva-derived cues. However, the function of vulva-derived VANG-1 is likely not involved in the initial polarization of neurites toward the vulva as loss of *vang-1* does not affect L/R directed outgrowth. It is reasonable to speculate that the non-cell-autonomous partial rescue is achieved by communication between epithelia-expressed VANG-1 and unidentified receptors present in VC4 and VC5 neurons. Moreover, the finding that combined cell and non-cell-autonomously expressed VANG-1 results in full rescue of *vang-1* defects suggest that cell and non-cell-autonomously expressed *vang-1* act in parallel pathways.

4.3 Does DSH-1 act in the same pathway or in a parallel pathway with VANG-1 and PRKL-1?

Our analysis of A/P directed ectopic neurites penetrance in *prkl-1* single and *vang-1;prkl-1* double mutants suggest that *prkl-1* acts in the same pathway as *vang-1* to suppress ectopic A/P neurite outgrowth. We also showed that *dsh-1* is involved in controlling neurite polarity as *dsh-1* mutants display A/P neurite polarity defects. In addition, work from our group showed that *dsh-1* acts both cell and non-cell-autonomously. Unlike *vang-1* and *prkl-1* mutants which show a relatively low penetrance

of bipolar A/P neurite polarity defects, *dsh-1 mutants* show a relatively high penetrance of bipolar A/P neurite polarity defects. In addition, *dsh-1;vang-1* and *dsh-1;prkl-1* mutant backgrounds exhibited an increase in bipolar A/P neurite polarity defects (Sanchez-Alvarez et al., 2011), indicating the possibility of *dsh-1* acting in a pathway parallel to *vang-1* and *prkl-1*. However, *dsh-1;vang-1* and *dsh-1;prkl-1* double mutants also showed defective vulva morphology, suggesting that bipolar A/P polarity defects may be a secondary effect resulting from vulval defects. Alternatively, the increase in A/P bipolar defects can also suggest *dsh-1* and *vang-1/prkl-1* acting in partially redundant pathways to regulate neurite extension along the L/R axis of the vulva. Interestingly, *vang-1* and *dsh-1* A/P tripolar neurite polarity defects can be rescued by the expression of genomic *prkl-1* (Sanchez-Alvarez et al., 2011). The rescue of *dsh-1* A/P tripolar defects suggests that *prkl-1* acts downstream of both *vang-1* and *dsh-1* to regulate neuronal polarity.

Taken together, it is reasonable to speculate that *dsh-1* may control different aspects of neuronal polarity in two distinct *vang-1*/*prkl-1*-dependent and *vang-1/prkl-1*-independent pathways; the former pathway involved in maintaining neuronal polarity and the latter in controlling L/R neurite extension. *dsh* is known to function in both the canonical β-catenin-dependent *wnt* and the non-canonical *wnt*-PCP signalling pathways (Gao and Chen, 2009). Therefore, it is possible that a *wnt* canonical pathway may also regulate neuronal polarity. Indeed, it has been shown that two distinct WNT-induced pathways can regulate the orientation of the VPC's (Green et al., 2008). In addition, several studies have revealed that *dsh-1* functions in a *vang-1*-independent manner via WNT-activated FZ signalling pathways to regulate synaptic formations (Klassen and Shen, 2007) and neurite outgrowth (Song et al., 2010) in *C. elegans*. It has been reported

that WNT/LIN-44 localizes FZ/LIN-17 to specific domains in axons where presynaptic vesicles are excluded and FZ/LIN-17 in turn activates DSH-1 to inhibit ectopic synaptic formations (Klassen and Shen, 2007). Moreover, DSH-1 binds to the ROR receptor tyrosine kinase ROR-2/CAM-1 and functions downstream of WNT/CWN2 and the FZs CFZ-2 and MIG-1 to regulate head motor neurons neurite outgrowth (Song et al., 2010). Therefore, these studies provide examples that *dsh-1* can modulate some aspects of neuronal development, including synaptic formation and neurite polarity independent of *vang-1*.

4.4 Polarized PCP protein localization does not appear to be required to maintain VC4/5 polarity

Asymmetric localization of PCP proteins is required for correct tissue polarity of *Drosophila* epithelia cells and for some aspects of vertebrate development. In *Drosophila* wing epithelia cells, VANG and PK are localized at proximal edges and FZ and DSH are localized at the distal edges of the membrane (Bastock et al., 2003; Das et al., 2004; Jenny et al., 2003; Jenny et al., 2005; McNeill, 2010). In zebrafish dorsal mesodermal cells undergoing CE, PK and DSH were respectively localized at the anterior and posterior side of the cell membrane (Ciruna et al., 2006; Yin et al., 2008). In mouse cochlea, *vang-1* homolog VANGL2 localizes at the proximal edges and the *dsh* homologs DVL1 and DVL2 localize at the distal edges of hair cells (Montcouquiol et al., 2006; Wang et al., 2006a; Wang et al., 2005b). However, asymmetric localizations were not observed in a number of PCP-regulated developmental events. In mouse, VANGL2 and DSH localized in a symmetric manner in neuroepithelium cells undergoing neural tube closure (Torban et al., 2008; Wang et al., 2006a). Similarly, chicken PRICKLE1 and

DVL have been shown to localize symmetrically in the elongating myocytes (Gros et al., 2009). It has been proposed that the variability of localization patterns reported in different vertebrate models may be evidence of dynamic and transient expressions of PCP proteins. Therefore, it may be difficult to observe the same expressions at a specific time point as cells make and break contacts with adjacent cells during the course of their migration (Vladar et al., 2009; Zallen, 2007). In addition, there is no evidence of asymmetric localizations of FZ, PK, VANG, and DSH reported in *Drosophila* Mushroom Body axons undergoing axonal branching (Ng, 2012).

We found that VANG-1, PRKL-1, and DSH-1 are localized symmetrically around the plasma membrane of VC4 neurons. While the localization of PRKL-1 and DSH-1 in the form of puncta resembles the localization of PK and DSH observed in zebrafish mesodermal cells, the composition and significance of the puncta are not well understood. In zebrafish, PK puncta appeared to be dynamic as the puncta were randomly distributed around the membrane prior to being anteriorly localized as the cells undergo CE (Yin et al., 2008). Similarly, *in vitro* characterization of DSH puncta suggested that DSH puncta are dynamic assemblies of proteins (Schwarz-Romond et al., 2005; Smalley et al., 2005). The symmetric localizations reported in our study can be attributed to the dynamic nature of developing neurons. In *Drosophila*, it has been proposed that the arrangement and packing of epithelia cells affect PCP signalling (Ma et al., 2008a). Unlike *Drosophila* epithelia cells where PCP signalling propagates planar polarity in static group of tightly packed cells, neurons are highly dynamic as they break symmetrical shape by extending and retracting lamellipodia/filopodia and eventually forming neurites in response to extracellular cues. In addition, neurons also communicate with the underlying

neuroepithelium and guidepost cells (Randlett et al., 2011; Tada and Kai, 2009; Wada et al., 2006; Zhou et al., 2008). In this respect, neurons more or less resemble the migrating mouse neuroectodermal cells undergoing directed movement as they undergo cell shape deformation to retract and extend lamellipodia/filopodia according to the specified direction. Moreover, the GFP::VANG-1 fusion labels all VANG-1 isoforms, making visualization of post-translationally modified VANG-1, which may be asymmetrically localized, indistinguishable. Indeed, the activity and localization of mouse *vang* homolog VANGL2 is dependent on a graded level of Wnt5a-induced phosphorylation (Gao et al., 2011).

We did not observe any detectable change of VANG-1, PRKL-1, and DSH-1 localization in mutant backgrounds. Therefore, our findings suggest that membrane localization of VANG-1, PRKL-1, and DSH-1 is not dependent on one another. Our results are consistent with *Drosophila* studies which showed VANG localization is not affected by *pk* and *dsh* mutations as *vang* acts upstream of *pk* and *dsh* (Ng, 2012; Strutt and Strutt, 2007; Strutt, 2001). Indeed, work from our group indicates that *prkl-1* may function downstream of *vang-1* in some aspects of neuronal polarity as overexpression of PRKL-1 can rescue *vang-1* and *dsh-1* neurite polarity defects (Sanchez-Alvarez et al., 2011). In addition, it has also been demonstrated that in mouse neuroepithelium cells, DVL localization does not required VANGL2 activity (Wang et al., 2006a). Nonetheless, it is intriguing that the localization of PRKL-1 was not affected in *vang-1* backgrounds as *vang-1* likely acts upstream of *prkl-1* and is required to suppress A/P ectopic neurite outgrowth. It is plausible that in the absence of VANG-1, PRKL-1 may retain its

interaction with an unknown gene as neuronal polarity was not completely abolished in *vang-1* mutants.

Taken together with our *dsh-1* genetic analysis results and the rescue of neuronal polarity defects by *prkl-1*, the finding that DSH-1 localization was not disturbed in *vang-1* is consistent with *dsh-1* and *vang-1* interacting in parallel pathways. While *Van Gogh* has been shown to genetically and physically interact with *dsh* in invertebrate and vertebrate models (Bastock et al., 2003; Hoffmann et al., 2010; Jenny et al., 2003; Park and Moon, 2002; Shafer et al., 2011; Wang et al., 2006a), *dsh* is also capable of transducing PCP-like signalling independently of *Van Gogh* (Song et al., 2010; Wu and Herman, 2006). Conversely, it is also a possibility that V*an Gogh* can modulate cell polarity independently of *dsh* as the planar polarity of mouse limb bud elongation is modulated by a WNT5A-VANGL2-activated pathway (Gao et al., 2011). This study demonstrates that WNTs can bind to ligands other than FZ's and suggest that *dsh* activity is not required as *dsh* is generally activated upon binding with FZ's (Gao and Chen, 2009).

4.5 A model for VANG-1 and PRKL-1 mediated regulation of neuronal polarity

We show here the core PCP genes *vang-1*, *prkl-1*, and *dsh-1* modulate *C. elegans* neuronal polarity. Based on our findings, we propose that *vang-1*, *prkl-1*, and *dsh-1* are not involved in the establishment of neuronal polarity but rather function to maintain neuronal polarity by suppressing the emergence of ectopic neurites along the A/P body axis. Several studies have shown that vulval cells may act as guideposts to impart directionality to emerging neurites (Adler et al., 2006; Asakura et al., 2007; Li and Chalfie, 1990). We suggest the regulation of VC motor neuron polarity is controlled by

two polarity cues: the default A/P cues and the vulva-derived L/R cues. The vulva-flanking VC4 and VC5 are the only members of the VC motor neurons that are polarized along the L/R axis. In the absence of the vulva, VC4/5 take on the polarity of the vulva-distant VC1-3 and VC6 neurons (Li and Chalfie, 1990), indicating that all VC motor neurons are responsive to the default A/P cues. Therefore, cell-cell contacts between VC4/5 and the vulva cells likely re-polarize the orientation of neurite extension as contact-mediated cues have been shown to play a role in axon emergence (Randlett et al., 2011).

In support of vulva-mediated neurite orientation, our work demonstrated that *vang-1* and *dsh-1* are expressed in VC neurons and in the vulva epithelial cells and, in addition, act both cell and non-cell autonomously. We showed that *vang-1* expression in the epithelial cells brought about partial rescue of neurite polarity defects, suggesting the possibility that *vang-1* activity in the epithelial cells plays a role in regulating neuronal polarity. We also revealed that cell-autonomously expressed *vang-1* was able to partially rescue neuronal polarity defects. Moreover, full rescue was achieved by the combined expression of cell and non-cell autonomous expression of *vang-1*. Therefore, we reason that *vang-1* may function in two pathways and interact additively with one another to suppress ectopic A/P directed neurite outgrowths.

While our findings indicate that *vang-1* activity in the epithelial cells is required in silencing VC4/5 neurons' response to A/P outgrowth cues, we can only speculate what genes may communicate with the epithelial-expressed *vang-1*. Although Wnt/EGL-20 has been shown to interact with VANG-1 (Hoffmann et al., 2010), the WNTs ligands are unlikely candidates as they are secreted factors and are not expressed from the VC

neurons. However, it is possible *wnt*s may function in a *vang-1*-independent manner. Indeed, Wnt/CWN-2 has been shown to regulate *C. elegans* neuronal polarity via DSH-1 (Song et al., 2010), supporting our suggestion of the possibility of *dsh-1* acting in parallel to *vang-1*. The FZ receptors should also be considered as interacting partners of the vulva-expressed *vang-1* as we have not conclusively determined their roles and in addition, *Drosophila* FZ can bind directly to VANG (Wu and Mlodzik, 2008). Similarly, the seven-pass transmembrane FMI is also a viable candidate as it interacts and can bind with VANG in *Drosophila* (Strutt and Strutt, 2007). While strong *lof fmi-1* single mutants do not show VC4/5 neurite polarity defects, the *vang-1,fmi-1* double mutant showed a decrease of A/P ectopic neurites (Sanchez-Alvarez et al., 2011). This finding implies that *fmi-1* acts as a positive factor to promote neurite outgrowth. Taken together with *fmi-1* mutant phenotype, these findings suggest that PCP components involved in controlling VC4/5 neuronal polarity function in distinct manners from *Drosophila* PCP signalling. Our findings presented here point to the need of further investigation of *fz*s and *fmi-1* and identification of interacting partners of epithelial-expressed *vang-1*.

Our group showed that *prkl-1* acts cell-autonomously in the VC neurons and is expressed in a small subset of neurons including the VC neurons, the HSN neuron, and some neurons in the head and tail region (Sanchez-Alvarez et al., 2011). Taken together with our finding that *vang-1* and *prkl-1* function in the same pathway, it can be argued that *vang-1* in VC neurons interacts with *prkl-1* to maintain neuronal polarity. Indeed, several findings suggest that the interaction with *prkl-1* likely mediates the cell-autonomous function of *vang-1*. Overexpressed *prkl-1* prevents neurite formations in VC neurons and restores correct neurite polarity in *vang-1* and *dsh-1* mutants. Moreover,

RNAi-induced knockdown of *prkl-1* in wild-type animals at L4 stage results in A/P ectopic neurites emergence. Taken together with the rescue of *vang-1* neuronal polarity defects by *prkl-1* overexpression, PRKL-1 likely mediates VC4 and VC5 neuronal polarity through its interaction with cell-autonomously-expressed VANG-1.

In summary, I propose that the neuronal polarity of VC4 and VC5 is dependent on neuron-vulva cell contacts that first establish and subsequently maintain neuronal polarity via VANG-1 and/or DSH-1 induced activity of PRKL-1. Once activated, PRKL-1 is persistently required throughout neuritogenesis to maintain correct L/R neuronal polarity by silencing the default A/P-directed neurite outgrowth cues (Fig. 30). *vang-1/prkl-1* and *dsh-1* may function in parallel pathways to suppress ectopic neurite outgrowth. Additionally, work from our group indicates that *fmi-1* promotes neurite outgrowth (Sanchez-Alvarez et al., 2011). Therefore, the interaction between *fmi-1*'s neurite outgrowth promoting activity and *vang-1/prkl-1*'s neurite outgrowth inhibiting activity likely modulates the polarization of VC4/5 neurons (Fig. 30)

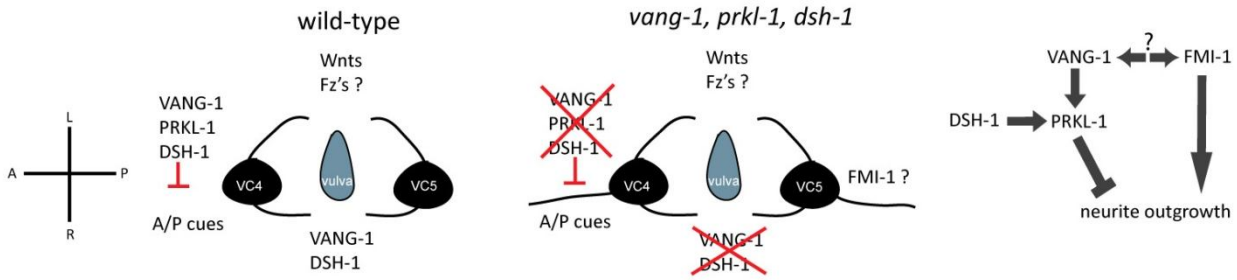

Figure 30. *vang-1*, *prkl-1*, and *dsh-1* cooperate in a PCP-like pathway to maintain the correct neuronal polarity. *vang-1*, *prkl-1*, and *dsh-1* suppress VC4/5 neurons' response to the default anterior-posterior (A/P) neurite outgrowth cues. In *vang-1*, *prkl-1*, and *dsh-1* mutants, the absence of PRKL-1 activity in the VC4/5 neurons, and loss of VANG-1 and DSH-1 activity in both VC4/5 and the epithelial cells, including the vulval epithelia, lead A/P ectopic neurite outgrowths as VC4/5 neurons respond to the default A/P neurite outgrowth cues. PRKL-1 appears to act downstream of VANG-1 and DSH-1 to inhibit ectopic neurite outgrowth. Additionally, DSH-1 may function in parallel to VANG-1 and PRKL-1 to polarize VC4/5 neurons in the early stage of neuritogenesis and to suppress VC4/5 response to A/P neurite outgrowth cues. In contrast, FMI-1 acts to promote neurite outgrowth. The role of FMI-1 in the *vang-1/prkl-1* PCP-like pathway remains to be determined.

4.6 Future Directions

The proposed speculative model contains a number of unanswered questions. What other genes are involved in *vang-1/prkl-1* neuronal polarity pathway? Forward genetic screens can be performed to identify new neurite defective mutants. A *vang-1* suppressor screen can also be carried out in order to identify new pathway components. Given the possibility of *dsh-1* acting in parallel pathway to *vang-1/prkl-1* in controlling L/R neurite extension, it is important to identify genes that interact with *dsh-1*. Forward genetic screens of *vang-1;prkl-1* double mutants for mutants that show an increase in A/P bipolar defects can be performed to obtain genes that function in the same pathway as *dsh-1*. In addition, what are the possible candidates for A/P guidance cues and receptors? Wnts have been shown to regulate neuronal polarity, and therefore represent likely candidates. Further genetic analysis of single and multiple *wnt* mutants will offer better understanding of the function of *wnt*s. Furthermore, what is the role of VANG-1 in vulval cells? It would be interesting to see if VANG-1 is one of the vulva-derived cues by using cell-specific promoters to drive the expression of *vang-1* dsRNA in the vulva cells to knockdown *vang-1* function. Moreover, the neurite promoting activity of *fmi-1* and its interaction with *vang-1*, *prkl-1*, and *dsh-1* remain to be explored. If *vang-1/prkl-1* and *fmi-1* act in separate pathways, overexpression of *fmi-1* in a *prkl-1* overexpression background may restore the correct neurite polarization.

Additionally, we are aware that our translational expression transgenes are expressed in wild-type animals and therefore represent subcellular localizations of overexpressed GFP-tagged proteins and do not represent the localization of endogenous proteins. Polyclonal antibodies stainings against endogenous PRKL-1, VANG-1, and

DSH-1 will illustrate more accurate localizations of endogenous PCP proteins. It would also be interesting to observe either the subcellular localizations of the existing overexpressed translational transgenes or antibodies stainings in vulva ablated animals to see how the localizations would be affected in the absence of the vulva.

4.7 Conclusion and Significance

In conclusion, we found that *vang-1*, a *C. elegans* homolog of a core component of the PCP signalling pathway *Van Gogh*, plays a role in modulating neuronal polarity. Subsequent candidate approach and forward genetic screens revealed alleles of *prkl-1* and *dsh-1*, homologs of the PCP-signalling genes *prickle* and *dishevelled* to also be modulators of VC4/5 neuronal polarity. Through genetic analysis, cell-rescue and overexpression experiments, we found that VANG-1/PRKL-1 and DSH-1 may act in parallel pathways to maintain neuronal polarity by silencing VC4 and VC5 response to an A/P neurite outgrowth cue. Moreover, asymmetrical localizations of VANG-1, PRKL-1, and DSH-1 are not required to maintain neuronal polarity. We show that VANG-1 and PRKL-1 interact in a PCP-like signalling pathway to maintain neuronal polarity by suppressing nascent neurite outgrowth responses to extrinsic cues.

While the biological significance of ectopic neurite suppression is not obvious as *vang-1*, *prkl-1*, and *dsh-1* do not display noticeable aberration in egg-laying behaviour, it is likely that *vang-1*, *prkl-1*, and *dsh-1* function to prevent aberrant innervations of ventral muscles by VC4 and VC5 as muscle innervations are accomplished by VC1-3 and VC6. Nonetheless, the results from this work provide novel information on the genetic pathways neurons employ to break neuronal symmetry as they project neurite extensions and maintain neuronal polarity. In addition, our findings shed more light on yet another

biological development mediated by the PCP signalling pathway. Since the PCP signalling pathway regulates a wide range of developmental events, elucidating the genetic interactions and molecular mechanisms used by such a highly conserved pathway may lead to possible therapeutic treatments for a variety of diseases, including nervous-system and neural tube closure-related diseases such as Parkinson's disease and spina bifida.

LITERATURE CITED

Adler, C. E., Fetter, R. D. and Bargmann, C. I. (2006). UNC-6/Netrin induces neuronal asymmetry and defines the site of axon formation. *Nat Neurosci* **9**, 511-8.

Adler, P. N., Krasnow, R. E. and Liu, J. (1997). Tissue polarity points from cells that have higher Frizzled levels towards cells that have lower Frizzled levels. *Curr Biol* **7**, 940-9.

Adler, P. N., Zhu, C. and Stone, D. (2004). Inturned localizes to the proximal side of wing cells under the instruction of upstream planar polarity proteins. *Curr Biol* **14**, 2046-51.

Anderson, P. (1995). Mutagenesis. *Methods Cell Biol* **48**, 31-58.

Artal-Sanz, M., de Jong, L. and Tavernarakis, N. (2006). *Caenorhabditis* elegans: a versatile platform for drug discovery. *Biotechnol J* **1**, 1405-18.

Asakura, T., Ogura, K. and Goshima, Y. (2007). UNC-6 expression by the vulval precursor cells of *Caenorhabditis* elegans is required for the complex axon guidance of the HSN neurons. *Dev Biol* **304**, 800-10.

Axelrod, J. D. (2001). Unipolar membrane association of Dishevelled mediates Frizzled planar cell polarity signaling. *Genes Dev* **15**, 1182-7.

Axelrod, J. D. (2009). Progress and challenges in understanding planar cell polarity signaling. *Semin Cell Dev Biol* **20**, 964-71.

Barnes, A. P., Lilley, B. N., Pan, Y. A., Plummer, L. J., Powell, A. W., Raines, A. N., Sanes, J. R. and Polleux, F. (2007). LKB1 and SAD kinases define a pathway required for the polarization of cortical neurons. *Cell* **129**, 549-63.

Barnes, A. P. and Polleux, F. (2009). Establishment of axon-dendrite polarity in developing neurons. *Annu Rev Neurosci* **32**, 347-81.

Barnes, A. P., Solecki, D. and Polleux, F. (2008). New insights into the molecular mechanisms specifying neuronal polarity in vivo. *Curr Opin Neurobiol* **18**, 44-52.

Bastock, R., Strutt, H. and Strutt, D. (2003). Strabismus is asymmetrically localised and binds to Prickle and Dishevelled during *Drosophila* planar polarity patterning. *Development* **130**, 3007-14.

Behrens, J., von Kries, J. P., Kuhl, M., Bruhn, L., Wedlich, D., Grosschedl, R. and Birchmeier, W. (1996). Functional interaction of β-catenin with the transcription factor LEF-1. *Nature* **382**, 638-42.

Bellaiche, Y., Beaudoin-Massiani, O., Stuttem, I. and Schweisguth, F. (2004). The planar cell polarity protein Strabismus promotes Pins anterior localization during asymmetric division of sensory organ precursor cells in *Drosophila*. *Development* **131**, 469-78.

Bellaiche, Y., Gho, M., Kaltschmidt, J. A., Brand, A. H. and Schweisguth, F. (2001). Frizzled regulates localization of cell-fate determinants and mitotic spindle rotation during asymmetric cell division. *Nat Cell Biol* **3**, 50-7.

Benazeraf, B. and Pourquie, O. (2008). Developmental biology: cell intercalation one step beyond. *Curr Biol* **18**, R119-21.

Bienz, M. (2005). β-Catenin: a pivot between cell adhesion and Wnt signalling. *Curr Biol* **15**, R64-7.

Bingham, S., Higashijima, S., Okamoto, H. and Chandrasekhar, A. (2002). The Zebrafish trilobite gene is essential for tangential migration of branchiomotor neurons. *Dev Biol* **242**, 149-60.

Brenner, S. (1974). The genetics of *Caenorhabditis* elegans. *Genetics* **77**, 71-94.

Brittle, A. L., Repiso, A., Casal, J., Lawrence, P. A. and Strutt, D. (2010). Four-jointed modulates growth and planar polarity by reducing the affinity of Dachsous for Fat. *Curr Biol* **20**, 803-10.

Cadigan, K. M. and Nusse, R. (1997). Wnt signaling: a common theme in animal development. *Genes Dev* **11**, 3286-305.

Carreira-Barbosa, F., Concha, M. L., Takeuchi, M., Ueno, N., Wilson, S. W. and Tada, M. (2003). Prickle 1 regulates cell movements during gastrulation and neuronal migration in zebrafish. *Development* **130**, 4037-46.
Chang, C., Adler, C. E., Krause, M., Clark, S. G., Gertler, F. B., Tessier-Lavigne, M. and Bargmann, C. I. (2006). MIG-10/lamellipodin and AGE-1/PI3K promote axon guidance and outgrowth in response to Slit and Netrin. *Curr Biol* **16**, 854-62.
Chen, W. S., Antic, D., Matis, M., Logan, C. Y., Povelones, M., Anderson, G. A., Nusse, R. and Axelrod, J. D. (2008). Asymmetric homotypic interactions of the atypical cadherin Flamingo mediate intercellular polarity signaling. *Cell* **133**, 1093-105.
Choi, J. H., Law, M. Y., Chien, C. B., Link, B. A. and Wong, R. O. (2010). *In vivo* development of dendritic orientation in wild-type and mislocalized retinal ganglion cells. *Neural Dev* **5**, 29.
Chuai, M. and Weijer, C. J. (2009). Regulation of cell migration during chick gastrulation. *Curr Opin Genet Dev* **19**, 343-9.
Chung, S., Kim, S., Yoon, J., Adler, P. N. and Yim, J. (2007). The balance between the novel protein target of wingless and the *Drosophila* Rho-associated kinase pathway regulates planar cell polarity in the *Drosophila* wing. *Genetics* **176**, 891-903.
Ciruna, B., Jenny, A., Lee, D., Mlodzik, M. and Schier, A. F. (2006). Planar cell polarity signalling couples cell division and morphogenesis during neurulation. *Nature* **439**, 220-4.
Coghlan, A. (2005). Nematode genome evolution. *WormBook*, 1-15.
Colavita, A. and Culotti, J. G. (1998). Suppressors of ectopic UNC-5 growth cone steering identify eight genes involved in axon guidance in *Caenorhabditis elegans*. *Dev Biol* **194**, 72-85.
Cooper, O., Sweetman, D., Wagstaff, L. and Munsterberg, A. (2008). Expression of avian *prickle* genes during early development and organogenesis. *Dev Dyn* **237**, 1442-8.
Culotti, J. G. and Kolodkin, A. L. (1996). Functions of netrins and semaphorins in axon guidance. *Curr Opin Neurobiol* **6**, 81-8.
Curtin, J. A., Quint, E., Tsipouri, V., Arkell, R. M., Cattanach, B., Copp, A. J., Henderson, D. J., Spurr, N., Stanier, P., Fisher, E. M. et al. (2003). Mutation of Celsr1 disrupts planar polarity of inner ear hair cells and causes severe neural tube defects in the mouse. *Curr Biol* **13**, 1129-33.
Dabdoub, A., Donohue, M. J., Brennan, A., Wolf, V., Montcouquiol, M., Sassoon, D. A., Hseih, J. C., Rubin, J. S., Salinas, P. C. and Kelley, M. W. (2003). Wnt signaling mediates reorientation of outer hair cell stereociliary bundles in the mammalian cochlea. *Development* **130**, 2375-84.
Dale, R. M., Sisson, B. E. and Topczewski, J. (2009). The emerging role of Wnt/PCP signaling in organ formation. *Zebrafish* **6**, 9-14.
Das, G., Jenny, A., Klein, T. J., Eaton, S. and Mlodzik, M. (2004). Diego interacts with Prickle and Strabismus/Van Gogh to localize planar cell polarity complexes. *Development* **131**, 4467-76.
de la Roche, M., Worm, J. and Bienz, M. (2008). The function of BCL9 in Wnt/β-catenin signaling and colorectal cancer cells. *BMC Cancer* **8**, 199.
Deppe, U., Schierenberg, E., Cole, T., Krieg, C., Schmitt, D., Yoder, B. and von Ehrenstein, G. (1978). Cell lineages of the embryo of the nematode *Caenorhabditis elegans*. *Proc Natl Acad Sci U S A* **75**, 376-80.
Devenport, D. and Fuchs, E. (2008). Planar polarization in embryonic epidermis orchestrates global asymmetric morphogenesis of hair follicles. *Nat Cell Biol* **10**, 1257-68.
Dotti, C. G., Sullivan, C. A. and Banker, G. A. (1988). The establishment of polarity by hippocampal neurons in culture. *J Neurosci* **8**, 1454-68.
Endo, Y. and Rubin, J. S. (2007). Wnt signaling and neurite outgrowth: insights and questions. *Cancer Sci* **98**, 1311-7.
Evans, T. A. and Bashaw, G. J. (2010). Axon guidance at the midline: of mice and flies. *Curr Opin Neurobiol* **20**, 79-85.

Fenstermaker, A. G., Prasad, A. A., Bechara, A., Adolfs, Y., Tissir, F., Goffinet, A., Zou, Y. and Pasterkamp, R. J. (2010). Wnt/planar cell polarity signaling controls the anterior-posterior organization of monoaminergic axons in the brainstem. *J Neurosci* **30**, 16053-64.
Fire, A., Harrison, S. W. and Dixon, D. (1990). A modular set of lacZ fusion vectors for studying gene expression in *Caenorhabditis elegans*. *Gene* **93**, 189-98.
Fischer, E., Legue, E., Doyen, A., Nato, F., Nicolas, J. F., Torres, V., Yaniv, M. and Pontoglio, M. (2006). Defective planar cell polarity in polycystic kidney disease. *Nat Genet* **38**, 21-3.
Formstone, C. J. and Mason, I. (2005a). Combinatorial activity of Flamingo proteins directs convergence and extension within the early zebrafish embryo via the planar cell polarity pathway. *Dev Biol* **282**, 320-35.
Formstone, C. J. and Mason, I. (2005b). Expression of the *celsr/flamingo* homologue, *c-fmi1*, in the early avian embryo indicates a conserved role in neural tube closure and additional roles in asymmetry and somitogenesis. *Dev Dyn* **232**, 408-13.
Gao, B., Song, H., Bishop, K., Elliot, G., Garrett, L., English, M. A., Andre, P., Robinson, J., Sood, R., Minami, Y. et al. (2011). Wnt signaling gradients establish planar cell polarity by inducing Vangl2 phosphorylation through Ror2. *Dev Cell* **20**, 163-76.
Gao, C. and Chen, Y. G. (2009). Dishevelled: The hub of Wnt signaling. *Cell Signal* **22**, 717-27.
Gilbert, S. F. (2000). Developmental Biology. Sunderland: Sinauer Associates, Inc.
Gomes, J. E., Corado, M. and Schweisguth, F. (2009). Van Gogh and Frizzled act redundantly in the *Drosophila* sensory organ precursor cell to orient its asymmetric division. *PLoS One* **4**, e4485.
Gong, Y., Mo, C. and Fraser, S. E. (2004). Planar cell polarity signalling controls cell division orientation during zebrafish gastrulation. *Nature* **430**, 689-93.
Goodrich, L. V. and Strutt, D. (2011). Principles of planar polarity in animal development. *Development* **138**, 1877-92.
Govek, E. E., Newey, S. E. and Van Aelst, L. (2005). The role of the Rho GTPases in neuronal development. *Genes Dev* **19**, 1-49.
Green, J. L., Inoue, T. and Sternberg, P. W. (2008). Opposing Wnt pathways orient cell polarity during organogenesis. *Cell* **134**, 646-56.
Greene, N. D., Gerrelli, D., Van Straaten, H. W. and Copp, A. J. (1998). Abnormalities of floor plate, notochord and somite differentiation in the *loop-tail (lp)* mouse: a model of severe neural tube defects. *Mech Dev* **73**, 59-72.
Grishok, A. (2005). RNAi mechanisms in *Caenorhabditis elegans*. *FEBS Lett* **579**, 5932-9.
Gros, J., Serralbo, O. and Marcelle, C. (2009). WNT11 acts as a directional cue to organize the elongation of early muscle fibres. *Nature* **457**, 589-93.
Gubb, D. and Garcia-Bellido, A. (1982). A genetic analysis of the determination of cuticular polarity during development in *Drosophila melanogaster*. *J Embryol Exp Morphol* **68**, 37-57.
Hamelin, M., Zhou, Y., Su, M. W., Scott, I. M. and Culotti, J. G. (1993). Expression of the UNC-5 guidance receptor in the touch neurons of *C. elegans* steers their axons dorsally. *Nature* **364**, 327-30.
Hand, R., Bortone, D., Mattar, P., Nguyen, L., Heng, J. I., Guerrier, S., Boutt, E., Peters, E., Barnes, A. P., Parras, C. et al. (2005). Phosphorylation of Neurogenin2 specifies the migration properties and the dendritic morphology of pyramidal neurons in the neocortex. *Neuron* **48**, 45-62.
Hao, J. C., Yu, T. W., Fujisawa, K., Culotti, J. G., Gengyo-Ando, K., Mitani, S., Moulder, G., Barstead, R., Tessier-Lavigne, M. and Bargmann, C. I. (2001). *C. elegans* Slit acts in midline, dorsal-ventral, and anterior-posterior guidance via the SAX-3/Robo receptor. *Neuron* **32**, 25-38.

Harumoto, T., Ito, M., Shimada, Y., Kobayashi, T. J., Ueda, H. R., Lu, B. and Uemura, T. (2010). Atypical cadherins Dachsous and Fat control dynamics of noncentrosomal microtubules in planar cell polarity. *Dev Cell* **19**, 389-401.
He, X., Semenov, M., Tamai, K. and Zeng, X. (2004). LDL receptor-related proteins 5 and 6 in Wnt/β-catenin signaling: arrows point the way. *Development* **131**, 1663-77.
Hilliard, M. A. and Bargmann, C. I. (2006). Wnt signals and frizzled activity orient anterior-posterior axon outgrowth in *C. elegans*. *Dev Cell* **10**, 379-90.
Hoffmann, M., Segbert, C., Helbig, G. and Bossinger, O. (2010). Intestinal tube formation in *Caenorhabditis elegans* requires *vang-1* and *egl-15* signaling. *Dev Biol* **339**, 268-79.
Hou, S. T., Jiang, S. X. and Smith, R. A. (2008). Permissive and repulsive cues and signalling pathways of axonal outgrowth and regeneration. *Int Rev Cell Mol Biol* **267**, 125-81.
Insolera, R., Chen, S. and Shi, S. H. (2011). Par proteins and neuronal polarity. *Dev Neurobiol* **71**, 483-94.
Jenny, A., Darken, R. S., Wilson, P. A. and Mlodzik, M. (2003). Prickle and Strabismus form a functional complex to generate a correct axis during planar cell polarity signaling. *EMBO J* **22**, 4409-20.
Jenny, A., Reynolds-Kenneally, J., Das, G., Burnett, M. and Mlodzik, M. (2005). Diego and Prickle regulate Frizzled planar cell polarity signalling by competing for Dishevelled binding. *Nat Cell Biol* **7**, 691-7.
Jessen, J. R. and Solnica-Krezel, L. (2004). Identification and developmental expression pattern of *van gogh-like 1*, a second zebrafish strabismus homologue. *Gene Expr Patterns* **4**, 339-44.
Jessen, J. R., Topczewski, J., Bingham, S., Sepich, D. S., Marlow, F., Chandrasekhar, A. and Solnica-Krezel, L. (2002). Zebrafish trilobite identifies new roles for Strabismus in gastrulation and neuronal movements. *Nat Cell Biol* **4**, 610-5.
Johnson, N. M., Behm, C. A. and Trowell, S. C. (2005). Heritable and inducible gene knockdown in *C. elegans* using Wormgate and the ORFeome. *Gene* **359**, 26-34.
Jorgensen, E. M. and Mango, S. E. (2002). The art and design of genetic screens: *Caenorhabditis elegans*. *Nat Rev Genet* **3**, 356-69.
Kamath, R. S. and Ahringer, J. (2003). Genome-wide RNAi screening in *Caenorhabditis elegans*. *Methods* **30**, 313-21.
Kamath, R. S., Fraser, A. G., Dong, Y., Poulin, G., Durbin, R., Gotta, M., Kanapin, A., Le Bot, N., Moreno, S., Sohrmann, M. et al. (2003). Systematic functional analysis of the *Caenorhabditis elegans* genome using RNAi. *Nature* **421**, 231-7.
Kamath, R. S., Martinez-Campos, M., Zipperlen, P., Fraser, A. G. and Ahringer, J. (2001). Effectiveness of specific RNA-mediated interference through ingested double-stranded RNA in *Caenorhabditis elegans*. *Genome Biol* **2**, RESEARCH0002.
Karner, C. M., Chirumamilla, R., Aoki, S., Igarashi, P., Wallingford, J. B. and Carroll, T. J. (2009). Wnt9b signaling regulates planar cell polarity and kidney tubule morphogenesis. *Nat Genet* **41**, 793-9.
Kennedy, S., Wang, D. and Ruvkun, G. (2004). A conserved siRNA-degrading RNase negatively regulates RNA interference in *C. elegans*. *Nature* **427**, 645-9.
Kenyon, C. (1988). The nematode *Caenorhabditis elegans*. *Science* **240**, 1448-53.
Kibar, Z., Vogan, K. J., Groulx, N., Justice, M. J., Underhill, D. A. and Gros, P. (2001). Ltap, a mammalian homolog of *Drosophila* Strabismus/Van Gogh, is altered in the mouse neural tube mutant *Loop-tail*. *Nat Genet* **28**, 251-5.
Kilian, B., Mansukoski, H., Barbosa, F. C., Ulrich, F., Tada, M. and Heisenberg, C. P. (2003). The role of Ppt/Wnt5 in regulating cell shape and movement during zebrafish gastrulation. *Mech Dev* **120**, 467-76.

Killeen, M. T. and Sybingco, S. S. (2008). Netrin, Slit and Wnt receptors allow axons to choose the axis of migration. *Dev Biol* **323**, 143-51.
Kishi, M., Pan, Y. A., Crump, J. G. and Sanes, J. R. (2005). Mammalian SAD kinases are required for neuronal polarization. *Science* **307**, 929-32.
Klassen, M. P. and Shen, K. (2007). Wnt signaling positions neuromuscular connectivity by inhibiting synapse formation in *C. elegans*. *Cell* **130**, 704-16.
Koster, I., Jungwirth, M. S. and Steinbeisser, H. (2010). xGit2 and xRhoGAP 11A regulate convergent extension and tissue separation in *Xenopus* gastrulation. *Dev Biol* **344**, 26-35.
Kuriyama, S. and Mayor, R. (2008). Molecular analysis of neural crest migration. *Philos Trans R Soc Lond B Biol Sci* **363**, 1349-62.
Lawrence, P. A., Casal, J. and Struhl, G. (2004). Cell interactions and planar polarity in the abdominal epidermis of *Drosophila*. *Development* **131**, 4651-64.
Levy-Strumpf, N. and Culotti, J. G. (2007). VAB-8, UNC-73 and MIG-2 regulate axon polarity and cell migration functions of UNC-40 in *C. elegans*. *Nat Neurosci* **10**, 161-8.
Li, C. and Chalfie, M. (1990). Organogenesis in *C. elegans*: positioning of neurons and muscles in the egg-laying system. *Neuron* **4**, 681-95.
Lickteig, K. M., Duerr, J. S., Frisby, D. L., Hall, D. H., Rand, J. B. and Miller, D. M., 3rd. (2001). Regulation of neurotransmitter vesicles by the homeodomain protein UNC-4 and its transcriptional corepressor UNC-37/groucho in *Caenorhabditis elegans* cholinergic motor neurons. *J Neurosci* **21**, 2001-14.
Lim, J., Norga, K. K., Chen, Z. and Choi, K. W. (2005). Control of planar cell polarity by interaction of DWnt4 and Four-jointed. *Genesis* **42**, 150-61.
Lin, Y. Y. and Gubb, D. (2009). Molecular dissection of *Drosophila* Prickle isoforms distinguishes their essential and overlapping roles in planar cell polarity. *Dev Biol* **325**, 386-99.
Lu, X., Borchers, A. G., Jolicoeur, C., Rayburn, H., Baker, J. C. and Tessier-Lavigne, M. (2004). PTK7/CCK-4 is a novel regulator of planar cell polarity in vertebrates. *Nature* **430**, 93-8.
Lyuksyutova, A. I., Lu, C. C., Milanesio, N., King, L. A., Guo, N., Wang, Y., Nathans, J., Tessier-Lavigne, M. and Zou, Y. (2003). Anterior-posterior guidance of commissural axons by Wnt-frizzled signaling. *Science* **302**, 1984-8.
Ma, D., Amonlirdviman, K., Raffard, R. L., Abate, A., Tomlin, C. J. and Axelrod, J. D. (2008a). Cell packing influences planar cell polarity signaling. *Proc Natl Acad Sci U S A* **105**, 18800-5.
Ma, Y. C., Song, M. R., Park, J. P., Henry Ho, H. Y., Hu, L., Kurtev, M. V., Zieg, J., Ma, Q., Pfaff, S. L. and Greenberg, M. E. (2008b). Regulation of motor neuron specification by phosphorylation of Neurogenin 2. *Neuron* **58**, 65-77.
Macdonald, B. T., Semenov, M. V. and He, X. (2007). SnapShot: Wnt/β-catenin signaling. *Cell* **131**, 1204.
Maduro, M. F. (2010). Cell fate specification in the *C. elegans* embryo. *Dev Dyn* **239**, 1315-29.
Mao, Y., Rauskolb, C., Cho, E., Hu, W. L., Hayter, H., Minihan, G., Katz, F. N. and Irvine, K. D. (2006). Dachs: an unconventional myosin that functions downstream of Fat to regulate growth, affinity and gene expression in *Drosophila*. *Development* **133**, 2539-51.
Mapp, O. M., Wanner, S. J., Rohrschneider, M. R. and Prince, V. E. (2010). Prickle1b mediates interpretation of migratory cues during zebrafish facial branchiomotor neuron migration. *Dev Dyn* **239**, 1596-608.
McNeill, H. (2009). Planar cell polarity and the kidney. *J Am Soc Nephrol* **20**, 2104-11.
McNeill, H. (2010). Planar cell polarity: keeping hairs straight is not so simple. *Cold Spring Harb Perspect Biol* **2**, a003376.
Mello, C. and Fire, A. (1995). DNA transformation. *Methods Cell Biol* **48**, 451-82.

Mello, C. C., Kramer, J. M., Stinchcomb, D. and Ambros, V. (1991). Efficient gene transfer in *C.elegans*: extrachromosomal maintenance and integration of transforming sequences. *EMBO J* **10**, 3959-70.
Mitchell, K. J., Doyle, J. L., Serafini, T., Kennedy, T. E., Tessier-Lavigne, M., Goodman, C. S. and Dickson, B. J. (1996). Genetic analysis of Netrin genes in *Drosophila*: Netrins guide CNS commissural axons and peripheral motor axons. *Neuron* **17**, 203-15.
Molenaar, M., van de Wetering, M., Oosterwegel, M., Peterson-Maduro, J., Godsave, S., Korinek, V., Roose, J., Destree, O. and Clevers, H. (1996). XTcf-3 transcription factor mediates β-catenin-induced axis formation in *Xenopus* embryos. *Cell* **86**, 391-9.
Montcouquiol, M., Rachel, R. A., Lanford, P. J., Copeland, N. G., Jenkins, N. A. and Kelley, M. W. (2003). Identification of Vangl2 and Scrb1 as planar polarity genes in mammals. *Nature* **423**, 173-7.
Montcouquiol, M., Sans, N., Huss, D., Kach, J., Dickman, J. D., Forge, A., Rachel, R. A., Copeland, N. G., Jenkins, N. A., Bogani, D. et al. (2006). Asymmetric localization of Vangl2 and Fz3 indicate novel mechanisms for planar cell polarity in mammals. *J Neurosci* **26**, 5265-75.
Morgan, J. L., Dhingra, A., Vardi, N. and Wong, R. O. (2006). Axons and dendrites originate from neuroepithelial-like processes of retinal bipolar cells. *Nat Neurosci* **9**, 85-92.
Murdoch, J. N., Doudney, K., Paternotte, C., Copp, A. J. and Stanier, P. (2001). Severe neural tube defects in the *loop-tail* mouse result from mutation of *Lpp1*, a novel gene involved in floor plate specification. *Hum Mol Genet* **10**, 2593-601.
Nachury, M. V., Loktev, A. V., Zhang, Q., Westlake, C. J., Peranen, J., Merdes, A., Slusarski, D. C., Scheller, R. H., Bazan, J. F., Sheffield, V. C. et al. (2007). A core complex of BBS proteins cooperates with the GTPase Rab8 to promote ciliary membrane biogenesis. *Cell* **129**, 1201-13.
Ng, J. (2012). Wnt/PCP proteins regulate stereotyped axon branch extension in *Drosophila*. *Development* **139**, 165-77.
Nishimura, T., Kato, K., Yamaguchi, T., Fukata, Y., Ohno, S. and Kaibuchi, K. (2004). Role of the PAR-3-KIF3 complex in the establishment of neuronal polarity. *Nat Cell Biol* **6**, 328-34.
Nishimura, T., Yamaguchi, T., Kato, K., Yoshizawa, M., Nabeshima, Y., Ohno, S., Hoshino, M. and Kaibuchi, K. (2005). PAR-6-PAR-3 mediates Cdc42-induced Rac activation through the Rac GEFs STEF/Tiam1. *Nat Cell Biol* **7**, 270-7.
Okuda, H., Miyata, S., Mori, Y. and Tohyama, M. (2007). Mouse Prickle1 and Prickle2 are expressed in postmitotic neurons and promote neurite outgrowth. *FEBS Lett* **581**, 4754-60.
Ou, C. Y. and Shen, K. (2010). Neuronal polarity in C. elegans. *Dev Neurobiol*.
Pan, C. L., Howell, J. E., Clark, S. G., Hilliard, M., Cordes, S., Bargmann, C. I. and Garriga, G. (2006). Multiple Wnts and Frizzled receptors regulate anteriorly directed cell and growth cone migrations in *Caenorhabditis elegans*. *Dev Cell* **10**, 367-77.
Park, M. and Moon, R. T. (2002). The planar cell-polarity gene *stbm* regulates cell behaviour and cell fate in vertebrate embryos. *Nat Cell Biol* **4**, 20-5.
Quinn, C. C., Pfeil, D. S., Chen, E., Stovall, E. L., Harden, M. V., Gavin, M. K., Forrester, W. C., Ryder, E. F., Soto, M. C. and Wadsworth, W. G. (2006). UNC-6/netrin and SLT-1/slit guidance cues orient axon outgrowth mediated by MIG-10/RIAM/lamellipodin. *Curr Biol* **16**, 845-53.
Randlett, O., Poggi, L., Zolessi, F. R. and Harris, W. A. (2011). The oriented emergence of axons from retinal ganglion cells is directed by laminin contact in vivo. *Neuron* **70**, 266-80.
Riddle, D. L., Blumenthal, T., Meyer, B. J. and Priess, J. R. (1997). Introduction to *C. elegans*.
Rieckher, M., Kourtis, N., Pasparaki, A. and Tavernarakis, N. (2009). Transgenesis in *Caenorhabditis elegans*. *Methods Mol Biol* **561**, 21-39.

Rocheleau, C. E., Howard, R. M., Goldman, A. P., Volk, M. L., Girard, L. J. and Sundaram, M. V. (2002). A *lin-45 raf* enhancer screen identifies *eor-1, eor-2* and unusual alleles of Ras pathway genes in *Caenorhabditis elegans*. *Genetics* **161**, 121-31.
Rohrschneider, M. R., Elsen, G. E. and Prince, V. E. (2007). Zebrafish Hoxb1a regulates multiple downstream genes including *prickle1b*. *Dev Biol* **309**, 358-72.
Rohrschneider, M. R. and Nance, J. (2009). Polarity and cell fate specification in the control of *Caenorhabditis elegans* gastrulation. *Dev Dyn* **238**, 789-96.
Ross, A. J., May-Simera, H., Eichers, E. R., Kai, M., Hill, J., Jagger, D. J., Leitch, C. C., Chapple, J. P., Munro, P. M., Fisher, S. et al. (2005). Disruption of Bardet-Biedl syndrome ciliary proteins perturbs planar cell polarity in vertebrates. *Nat Genet* **37**, 1135-40.
Roszko, I., Sawada, A. and Solnica-Krezel, L. (2009). Regulation of convergence and extension movements during vertebrate gastrulation by the Wnt/PCP pathway. *Semin Cell Dev Biol* **20**, 986-97.
Sanchez-Alvarez, L., Visanuvimol, J., McEwan, A., Su, A., Imai, J. H. and Colavita, A. (2011). VANG-1 and PRKL-1 Cooperate to Negatively Regulate Neurite Formation in *Caenorhabditis elegans*. *PLoS Genet* **7**, e1002257.
Sassi, H. E., Renihan, S., Spence, A. M. and Cooperstock, R. L. (2005). Gene CATCHR--gene cloning and tagging for *Caenorhabditis elegans* using yeast homologous recombination: a novel approach for the analysis of gene expression. *Nucleic Acids Res* **33**, e163.
Schafer, W. R. (2005). Egg-laying. *WormBook*, 1-7.
Schambony, A. and Wedlich, D. (2007). Wnt-5A/Ror2 regulate expression of XPAPC through an alternative noncanonical signaling pathway. *Dev Cell* **12**, 779-92.
Schmitz, C., Kinge, P. and Hutter, H. (2007). Axon guidance genes identified in a large-scale RNAi screen using the RNAi-hypersensitive *Caenorhabditis elegans* strain *nre-1(hd20) lin-15b(hd126)*. *Proc Natl Acad Sci U S A* **104**, 834-9.
Schwamborn, J. C. and Puschel, A. W. (2004). The sequential activity of the GTPases Rap1B and Cdc42 determines neuronal polarity. *Nat Neurosci* **7**, 923-9.
Schwarz-Romond, T., Merrifield, C., Nichols, B. J. and Bienz, M. (2005). The Wnt signalling effector Dishevelled forms dynamic protein assemblies rather than stable associations with cytoplasmic vesicles. *J Cell Sci* **118**, 5269-77.
Seifert, J. R. and Mlodzik, M. (2007). Frizzled/PCP signalling: a conserved mechanism regulating cell polarity and directed motility. *Nat Rev Genet* **8**, 126-38.
Serafini, T., Colamarino, S. A., Leonardo, E. D., Wang, H., Beddington, R., Skarnes, W. C. and Tessier-Lavigne, M. (1996). Netrin-1 is required for commissural axon guidance in the developing vertebrate nervous system. *Cell* **87**, 1001-14.
Shafer, B., Onishi, K., Lo, C., Colakoglu, G. and Zou, Y. (2011). Vangl2 Promotes Wnt/Planar Cell Polarity-like Signaling by Antagonizing Dvl1-Mediated Feedback Inhibition in Growth Cone Guidance. *Dev Cell* **20**, 407.
Shelly, M., Cancedda, L., Heilshorn, S., Sumbre, G. and Poo, M. M. (2007). LKB1/STRAD promotes axon initiation during neuronal polarization. *Cell* **129**, 565-77.
Shi, S. H., Jan, L. Y. and Jan, Y. N. (2003). Hippocampal neuronal polarity specified by spatially localized mPar3/mPar6 and PI 3-kinase activity. *Cell* **112**, 63-75.
Shimada, Y., Yonemura, S., Ohkura, H., Strutt, D. and Uemura, T. (2006). Polarized transport of Frizzled along the planar microtubule arrays in *Drosophila* wing epithelium. *Dev Cell* **10**, 209-22.
Shimizu, K., Sato, M. and Tabata, T. (2011). The Wnt5/planar cell polarity pathway regulates axonal development of the *Drosophila* mushroom body neuron. *J Neurosci* **31**, 4944-54.
Shnitsar, I. and Borchers, A. (2008). PTK7 recruits dsh to regulate neural crest migration. *Development* **135**, 4015-24.

Sieburth, D., Ch'ng, Q., Dybbs, M., Tavazoie, M., Kennedy, S., Wang, D., Dupuy, D., Rual, J. F., Hill, D. E., Vidal, M. et al. (2005). Systematic analysis of genes required for synapse structure and function. *Nature* **436**, 510-7.
Simmer, F., Tijsterman, M., Parrish, S., Koushika, S. P., Nonet, M. L., Fire, A., Ahringer, J. and Plasterk, R. H. (2002). Loss of the putative RNA-directed RNA polymerase RRF-3 makes *C. elegans* hypersensitive to RNAi. *Curr Biol* **12**, 1317-9.
Simon, M. A. (2004). Planar cell polarity in the *Drosophila* eye is directed by graded Four-jointed and Dachsous expression. *Development* **131**, 6175-84.
Simon, M. A., Xu, A., Ishikawa, H. O. and Irvine, K. D. (2010). Modulation of Fat:Dachsous binding by the cadherin domain kinase Four-jointed. *Curr Biol* **20**, 811-7.
Simons, M., Gloy, J., Ganner, A., Bullerkotte, A., Bashkurov, M., Kronig, C., Schermer, B., Benzing, T., Cabello, O. A., Jenny, A. et al. (2005). Inversin, the gene product mutated in nephronophthisis type II, functions as a molecular switch between Wnt signaling pathways. *Nat Genet* **37**, 537-43.
Sisson, B. E. and Topczewski, J. (2009). Expression of five Frizzleds during zebrafish craniofacial development. *Gene Expr Patterns* **9**, 520-7.
Smalley, M. J., Signoret, N., Robertson, D., Tilley, A., Hann, A., Ewan, K., Ding, Y., Paterson, H. and Dale, T. C. (2005). Dishevelled (Dvl-2) activates canonical Wnt signalling in the absence of cytoplasmic puncta. *J Cell Sci* **118**, 5279-89.
Solnica-Krezel, L. (2006). Gastrulation in zebrafish -- all just about adhesion? *Curr Opin Genet Dev* **16**, 433-41.
Song, S., Zhang, B., Sun, H., Li, X., Xiang, Y., Liu, Z., Huang, X. and Ding, M. (2010). A Wnt-Frz/Ror-Dsh pathway regulates neurite outgrowth in *Caenorhabditis elegans*. *PLoS Genet* **6**.
Strutt, D., Johnson, R., Cooper, K. and Bray, S. (2002). Asymmetric localization of Frizzled and the determination of notch-dependent cell fate in the *Drosophila* eye. *Curr Biol* **12**, 813-24.
Strutt, D. and Strutt, H. (2007). Differential activities of the core planar polarity proteins during *Drosophila* wing patterning. *Dev Biol* **302**, 181-94.
Strutt, D. and Warrington, S. J. (2008). Planar polarity genes in the *Drosophila* wing regulate the localisation of the FH3-domain protein Multiple Wing Hairs to control the site of hair production. *Development* **135**, 3103-11.
Strutt, D. I. (2001). Asymmetric localization of frizzled and the establishment of cell polarity in the *Drosophila* wing. *Mol Cell* **7**, 367-75.
Strutt, D. I. (2002). The asymmetric subcellular localisation of components of the planar polarity pathway. *Semin Cell Dev Biol* **13**, 225-31.
Strutt, H. and Strutt, D. (2008). Differential stability of Flamingo protein complexes underlies the establishment of planar polarity. *Curr Biol* **18**, 1555-64.
Strutt, H. and Strutt, D. (2009). Asymmetric localisation of planar polarity proteins: mechanisms and consequences. *Semin Cell Dev Biol* **20**, 957-63.
Sugimura, R. and Li, L. (2010). Noncanonical Wnt signaling in vertebrate development, stem cells, and diseases. *Birth Defects Res C Embryo Today* **90**, 243-56.
Sulston, J. E., Schierenberg, E., White, J. G. and Thomson, J. N. (1983). The embryonic cell lineage of the nematode *Caenorhabditis elegans*. *Dev Biol* **100**, 64-119.
Sweede, M., Ankem, G., Chutvirasakul, B., Azurmendi, H. F., Chbeir, S., Watkins, J., Helm, R. F., Finkielstein, C. V. and Capelluto, D. G. (2008). Structural and membrane binding properties of the Prickle PET domain. *Biochemistry* **47**, 13524-36.
Tada, M. and Kai, M. (2009). Noncanonical Wnt/PCP signaling during vertebrate gastrulation. *Zebrafish* **6**, 29-40.
Tahirovic, S. and Bradke, F. (2009). Neuronal polarity. *Cold Spring Harb Perspect Biol* **1**, a001644.

Taylor, J., Abramova, N., Charlton, J. and Adler, P. N. (1998). Van Gogh: a new *Drosophila* tissue polarity gene. *Genetics* **150**, 199-210.
Timmons, L. (2004). Endogenous inhibitors of RNA interference in *Caenorhabditis elegans*. *Bioessays* **26**, 715-8.
Tissir, F. and Goffinet, A. M. (2006). Expression of planar cell polarity genes during development of the mouse CNS. *Eur J Neurosci* **23**, 597-607.
Tissir, F. and Goffinet, A. M. (2010). Planar cell polarity signaling in neural development. *Curr Opin Neurobiol* **20**, 572-7.
Torban, E., Patenaude, A. M., Leclerc, S., Rakowiecki, S., Gauthier, S., Andelfinger, G., Epstein, D. J. and Gros, P. (2008). Genetic interaction between members of the Vangl family causes neural tube defects in mice. *Proc Natl Acad Sci U S A* **105**, 3449-54.
Torban, E., Wang, H. J., Groulx, N. and Gros, P. (2004). Independent mutations in mouse Vangl2 that cause neural tube defects in looptail mice impair interaction with members of the Dishevelled family. *J Biol Chem* **279**, 52703-13.
Tree, D. R., Shulman, J. M., Rousset, R., Scott, M. P., Gubb, D. and Axelrod, J. D. (2002). Prickle mediates feedback amplification to generate asymmetric planar cell polarity signaling. *Cell* **109**, 371-81.
Ulrich, F., Concha, M. L., Heid, P. J., Voss, E., Witzel, S., Roehl, H., Tada, M., Wilson, S. W., Adams, R. J., Soll, D. R. et al. (2003). Slb/Wnt11 controls hypoblast cell migration and morphogenesis at the onset of zebrafish gastrulation. *Development* **130**, 5375-84.
Valentine, M. and Collier, S. (2011). Planar cell polarity and tissue design: Shaping the *Drosophila* wing membrane. *Fly (Austin)* **5**.
Vervenne, H. B., Crombez, K. R., Lambaerts, K., Carvalho, L., Koppen, M., Heisenberg, C. P., Van de Ven, W. J. and Petit, M. M. (2008). Lpp is involved in Wnt/PCP signaling and acts together with Scrib to mediate convergence and extension movements during zebrafish gastrulation. *Dev Biol* **320**, 267-77.
Vladar, E. K., Antic, D. and Axelrod, J. D. (2009). Planar cell polarity signaling: the developing cell's compass. *Cold Spring Harb Perspect Biol* **1**, a002964.
Wada, H., Iwasaki, M., Sato, T., Masai, I., Nishiwaki, Y., Tanaka, H., Sato, A., Nojima, Y. and Okamoto, H. (2005). Dual roles of zygotic and maternal Scribble1 in neural migration and convergent extension movements in zebrafish embryos. *Development* **132**, 2273-85.
Wada, H. and Okamoto, H. (2009a). Roles of noncanonical Wnt/PCP pathway genes in neuronal migration and neurulation in zebrafish. *Zebrafish* **6**, 3-8.
Wada, H. and Okamoto, H. (2009b). Roles of planar cell polarity pathway genes for neural migration and differentiation. *Dev Growth Differ* **51**, 233-40.
Wada, H., Tanaka, H., Nakayama, S., Iwasaki, M. and Okamoto, H. (2006). Frizzled3a and Celsr2 function in the neuroepithelium to regulate migration of facial motor neurons in the developing zebrafish hindbrain. *Development* **133**, 4749-59.
Waggoner, L. E., Zhou, G. T., Schafer, R. W. and Schafer, W. R. (1998). Control of alternative behavioral states by serotonin in *Caenorhabditis elegans*. *Neuron* **21**, 203-14.
Wallingford, J. B. and Harland, R. M. (2002). Neural tube closure requires Dishevelled-dependent convergent extension of the midline. *Development* **129**, 5815-25.
Wallingford, J. B., Rowning, B. A., Vogeli, K. M., Rothbacher, U., Fraser, S. E. and Harland, R. M. (2000). Dishevelled controls cell polarity during Xenopus gastrulation. *Nature* **405**, 81-5.
Wallingford, J. B., Vogeli, K. M. and Harland, R. M. (2001). Regulation of convergent extension in Xenopus by Wnt5a and Frizzled-8 is independent of the canonical Wnt pathway. *Int J Dev Biol* **45**, 225-7.

Wang, D., Kennedy, S., Conte, D., Jr., Kim, J. K., Gabel, H. W., Kamath, R. S., Mello, C. C. and Ruvkun, G. (2005a). Somatic misexpression of germline P granules and enhanced RNA interference in retinoblastoma pathway mutants. *Nature* **436**, 593-7.
Wang, J., Hamblet, N. S., Mark, S., Dickinson, M. E., Brinkman, B. C., Segil, N., Fraser, S. E., Chen, P., Wallingford, J. B. and Wynshaw-Boris, A. (2006a). Dishevelled genes mediate a conserved mammalian PCP pathway to regulate convergent extension during neurulation. *Development* **133**, 1767-78.
Wang, J., Mark, S., Zhang, X., Qian, D., Yoo, S. J., Radde-Gallwitz, K., Zhang, Y., Lin, X., Collazo, A., Wynshaw-Boris, A. et al. (2005b). Regulation of polarized extension and planar cell polarity in the cochlea by the vertebrate PCP pathway. *Nat Genet* **37**, 980-5.
Wang, Y., Guo, N. and Nathans, J. (2006b). The role of Frizzled3 and Frizzled6 in neural tube closure and in the planar polarity of inner-ear sensory hair cells. *J Neurosci* **26**, 2147-56.
Wang, Y. and Nathans, J. (2007). Tissue/planar cell polarity in vertebrates: new insights and new questions. *Development* **134**, 647-58.
Wang, Y., Thekdi, N., Smallwood, P. M., Macke, J. P. and Nathans, J. (2002). Frizzled-3 is required for the development of major fiber tracts in the rostral CNS. *J Neurosci* **22**, 8563-73.
Warchol, M. E. and Montcouquiol, M. (2010). Maintained expression of the planar cell polarity molecule Vangl2 and reformation of hair cell orientation in the regenerating inner ear. *J Assoc Res Otolaryngol* **11**, 395-406.
White, J. G., Southgate, E., Thomson, J. N. and Brenner, S. (1976). The structure of the ventral nerve cord of *Caenorhabditis elegans*. *Philos Trans R Soc Lond B Biol Sci* **275**, 327-48.
Wiggin, G. R., Fawcett, J. P. and Pawson, T. (2005). Polarity proteins in axon specification and synaptogenesis. *Dev Cell* **8**, 803-16.
Winter, C. G., Wang, B., Ballew, A., Royou, A., Karess, R., Axelrod, J. D. and Luo, L. (2001). *Drosophila* Rho-associated kinase (Drok) links Frizzled-mediated planar cell polarity signaling to the actin cytoskeleton. *Cell* **105**, 81-91.
Wu, J. and Mlodzik, M. (2008). The Frizzled extracellular domain is a ligand for Van Gogh/Stbm during nonautonomous planar cell polarity signaling. *Dev Cell* **15**, 462-9.
Wu, J. and Mlodzik, M. (2009). A quest for the mechanism regulating global planar cell polarity of tissues. *Trends Cell Biol* **19**, 295-305.
Wu, M. and Herman, M. A. (2006). A novel noncanonical Wnt pathway is involved in the regulation of the asymmetric B cell division in *C. elegans*. *Dev Biol* **293**, 316-29.
Yates, L. L., Papakrivopoulou, J., Long, D. A., Goggolidou, P., Connolly, J. O., Woolf, A. S. and Dean, C. H. (2010). The planar cell polarity gene Vangl2 is required for mammalian kidney-branching morphogenesis and glomerular maturation. *Hum Mol Genet* **19**, 4663-76.
Ybot-Gonzalez, P., Savery, D., Gerrelli, D., Signore, M., Mitchell, C. E., Faux, C. H., Greene, N. D. and Copp, A. J. (2007). Convergent extension, planar-cell-polarity signalling and initiation of mouse neural tube closure. *Development* **134**, 789-99.
Yin, C., Kiskowski, M., Pouille, P. A., Farge, E. and Solnica-Krezel, L. (2008). Cooperation of polarized cell intercalations drives convergence and extension of presomitic mesoderm during zebrafish gastrulation. *J Cell Biol* **180**, 221-32.
Yoshimura, T., Arimura, N. and Kaibuchi, K. (2006). Signaling networks in neuronal polarization. *J Neurosci* **26**, 10626-30.
Zallen, J. A. (2007). Planar polarity and tissue morphogenesis. *Cell* **129**, 1051-63.
Zhou, L., Bar, I., Achouri, Y., Campbell, K., De Backer, O., Hebert, J. M., Jones, K., Kessaris, N., de Rouvroit, C. L., O'Leary, D. et al. (2008). Early forebrain wiring: genetic dissection using conditional Celsr3 mutant mice. *Science* **320**, 946-9.

Ziel, J. W., Hagedorn, E. J., Audhya, A. and Sherwood, D. R. (2009). UNC-6 (netrin) orients the invasive membrane of the anchor cell in *C. elegans*. *Nat Cell Biol* **11**, 183-9.
Zinovyeva, A. Y., Yamamoto, Y., Sawa, H. and Forrester, W. C. (2008). Complex network of Wnt signaling regulates neuronal migrations during *Caenorhabditis elegans* development. *Genetics* **179**, 1357-71.
Zolessi, F. R., Poggi, L., Wilkinson, C. J., Chien, C. B. and Harris, W. A. (2006). Polarization and orientation of retinal ganglion cells *in vivo*. *Neural Dev* **1**, 2.

APPENDIX: List of primers

vang-1 sequencing primers

5’-aaaatgttatgacggcgtgtg-3’

3’-tggtacccagagccgttactc-5’

5’-aaaatgtcataaacgccgagtc-3’

3’-ttttagggtacctagcttgtgc-5’

5’-tcagaagcgggtatactgttcg-3’

3’-caacagttgtgacagggaaaag-5’

5’-aaattatggcggttcaaagc-3’

3’-gtgttcgaactttgtaagtgtcc-5’

5’-gattcactcaaacttcgctcg-3’

Mutants genotyping primers

Strain		Primers/ genotyping methods	Restriction enzyme	Restriction enzyme/PCR product sizes
LGI	*lin-44(n1792)*	visual inspection for vulva defects	NA	–
	lin-17(n677)	5’-atcgatgctccgatccgatcc-3’	BshNI	N2: 200bp/ *lin-17(n677)* : 500bp
		3’-attctctctctgcacatgctc-5’		
	mig-1(n687)	5’-ctacttcccgatgtgcaacgag-3’	MseI	N2: 383bp/ *mig-1(n687)* : 120bp and 263bp
		3’-aatccctctaaacttttccggc-5’		
	mom-5(or57)	progeny of *dpy-5 mom-5/nt2* parents and are *dpy-5 mom-5* homozygous.	NA	–
LGII	*dsh-1(ok1445)*	5’-caacattctcccttcctcca-3’	NA (deletion allele)	N2: 411bp, *dsh-1(ok1445)*/+ : 411bp and 525bp, *dsh-1(ok1445)* : 525 bp
		3’-aggcaaaatgaaaaccatcg-5’		
		3’-gcggaaccaccaccggactc-5’		
LGIV	*prkl-1(ok3182)*	5'-cacgttcacaattgtaattc-3’	NA (deletion allele)	N2: 1.5kbp, *prkl-1(ok3182)* : 650bp
		3’-aatagtctcccagggccaag-5’		
		3’-cgataagaagtactctcatg-5’		
	egl-20(n585)	5’-aacaggcactttgcgcggag-3’	BsmI	N2: 393bp, *egl-20(n585):* 129bp and 264bp
		3’-aaacactttcttagttggcc-5’		
LGV	*fmi-1(tm306)*	5’-gaagatccaacagttccatg-3’	NA (deletion allele)	N2: 1185bp, *fmi-1(tm306)* : 363bp
		3’-gaaatggcttttcttgcactg-5’		
	cfz-2(ok1201)	5’-catgctgcgtgctagcctcc-3’	NA (deletion allele)	N2: 1.6kbp, *cfz-2(ok1201)* : 500bp
		3’-ctacagcttgtcaggaatgc-5’		
LGX	*vang-1(zy1)*	5’- aaaatgtcataaacgccgagtc-3’	NA	missence mutation identified via DNA sequencing
		3’-ttttagggtacctagcttgtgc-5’		
	vang-1(zy2)	5’-aaattatggcggttcaaagc-3’	TspE1	N2: 160bp, *vang-1(zy2)* : 110bp
		3’-gtgttcgaactttgtaagtgtcc-5’		
	vang-1(zy10)	5'-aaaatgtcataaacgccgagtc-3'	NA	missence mutation identified via DNA sequencing
		3'-ttttagggtacctagcttgtgc-5'		
	vang-1(tm1422)	5’-aaaatgtcataaacgccgagtc-3’	NA (deletion allele)	N2: 800bp, *vang-1(tm1422)* : 200bp
		3’-ttttagggtacctagcttgtgc-5’		
	bar-1(ga80)	5’-cgagctattcggatatacac-3’	MseI	N2: 420bp, *bar-1(ga80)* : 148bp and 272bp
		3’- ataagcatagtgagttctgg-5’		

Expression and cell-specific rescue constructs primers

Expression and rescue constructs	Primers	PCR product
Pvang-1::vang-1	5'-cgcggatccatgtcgtatcaagataacaggaaac-3’	*vang-1* cDNA
	3’-tgctctagaacaaatcaaactgccgactcattgc-5’	
	5’-aacaaccagatggactcactgaccg-3’	*vang-1* genomic fragments and 3'UTR
	3’-aacgagctcccgagacttttgtgtaatccaac-5’	
	5’-ttactgcagatgctctgtagaggttacatgc-3’	3kb upstream of *vang-1* start codon
	3’-tatgtcgacttgatacgacatgttccacctg-5’	
gfp::vang-1	5’-cgcggatccatgagtaaaggagaagaacttttc-3’	GFP cassette from pPD95.77
	3’-cgcggatcctttgtatagttcatccatgccatg-5’	
myr::gfp	5' -attaccggtatgggttgcctgttttcaaaagagcggcgaagtaaaggagaagaacttttcactg-3'	*myr* -tagged GFP cassette from pPD95.77
	3'-tattaacaagggtatcaccttc-5'	
Pcat-1::vang-1	5’-tataagcttcaaggctctgcagggt-3’	promoter region of *cat-1*
	3'-ttatctagacatacctccttcttccaagtttta-5'	
Pajm-1::gfp::vang-1	5’-tatctgcagccaacttttcagta-3’	promoter region of *ajm-1*
	3’- ttatctagagtccttggttctgtaaagac-5’	
Punc-129::gfp::vang-1	5’-tatctgcagcccgggaaacatgatatcgacgg-3’	promoter region of *unc-129*
	3’- ttatctagatgcttgctcttccaattttcctg-5’	
Pvang-1::gfp::vang-1	5’-atccgtcctaagaaaccattattatcatgacagcggccgctctgtagaggttacatgcgacag-3’	approximately 9.9kb of vang-1 exon and intron genomic regions
	3’-aagcgtggtgcactctcagtacaatctgctctgcggccgctactctcgatttgacatgttctctc-5’	